Gas-Phase Ion Chemistry: Kinetics and Thermodynamics

by

Charles M. Nichols

B. S., Chemistry – ACS Certified
University of Central Arkansas, 2009

A thesis submitted to the
Faculty of the Graduate School of the
University of Colorado in partial fulfillment
of the requirements for the degree of
Doctor of Philosophy
Department of Chemistry and Biochemistry
2016

This thesis entitled:

Gas-Phase Ion Chemistry: Kinetics and Thermodynamics

Written by Charles M. Nichols

has been approved for the Department of Chemistry and Biochemistry by:

_____

Veronica M. Bierbaum

_____

W. Carl Lineberger

Date: December 08, 2015

A final copy of this thesis has been examined by all signatories, and we find that both the content and the form meet acceptable presentation standards of scholarly work in the above mentioned discipline.

Nichols, Charles M. (Ph.D., Physical Chemistry)

Gas Phase Ion Chemistry: Kinetics and Thermodynamics

Thesis directed by Professors Veronica M. Bierbaum and W. Carl Lineberger

Abstract:

This thesis employs gas-phase ion chemistry to study the kinetics and thermodynamics of chemical reactions and molecular properties. Gas-phase ion chemistry is important in diverse regions of the universe. It is directly relevant to the chemistry occurring in the atmospheres of planets and moons as well as the molecular clouds of the interstellar medium. Gas-phase ion chemistry is also employed to determine fundamental properties, such as the proton and electron affinities of molecules. Furthermore, gas-phase ion chemistry can be used to study chemical events that typically occur in the condensed-phase, such as prototypical organic reactions, in an effort to reveal the intrinsic properties and mechanisms of chemical reactions.

Mass spectrometry is used to investigate the reactivity and fundamental properties of ions. Kinetic data for reactions between cations or anions with neutral atoms or molecules is acquired using the selected ion flow tube (SIFT). These data are interpreted mechanistically and thermodynamically using literature data and theoretical computations. Additionally, the proton affinities of a series of anions are determined using a triple quadrupole mass spectrometer by investigating the collision induced dissociation of proton-bound, anionic heterodimers.

The SIFT is coupled with a variety of ion-generation techniques. This thesis reports the design and operation of a new electrospray ion source for the SIFT in detail. The electrospray ionization technique allows ions that are pre-formed in the condensed-phase to be transmitted into the gas-phase for studies of their reactivity.

To my friends, family, teachers, and Alex. Thanks for all of your support.

Acknowledgements

The completion of this thesis would not be possible without the assistance of so many people in my life. First and foremost, I'd like to thank my scientific mentor and advisor, Veronica 'Ronnie' Bierbaum. I couldn't have picked a better research advisor for my time at the University of Colorado. Thank you for your support and guidance over the last six years. I wouldn't be the speaker, writer, or scientist that I am today without your help. I feel lucky to have Carl Lineberger as a co-advisor. His comments and insight into public speaking, experimental phenomena, and data analysis have been invaluable. Mathias Weber supported me through three oral examinations, a process that proved to be one of the hardest obstacles in my life. I must also thank William Old for helping me initiate the kinetic method experiments on East campus, and for helping me find the postdoc position at Vanderbilt University. To Barney Ellison, thanks for your patience when the lab sink would overflow or the water line of a diffusion pump would pop off and flood your lab. I owe you a copy of Pedley. To my undergraduate advisor, Bill Taylor, thanks for introducing me to gas-phase ion chemistry, and becoming a friend over the years.

I don't know what I would have done without my coworkers in the Bierbaum lab. To John, Callie, Nick, Ditte, Jennifer, Zhibo, Zhe-Chen, Nadine, and Scott, thanks for making the group office an awesome workplace! I appreciate all of the scientific and instrumental discussions, as well as the snack and coffee breaks. Many thanks to the Lineberger, Ellison, and Weber research labs for being part of the ion chemistry "supergroup." The supergroup has been a great way to practice public speaking, receive feedback on my work, and to keep up with some of the research that is taking place on campus. The work that follows would not have been possible without funding, and therefore I must thank the National Science Foundation and the Air Force Office of Scientific Research (Grants CHE-1012321, CHE-1300886, ACI-1053575, and FA-9550-12-1-0125).

I must thank the support staff for their assistance. In the CIRES shop, Don has always been fun to talk with about instrumentation and electronics in general. The staff in the chemistry department also provided much assistance from purchasing orders to academic advising. Furthermore, I'm lucky to have access to

the JILA staff; the electronics, machine shop, and computer staff have helped me resolve many problems on the fly.

I must give a special thanks to Casey Christopher. Casey helped me with homework in the first three semesters, teaching me linear algebra and other math tricks. Without his generous assistance, I'm not sure that I would be here today. Casey and Jon were my roommates for four unforgettable years; thanks for putting up with me, and reintroducing me to the joy of board-games. The rest of the Boulder crew, Michael, Brett, Joe, Phil, Kristin, Laura, Daniel, Mindy, Jessie, Jessica, Joel, Kelsey, Rajine, Silvio, and everyone else… I had such a good group of friends during my time in Boulder; I'll always remember our snowboarding, hiking, backpacking, and camping adventures. Alex has been both supporting and loving since we began dating approximately three years ago. I don't know what I would do without you. I can't wait to start a new life down in Nashville together. Finally, I need to thank my family. To my mom and dad, Roy and Melissa, thanks for all of your unconditional support throughout my life. My two sisters, Jessica and Rebekah, and brother-in-laws, thanks for putting up with and supporting me. To my two awesome nephews and my adorable niece, hopefully I'll get to see more of you while living in Nashville. Thanks to all of my cousins, cousin-in-laws, and cousins' babies, I'm lucky to have such a large supportive family. My cousin Jim in particular has joined me on so many adventures that I think of him like a brother. Finally, thanks to my grandma, Tater Bug. You have been one of the biggest supporters in my life. Thanks for everything, including the strong family values you have instilled in me.

Publications

John M. Garver, Zhibo Yang, **Charles M. Nichols**, Benjamin B. Worker, Scott Gronert, Veronica M. Bierbaum; "Resolving the α-Effect in Gas-Phase S_N2 Reactions: A Marcus Theory Approach," Int. J. Mass Spectrom., 2012, **316**, 244

John M. Garver, Zhibo Yang, Nadine Wehres, **Charles M. Nichols**, Benjamin B. Worker, Veronica M. Bierbaum; "The α-Effect in Elimination Reactions and Competing Mechanisms in the Gas-Phase," Int. J. Mass Spectrom., 2012, **330**, 182

Charles M. Nichols, Zhibo Yang, Benjamin B. Worker, Denver R. Hager, Nico M. M. Nibbering, Veronica M. Bierbaum; "Gas-Phase Reactions of the Atomic Oxygen Radical Cation with Halogenated Compounds," Phys. Chem. Chem. Phys., 2013, **15**, 561

Charles M. Nichols, Zhibo Yang, Veronica M. Bierbaum; "Gas-phase Organic Reactions of the Atomic Oxygen Radical Cation," Int. J. Mass Spectrom., 2013, **353**, 1

Ditte L. Thomsen, Jennifer N. Reece, **Charles M. Nichols**, Steen Hammerum, Veronica M. Bierbaum; "Investigating the α-Effect in Gas-Phase S_N2 Reactions of Microsolvated Anions," J. Am. Chem. Soc., 2013, **135**, 15508

Ditte L. Thomsen, **Charles M. Nichols**, Jennifer N. Reece, Steen Hammerum, Veronica M. Bierbaum. "The α-Effect and Competing Mechanisms: The Gas-Phase Reactions of Microsolvated Anions with Methyl Formate," J. Am. Soc. Mass Spectrom., 2014, **25**, 159.

Ditte L. Thomsen, Jennifer N. Reece, **Charles M. Nichols**, Steen Hammerum, Veronica M. Bierbaum; "The α-Effect in Gas-Phase S_N2 Reactions of Microsolvated Anions: Methanol as a Solvent," J. Phys. Chem. A, 2014, **118**, 8060.

Scott Gronert, John M. Garver, **Charles M. Nichols**, Benjamin B. Worker, Veronica M. Bierbaum; "Dehalogenation of Arenes via S_N2 Reactions at Bromine: Competition with Nucleophilic Aromatic Substitution," J. Org. Chem., 2014, **79**, 11020

Charles M. Nichols, William M. Old, W. Carl Lineberger, Veronica M. Bierbaum, "Gas-Phase Acidities of Nitrated Azoles as Determined by the Extended Kinetic Method and Computations," J. Phys. Chem. A, 2015, **119**, 395

Daniel J. Nelson, Wilson K. Gichuhi, **Charles M. Nichols**, Veronica M. Bierbaum, and W. Carl Lineberger; "Structure and Thermochemistry of o-, m-, and p-Dehydromethylphenol" – In preparation.

Charles M. Nichols, Zhe-Chen Wang, Zhibo Yang, W. Carl Lineberger, Veronica M. Bierbaum, "Experimental and theoretical studies of the reactivity and thermochemistry of dicyanamide: $N(CN)_2^-$" – In preparation.

Charles M. Nichols, Zhe-Chen Wang, W. Carl Lineberger, Veronica M. Bierbaum, "Gas-Phase Reactions of the deprotonated nucleobases with H, N, and O atom" – In preparation.

Table of Contents

List of Figures

List of Tables

1 Introduction: Gas-Phase Ion Chemistry

1.1 Overview

Gas-phase ion chemistry is the study of the interactions of ions with molecules or atoms in the gas-phase, including kinetics, mechanisms, and thermochemistry. Gas-phase ion chemistry is naturally occurring throughout the universe in diverse regions such as the atmospheres of planets and moons, and in the interstellar medium. In addition, gas-phase ion chemistry can be employed to study the intrinsic properties of molecules and reactions commonly found in the condensed-phase. Therefore, gas-phase ion chemistry can directly or indirectly tell us about the behavior of chemical species in virtually all aspects of the physical world!

Ions exist in abundance along the edge of planetary atmospheres where the flux of high-energy photons is large. In Earth's atmosphere, cations reach concentrations of 10^5 cm^{-3} at altitudes of ~100 km.[1] Anions are also found in the Earth's atmosphere, and they reach their peak concentration at lower elevations due in part to the pressure-dependent three body stabilization process that forms the primary[2] anion O_2^-, equation 1.1.

$$e^- + O_2 + M \rightarrow O_2^- + M \qquad \textbf{1.1}$$

The [O] increases at higher altitudes, therefore reducing the concentration of all anions by removing O_2^- through an associative detachment reaction, equation 1.2.

$$O_2^- + O \rightarrow O_3 + e^- \qquad \textbf{1.2}$$

Equations 1.1 and 1.2 provide examples of reactions that are of interest to gas-phase ion chemists. In particular, our laboratory measures rate constants for these types of chemical reactions.

Moving across the solar system, Saturn's moon, Titan, is rich in gas-phase ion chemistry. Thanks to the success of the Cassini spacecraft, the atmosphere of Titan has been directly sampled and analyzed,

Figure 1.1. Many believe that Titan's atmosphere resembles that of early Earth. Both atmospheres currently have large amounts of molecular nitrogen, but unlike modern Earth, Titan's atmosphere is also rich in methane (CH_4), shrouding the moon in an organic haze. Because of its unique chemical makeup, the ion-chemistry in Titan's atmosphere differs from that on Earth. Ion laboratories around the world are studying properties and reactions of ions found in Titan's atmosphere in an attempt to better understand its composition and chemistry.[3]

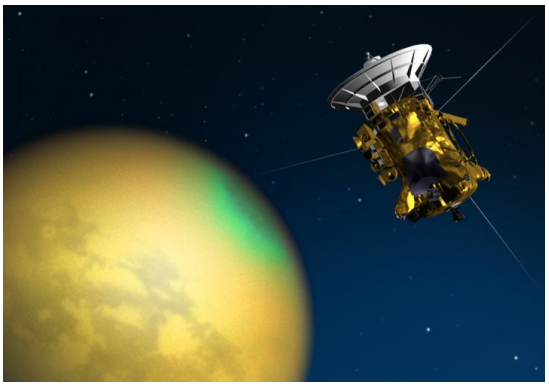

Figure 1.1 Artist rendition of the Cassini spacecraft's flyby of Titan
(Image credit: NASA/JPL)

The 'space between the stars,' or interstellar medium, was originally thought to be empty and devoid of any particles. However, researchers now know that this is not the case. Currently, over 200 chemical species have been detected in space, and this list continues to grow each year.[4] More than 30 of these observed species are ions! Gas-phase ion chemistry is very important within these regions as gas-phase ion neutral reactions will often proceed without a barrier. As the temperature in interstellar dense-molecular clouds, Figure 1.2, can be quite low—on the order of ~10 K—the barrier-less reactions between ions and molecules or atoms become very important because endothermic reactions and exothermic reactions with high activation barriers cannot proceed. Similar to the chemistry of the atmosphere, experimentally determined reaction rate constants are important for understanding the interplay within the complex chemical environments of the interstellar medium. Experimentally

determined ion-neutral rate constants are invaluable to astrochemical modelers, who attempt to understand the intrinsic origins and relative abundances of the molecular species observed in space.

Figure 1.2 The pillars of creation
Image captured by the Hubble telescope in 2014. Ion-chemistry is rich in interstellar clouds, or nebulae. (Image credit: NASA, ESA, and the Hubble Heritage Team (STScI/AURA))

Gas-phase ion chemistry can also provide information about the fundamental, intrinsic properties of molecules and reactions that occur in solvents because condensed-phase environments are difficult to understand on a fundamental level. In the condensed-phase, solvent molecules interact with the chemical species under study. These solvent interactions can vastly complicate quantitative physical descriptions of the chemistry taking place. For these reasons, molecular properties such as acidity, electron-affinity, and bond dissociation energy, are commonly determined in the gas-phase to ensure that the values obtained are intrinsic in origin. One example of how condensed-phase interactions can mask intrinsic thermodynamic properties involves the acidity ranking of simple organic alcohols. In the condensed-phase, the acidity of the alcohol decreases as the size of the alcohol increases, i.e., H_2O > CH_3OH > C_2H_5OH > i-C_3H_7OH > t-C_4H_9OH; the anionic conjugate bases are stabilized by solvation, and the

smaller species are more effectively solvated. However, the gas-phase acidity order is reversed: t-C_4H_9OH > i-C_3H_7OH > C_2H_5OH > CH_3OH > H_2O.[5] In the gas phase in the absence of solvent, the larger conjugate bases can more effectively stabilize/delocalize the negative charge.

Similar to molecular properties, reaction kinetics and mechanisms may be investigated in the gas-phase in efforts to understand the intrinsic nature of the processes observed. In addition, solvent molecules can be added incrementally to gas-phase reactions in a process known as micro-solvation, therefore linking observations in the gas-phase to those occurring in solution. One of the first micro-solvation studies investigated the reaction of hydroxide and methyl bromide.[6] The rate constant for the hydroxide-methyl bromide reaction decreases by a factor of ten upon the addition of a single water molecule to hydroxide, and the addition of three water molecules reduces the measured rate constant by over three orders of magnitude!

While the studies in this thesis may seem disparate, they are all united under the theme of gas-phase ion chemistry. I have studied highly reactive cations, such as the atomic oxygen radical cation, which reacts rapidly with every molecule that has been investigated. I have characterized anions, such as dicyanamide, that are so stable that they do not even react with atoms and electronically excited molecules. I have investigated fundamental physical properties of ions, such as the proton affinities of the nitrated azolates, and I have studied phenomena pertaining to prototypical organic chemical reactions, such as the intrinsic origin of the α-effect. Furthermore, the ion chemistry reported in this thesis is relevant to Earth's atmosphere; Saturn's moon, Titan; the interstellar medium; comets; ionic liquids; and physical-organic chemistry. This thesis, therefore, will offer a flavor of many of the aspects of research that are typical of gas-phase ion chemistry.

1.2 Potential Energy Surfaces

The changes in potential energy occurring during a chemical reaction are often summarized in a potential energy surface. For the generic S_N2 reaction portrayed in equation 1.3, Figure 1.3 illustrates the potential energy as a function of reaction coordinate.

$$X^- + CH_3Y \rightarrow CH_3X + Y^- \qquad \textbf{1.3}$$

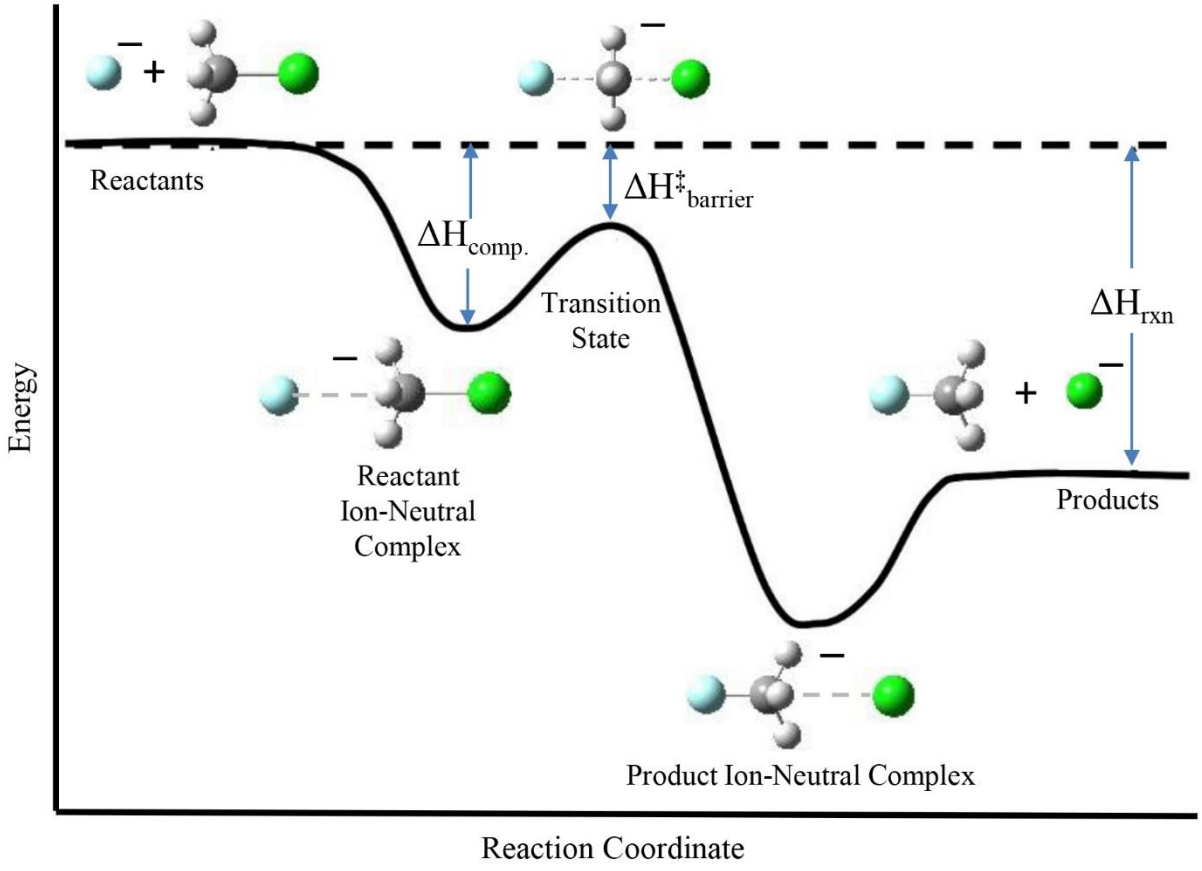

Figure 1.3 Potential energy surface for an S_N2 reaction
The double well potential for the S_N2 reaction of $X^- + CH_3Y$. The transition state barrier-height is indicated as well as the overall exothermicity of the reaction.

The energy of the reactants at infinite separation is usually assigned a value of zero. As the reactants approach, the attractive interaction causes a decrease in potential energy until the reactant ion-neutral

complex is formed with a binding energy of ΔH_{comp}. The reaction then proceeds through a transition state in which there is partial bond formation between the nucleophile and the substrate and partial bond cleavage of the leaving group. In the S_N2 process, the transition state is characterized by a Walden inversion. The reaction then proceeds to form the product ion-neutral complex, which separates into the ionic and neutral product. Since the products lie at lower energy than the reactants, the process is exothermic and the overall enthalpy change, ΔH_{rxn}, is negative in value.

$\Delta H^{\ddagger}_{barrier}$ represents the overall barrier height of the transition state. For this example, the transition state barrier falls below the energy of the reactants, and the reaction can proceed without an external source of energy. However, if $\Delta H^{\ddagger}_{barrier}$ is positive in value, the reaction will not occur; this situation explains the lack of reactivity of methyl bromide with hydroxide that is hydrated by three water molecules. Solvation lowers the energy of the reactants (with localized charge) more dramatically than solvation lowers the energy of the transition state (with diffuse charge); therefore, the transition state lies above the energy of the reactants.

As $\Delta H^{\ddagger}_{barrier}$ becomes smaller (or more negative), the rate of the chemical reaction usually increases. For example, catalysts increase the rate of a chemical reaction by providing an alternate pathway and lowering $\Delta H^{\ddagger}_{barrier}$.

Throughout this thesis, calculations are carried out to characterize the structures and energies of the reactants, ion-neutral complexes, transition states, and products. These results are presented in the form of potential energy surfaces that provide insight into the experimental results.

1.3 Thermochemistry

1.3.1 Gas-Phase Acidity

A thermodynamic value that can be experimentally determined with the selected-ion flow tube (SIFT; to be described in Chapter 2) is the gas-phase acidity of a molecule. The gas-phase acidity, $\Delta_{acid}G(AH)$, is defined as the change in free energy associated with equation 1.4.

$$AH \rightarrow A^- + H^+ \qquad \textbf{1.4}$$

Alternatively, the proton affinity of the anion, $PA(A^-)$ or $\Delta_aH_{298}(AH)$, is defined as the enthalpy change for equation 1.4.[7] Historically, the SIFT has been used to determine both $\Delta_aG_{298}(AH)$ and $\Delta_aH_{298}(AH)$.[8, 9] These quantities are directly related by the equation:

$$\Delta_aH_{298}(AH) = \Delta_aG_{298}(AH) + T\Delta_aS_{298}(AH) \qquad \textbf{1.5}$$

In general, $\Delta_aG_{298}(AH)$ is lower than $\Delta_aH_{298}(AH)$ by ~7 kcal/mol, which is the typical value of $T\Delta_aS_{298}(AH)$.

In favorable cases, we can experimentally determine $\Delta_aG_{298}(AH)$ by measuring the forward and reverse rate constants for proton transfer between an ion and a neutral acidic molecule. That is to say, we would measure the two rate constants of proton transfer, k_1 and k_2, for the following reactions:

$$A^- + HB \rightarrow AH + B^- \qquad \textbf{1.6}$$

$$B^- + HA \rightarrow BH + A^- \qquad \textbf{1.7}$$

This allows us to determine the equilibrium constant, $K_{eq} = k_1/k_2$, for reaction 1.8.

$$A^- + HB \rightleftarrows AH + B^- \qquad \textbf{1.8}$$

Subsequently, we can determine the free energy change using equation 1.9.

$$\Delta(\Delta_a G_{298}) = -RT\ln K_{eq} = \Delta_a G_{298}(AH) - \Delta_a G_{298}(BH) \quad \textbf{1.9}$$

In this example, $\Delta_a G_{298}(BH)$ is the known acidity of the 'reference acid,' and the previously unknown value, $\Delta_a G_{298}(AH)$, can be reported. However, this approach requires that the two molecules are close in intrinsic gas-phase acidity, within approximately 4 kcal/mol.[9] The experimentally determined $\Delta_a G_{298}(AH)$ can be converted to $\Delta_a H_{298}(AH)$ by using $T\Delta_a S_{298}(AH)$ values that are determined by electronic structure calculations.

The SIFT is also used for directly determining $\Delta_a H_{298}(AH)$ values, which are often referred to as the proton affinity of the conjugate base, $PA(A^-)$. For these studies, the 'bracketing' technique is often applied.[8] In this method, a series of reference acids with known $\Delta_a H_{298}$ are used, and their reactivity with an anion of unknown PA is monitored. If proton transfer from the reference acid to the anion is observed, the proton transfer process is assumed to be exothermic. Experimentally, this corresponds to a decrease in the parent anion signal and a proportional increase in the anion signal of the deprotonated reference acid. By reporting the PA at which the proton transfer switches from exothermic to endothermic, a 'bracket' is placed on the unknown PA.

Table 1.1 shows the results of a bracketing experiment used to determine the acidities of didehydro–1–, 2–, and 3–cresol. These studies were carried out in collaboration with Dan Nelson, and will be the subject of a forthcoming publication.

Table 1.1 Bracketing results for didehydro–1–, 2–, and 3–cresol

Reference Acid	Experimental	Proton Transfer Observed?		
	$\Delta_a H_{298}$ (kcal/mol)	1-cresol	2-cresol	3-cresol
3-trifluoromethylphenol	337.0±2.2	Yes	Yes	Yes
3-mercaptopropionic acid	339.4±2.2	Yes	Yes	Yes
1-chlorophenol	343.4±2.4	No	Yes	No
3-fluorophenol	346.8±2.2	No	Yes	No
propionic acid	347.4±2.2	No	Yes	No
acetic acid	348.1±2.2	No	Yes	No
phenol	350.0±2.0	No	No	No
pentafluoro-1-propanol	355.4±6.1	No	No	No

To determine the 'bracketed' PA of the didehydro–cresols, the average acidity of the two 'bracketing' acids is reported. For didehydro–1– and didehydro–3–cresol the two bracketing acids are 3–mercaptopropionic acid and 1–chlorophenol, and the experimentally determined acidity is Δ_aH_{298} = 341.4 ± 4.3 kcal/mol. For didehydro–2–cresol, the bracketing acids are acetic acid and phenol, and Δ_aH_{298} = 349.1 ± 3.1 kcal/mol. Note that the reported error for these experiments is quite large because the uncertainty in the PA from the two reference acids is considered.

Cook's kinetic method can also be used to measure the PA of an anion. In this thesis, Cook's kinetic method was used to determine the PA of six nitrated azolates (Chapter 5), using a commercial triple quadrupole instrument. Experimental and theoretical formulation of the kinetic method will be discussed in Chapter 5.

For all of the methods discussed above, the selection of appropriate reference acids is very important.

1.3.2 Electron Affinity/Electron Binding Energy

Using the negative ion photoelectron spectrometer (NIPES) the electron binding energy of an anion can be measured, i.e., the energy required to remove an electron from the anion. To perform this experiment, anions are generated and subsequently irradiated with photons of well-defined energy. If the energy of the photon is sufficiently large it can detach an electron from the anion. The kinetic energy of the electron can then be measured with a hemispherical analyzer. This process follows equation 1.10.

$$A^- + h\nu \rightarrow A + e^- \qquad \textbf{1.10}$$

The intensities of the photoelectrons are monitored versus their kinetic energies. The resulting photoelectron spectrum provides electron binding energies, the splitting of electronic energy levels, and vibrational frequencies. At the origin of the spectrum, the difference between the photon energy ($E^{h\nu}$) and the kinetic energy of the ejected electron (KE^{e-}) gives the electron affinity of A, equation 1.11.

$$EA(A) = E^{h\nu} - KE^{e-} \qquad \textbf{1.11}$$

1.3.3 Thermochemical Cycles

Hess's law states that, regardless of the multiple stages or steps of a reaction, the total enthalpy change for the reaction is the sum of all changes. When both $\Delta_a H_0(AH)$ and EA(A) are experimentally measured, a third thermochemical value, the bond dissociation energy, $D_0(AH)$, can be inferred. The routine of determining $D_0(AH)$ from $\Delta_a H_0(AH)$ and EA(A) is known as the negative ion cycle; to perform this operation the ionization energy of H, IE(H), must also be considered, equation 1.12.

$$H \rightarrow H^+ + e^- \qquad \textbf{1.12}$$

This value is well known, IE(H)=13.59844 eV. The Hess's law application of the negative ion cycle is provided in Figure 1.4a, and a schematic of the thermochemical cycle is provided in Figure 1.4b.

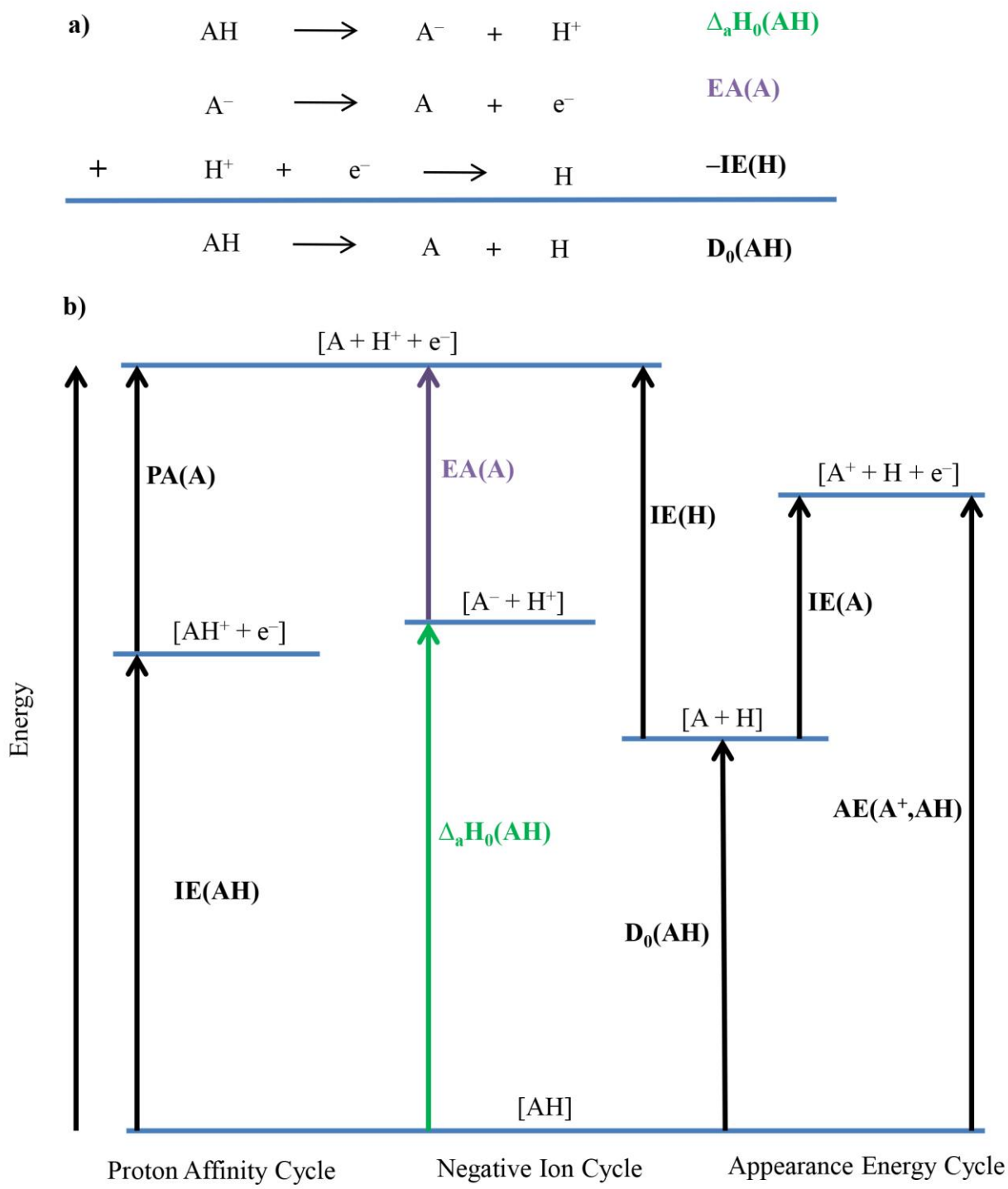

Figure 1.4 Thermochemical Cycles
(a) Using Hess's law to determine $D_0(AH)$ from EA(A) and $\Delta_a H_0(AH)$. (b) A schematic overview of the negative ion cycle as well as the proton affinity and appearance energy cycle.

1.3.4 Temperature Corrections

There is a small discrepancy between the PA values determined from our experiment, $\Delta_a H_{298}(AH)$ and those used to determine $D_0(AH)$ from the negative ion cycle, i.e. $\Delta_a H_0(AH)$. The difference in these values is due to the temperature at which they are measured. The acidity experiments are performed at room temperature when using the SIFT, but the EA(A) values determined using NIPES are intrinsically measured at 0 K. In order to determine the bond dissociation energy, $D_0(AH)$, the thermal contribution for $\Delta_a H_{298}(AH)$ must be corrected to 0 K. To perform this conversion, the heat capacities and their integral from 0–298 K must be considered, equation 1.13.

$$\Delta_a H_0(AH) = \Delta_a H_{298}(AH) - \int_0^{298} [C_p(A^-) + C_p(H^+) - C_p(AH)]dT \qquad \textbf{1.13}$$

When the heat capacities for a specific molecule or ion are unknown these values are theoretically determined with electronic structure calculations.

1.3.5 Thermochemistry and Mass Spectrometry for Ion-Neutral Reactions

This thesis will explore a wide variety of ion-neutral reactions illustrated generically in equation 1.14.

$$A^- + B \rightarrow C^- + D \qquad \textbf{1.14}$$

Equation 1.14 represents a reaction between an anion, A^-, and a neutral molecule, B, which advance to their anion-neutral products, C^- and D. This reaction also applies to cations where the charge is positive instead of negative. In the Bierbaum lab, mass spectrometry is used to monitor the reaction progress; the details of the experiment will be described in the next chapter. Mass spectrometry only provides detection of the ionic reactants and products, which can present some ambiguity for equation 1.14. As a reaction is studied using mass spectrometry, the reactants, A^- and B in equation 1.14, are usually well defined, but the exact structure of C^- and D must be inferred. The reactant ion, A^-, is usually formed under conditions that allow confident assignment of identity using the mass-to-charge ratio, m/z. The neutral reactant B is

generally supplied by commercial vendors. As products are formed, only the ionic product, i.e., C^- can be identified by its m/z. By understanding the nature of the reactants, the m/z of C^- will usually provide enough information to confidently determine its identity, but this task can sometimes be difficult when investigating the reactivity of large anions or molecules, especially when redundant atoms are present. Furthermore, the structure of the neutral product, D, must be inferred; this process can be complex, but thermodynamic arguments are used to suggest a reasonable structure for D.

Thermodynamics and a balanced chemical equation are used to report products for these ion-neutral reactions investigated through mass spectrometry. In the case of common ions and neutrals, the heats of formation of the inferred products will be readily available. When investigating systems where the heats of formation are unknown, theoretical heats of formation can be determined using computational software. In some cases, potential energy surfaces, such as Figure 1.3, are computationally generated to rationalize the structure and formula of the products. The experiments of this thesis explore only room-temperature exothermic reactions; therefore, if the proposed products are higher in energy than the reactants, they can be discarded as physically unreasonable.

1.4 Kinetics

Kinetics is the study of the rates and mechanisms of chemical reactions. For many of the chemical systems studied within this thesis, we report experimental reaction rate constants and compare them to theoretical collision rate constants.

1.4.1 Collision Theory

In order for an ion-neutral reaction to occur in the gas-phase, the ion and neutral must meet, or 'collide.' Therefore, a theoretical collision rate constant is useful to the experimentalist measuring reaction rate constants. Fortunately, theoretical ion-neutral collision rate constants have been studied somewhat comprehensively.

The development of capture collision theory began over a century ago when Langevin discussed the attractive potential between an ion, described as a point charge, and a polarizable neutral molecule.[10] With contributions from Gioumousis and Stevenson,[11] Langevin's theory resulted in equation 1.15 that can be used to predict the collision rate constant, k_L, between an ion and a polarizable neutral atom or molecule.

$$k_L = 2\pi e(\alpha_n/\mu)^{1/2} \qquad \textbf{1.15}$$

In equation 1.15, e, α_n, and μ correspond to the elementary charge, the polarizability of the neutral atom or molecule, and the reduced mass of the ion-neutral pair, respectively. Despite the simplicity of the formula, the Langevin collision rate provides a very good first-order approximation for the reaction rate constant of an efficient reaction.

The Langevin collision rate constant is derived by considering only the polarizability of the neutral, α_n. In the last 40 years, several other ion-neutral capture collision theories have emerged by a more thorough treatment of the ion-neutral potential. Average dipole orientation (ADO) capture collision theory includes the neutral permanent dipole moment, μ_D, in the treatment of the potential.[12] The result is a theoretical collision rate constant that better matches experimentally determined reaction rate constants. ADO theory was eventually simplified to parameterized trajectory theory (PTT) by applying an empirical fit to the ADO model in an attempt to make ADO theory more accessible to experimentalists.[13] Later, in 2003, Eichelberger et al. formulated point-polarizable ion (PPI) collision theory which incorporated the polarizability of the ion, α_i, into the ion-neutral potential.[14] This approach was developed because the experimentally measured rate constants for linear carbon anion chains, C_n^- and C_nH^-, with atomic oxygen were higher than the theoretical collision rate constants. The theory was successful, and PPI provided a better match to the experimental results. However, PPI only predicts substantial deviations from PTT when the polarizability of the ion is very large (anions), and the polarizability of the neutral is very low (atoms.) Recently, Kent Ervin published a paper summarizing the effect of several variables on the theoretical capture collision rate constant.[15] His new treatment uses numerical methods to calculate the

theoretical capture collision rate by considering the polarizability of the neutral, α_n; polarizability of the ion, α_i; dipole moment of the ion, μ_i; and quadrupole moment of the ion, Q_i.

In summary, the treatment of the ion-neutral effective potential affects the resulting theoretical collision rate constant. Theoretical collision rate constants provide, at best, an upper limit to the reaction rate constant for an ion-neutral pair that reacts upon every collision. When selecting a capture collision theory, the experimentalist must determine which variables are necessary to accurately describe the attractive potential between the ion-neutral pair.

1.4.2 Reaction Efficiencies

Throughout the thesis reaction efficiencies will be reported. Reaction efficiencies compare experimentally determined reaction rate constants to theoretical collision rate constants by taking the ratio of the rate constant (k_{exp}) to the collision rate constant (k_{col}). Reaction efficiencies effectively normalize experimentally determined rate constants, allowing for comparison of multiple ion-neutral reactions that have different collision rate constants.

Equation 1.16 shows an example calculation to determine the reaction efficiency of $O^{\bullet+}$ with CF_4. The theoretical collision rate constant for $O^{\bullet+}$ and CF_4 is 1.30×10^{-9} cm^3/s, and the measured reaction rate constant is 1.01×10^{-9} cm^3/s.

$$Reaction\ Efficiency = \frac{k_{exp}}{k_{col}} = \frac{1.01 \times 10^{-9}}{1.30 \times 10^{-9}} = 0.78 \qquad \textbf{1.16}$$

1.5 Electron Spin

The total sum of electron spin is highly relevant to some of the reactions in this thesis, particularly reactions involving the atomic cation $O^{\bullet+}$ (^4S) as well as the atomic neutrals H (^2P), N (^4S), and O (^3P). The ground-states of these atomic species are open-shell, i.e., they have one or more unpaired electrons

resulting in a total electron spin that is non-zero. The ground-state term symbols are presented in the parentheses to the right of the species; the superscripted number located to the left of the upper case letter designates the multiplicity. The multiplicity indicates the total electron spin of the species. If all electrons are paired, the atom or molecule is described as closed-shell with a multiplicity equal to one. If the atom or molecule has a single unpaired electron, such as H atom or hydroxyl radical, the multiplicity equals two. If the atom has two unpaired electron, such as O, the atom can have a multiplicity of 1 or 3 depending on the alignment (spin-up or spin-down) of the two unpaired electrons. Hund's rule indicates that the lowest energy configuration for O atom will have its two unpaired electrons spin-aligned, giving the ground state configuration of O atom a multiplicity of 3. Indeed, Hund's rule holds for O atom, and the electron configuration for O atom with a multiplicity of one is higher in energy than the configuration with a multiplicity of three. Multiplicities of 1, 2, 3, 4, etc. are designated singlets, doublets, triplets, and quartets, respectively. While a multiplicity larger than 4 is possible, it is less common and does not prevail in the studies presented herein.

As a general rule, the total electron-spin is conserved for a reaction, i.e., $\Delta S = 0$. However, small species with high spin-states such as $O^{\bullet+}$ (^4S), N (^4S), and O (^3P) are known to sometimes undergo spin conversion reactions where $\Delta S = -1$ in order to access more exothermic products. Spin-conversion reactions occur on two or more potential energy surfaces. For example, the atomic oxygen radical cation, $O^{\bullet+}$, has five valence electrons, and the ground-state electronic configuration is a quartet. On the contrary, a majority of molecules that contain an odd number of electrons will have a doublet ground state. Therefore, when $O^{\bullet+}$ reacts with a molecule, the reaction will often move from a quartet to a doublet potential energy surface.

An early account of spin-conversion for $O^{\bullet+}$ (^4S) was reported in 1966 by Fehsenfeld, Fergeson, and Schmeltekopf.[16] They observed spin-conversion for the reaction of $O^+(^4S) + CO_2(^1\Sigma) \rightarrow O_2^+(^2\Pi) + CO(^1\Sigma)$. In moving from reactants (S=3/2) to products (S=1/2), the total electron spin of the system has

changed by –1, i.e., $\Delta S = -1$. Therefore, this reaction violates the principle of spin-conservation. More examples of spin-conversion reactions with $O^{\bullet+}$ (^4S) will be discussed in Chapter 3.

1.6 Summary of This Work

A variety of gas-phase ion chemistry experiments relevant to environmental, materials, and physical-organic chemistry are reported within this thesis. Kinetics, mechanisms, and thermodynamics are the major foci of the ion chemistry that follows. This thesis will report a new electrospray ion source for the selected ion flow tube (SIFT), reactions of the atomic oxygen radical cation, the reactivity and thermochemistry of dicyanamide, the gas-phase acidities of the nitrated azoles, and experimental investigations into the intrinsic origin of the α-effect.

Kinetic data for ion-neutral reactions are obtained using the SIFT apparatus, which will be described in detail in the following chapter. In the SIFT, the rate constants are measured in the field-free reaction flow tube. Therefore, the SIFT provides a benchmark for studying the kinetics of ion-neutral reactions. Furthermore, a variety of ion generation techniques may be coupled to the SIFT, permitting the study of a wide variety of ions in the gas phase. For the experiments in this thesis, the ions are generated with electron ionization and electrospray ionization. Development of the electrospray ion source is a major component of this thesis, and its implementation will be discussed in detail in the next chapter.

The reactions of the atomic radical cation $O^{\bullet+}$ (^4S) will be discussed in Chapter 3. $O^{\bullet+}$ is an important ion in the atmosphere and the interstellar medium. With a recombination energy of 13.62 eV, $O^{\bullet+}$ is highly reactive. Furthermore, $O^{\bullet+}$ is characterized by a large multiplicity, and it will often undergo interesting spin-conversion reactions as outlined in section 1.5.

Chapter 4 will discuss the reactivity, or lack thereof, of the dicyanamide anion, $N(CN)_2^-$. This ion is a common anionic component of ionic liquids. Ionic liquids containing $N(CN)_2^-$ have been of great interest to the Air Force Office of Scientific Research due to their hypergolic behavior when mixed with nitric acid. Despite the hypergolic behavior, $N(CN)_2^-$ is an intrinsically stable anion in the gas phase. The study of dicyanamide contrasts that of $O^{\bullet+}$ in many ways because dicyanamide is extremely unreactive. In

addition to experimental studies of this anion, the hypergolic ignition mechanism of dicyanamide and nitric acid has been explored through electronic-structure calculations.

In Chapter 5, a study of the gas-phase acidities of the nitrated azoles will be reported. The acidities of the nitrated azoles were determined using Cook's kinetic method and a commercial triple quadrupole CID experiment. The details of the triple quadrupole instrument and of Cook's kinetic method will be discussed in Chapters 2 and 5, respectively. The gas-phase acidities of six nitrated azoles (2- and 3-nitropyrrole, 3- and 4-nitropyrazole, and 2- and 4-nitroimidazole) were experimentally measured with high precision. Because of agreement between the experimental and computational gas-phase acidities, the gas phase acidities and electron affinities of 24 nitrated azole compounds were investigated computationally. From these investigations, trends in the nitro-group placement and aza substitution's effect on the gas-phase acidity of the aromatic heterocycles are reported.

The final chapter of this thesis will summarize several gas-phase investigations of the α-effect. The α-effect describes an increased reactivity of α-nucleophiles, or nucleophiles in which the atom adjacent to the attacking center contains a lone pair of electrons. A multifaceted phenomenon, the origin of the α-effect has been the topic of many discussions over the last 50 years. The effect was first observed in solution, and this has prompted researchers to examine whether the α-effect is intrinsic in origin, or if it is a result of solvation effects. In Chapter 6, the reactivity of both un-solvated and micro-solvated α-nucleophiles will be investigated through gas-phase S_N2, E2, $B_{AC}2$, and PT organic reaction mechanisms. The results suggest that the α-effect does have a small intrinsic contribution, but the micro-solvation studies confirm that solvation plays an additional role in the α-effect.

1.7 References

[1] M.R. Torr, D.G. Torr, *The role of metastable species in the thermosphere*, Rev. Geophys., 20 (1982) 91-144.

[2] R.P. Wayne, *Chemistry of Atmospheres*, 2, Oxford University Press, New York, 1991.

[3] A. Somogyi, M.A. Smith, V. Vuitton, R. Thissen, I. Komaromi, *Chemical ionization in the atmosphere? A model study on negatively charged "exotic" ions generated from Titan's tholins by ultrahigh resolution MS and MS/MS*, Int. J. Mass Spectrom., 316 (2012) 157-163.

[4] D.E. Woon, *Interstellar and circumstellar molecules*, http://www.astrochymist.org, 2015.

[5] J.I. Brauman, L.K. Blair, *Gas-phase acidities of alcohols*, J. Am. Chem. Soc., 92 (1970) 5986-5992.

[6] D.K. Bohme, G.I. Mackay, *Bridging the gap between the gas-phase and solution - transition in the kinetics of nucleophilic displacement reactions*, J. Am. Chem. Soc., 103 (1981) 978-979.

[7] S.G. Lias, J.E. Bartmess, *Gas-phase ion thermochemistry*, http://webbook.nist.gov/chemistry/ion/, 2015.

[8] N. Eyet, V.M. Bierbaum, *Gas-phase acidities of thiocarboxylic acids*, Int. J. Mass Spectrom., 265 (2007) 267-270.

[9] A.J. Gianola, T. Ichino, R.L. Hoenigman, S. Kato, V.M. Bierbaum, W.C. Lineberger, *Thermochemistry and electronic structure of the pyrrolyl radical*, Journal of Physical Chemistry A, 108 (2004) 10326-10335.

[10] P. Langevin, *A fundamental formula of kinetic theory*, Ann. Chim. Phys., 5 (1905) 245-288.

[11] G. Gioumousis, D.P. Stevenson, *Reactions of gaseous molecule ions with gaseous molecules. V. Theory*, Journal of Chemical Physics, 29 (1957) 294-299.

[12] T. Su, M.T. Bowers, *Ion-polar molecular collisions. Effect of ion size on ion-polar molecular rate constants. Parameterization of the Average-Dipole-Orientation Theory*, Int. J. Mass Spectrom. Ion Process., 12 (1973) 347-356.

[13] T. Su, A.A. Viggiano, J.F. Paulson, *The effect of the dipole-induced dipole potential on ion polar molecule collision rate constants*, Journal of Chemical Physics, 96 (1992) 5550-5551.

[14] B.R. Eichelberger, T.P. Snow, V.M. Bierbaum, *Collision rate constants for polarizable ions*, J. Am. Soc. Mass Spectrom., 14 (2003) 501-505.

[15] K.M. Ervin, *Capture Collisions of Polyynide Anions with Hydrogen Atoms: Effect of the Ion Dipole, Quadrupole, and Anisotropic Polarizability*, Int. J. Mass Spectrom., 378 (2014) 48-53.

[16] F.C. Fehsenfeld, E.E. Ferguson, A.L. Schmeltekopf, *Thermal-Energy Ion-Neutral Reaction Rates. III. The Measured Rate Constant for the Reaction* $O^+(^4S)+CO_2(^1\Sigma)\rightarrow O_2^+(^2\Pi)+CO(^1\Sigma)$, Journal of Chemical Physics, 44 (1966) 3022-3024.

2 Experimental and Computational Methods

2.1 Selected Ion Flow Tube

The flowing-afterglow (FA) technique was developed in Boulder in the 1960s.[1] This technique revolutionized the field of gas-phase ion chemistry by providing a means to measure gas-phase rate constants of ion-neutral reactions. Versatility of the FA technique was limited by the co-existence of many ions and precursor gases in the reaction region.[2] This situation was remedied by the advent of the selected ion flow tube (SIFT) technique.[3] The SIFT technique allowed chemists to study the reactivity of ions of a single mass-to-charge ratio with a neutral species in the absence of precursor gases.

The selected ion flow tube (SIFT) instrument was used for most of the studies described in this thesis.[4] A schematic of the instrument is shown in Figure 2.1.

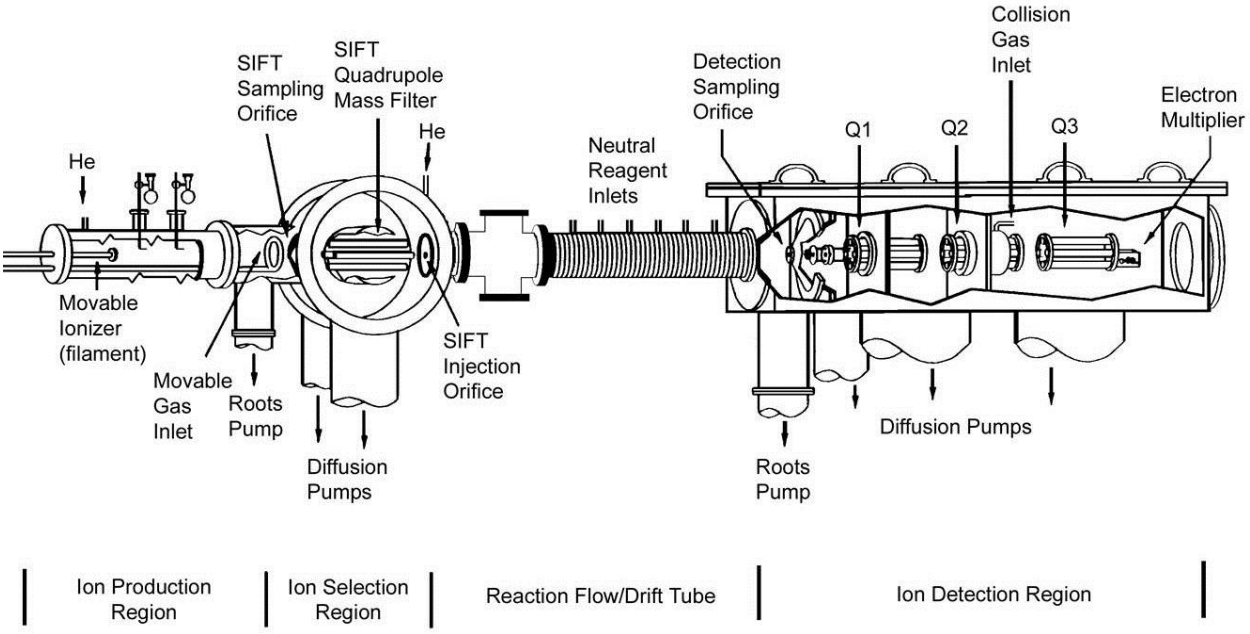

Figure 2.1 Schematic of Selected Ion Flow Tube (SIFT)

The instrument consists of four regions; ion-production, ion-selection, reaction flow tube, and ion-detection.

2.1.1 Ion Production Region

The SIFT technique employs a variety of ion sources. The Bierbaum lab has implemented electron ionization, electrospray ionization, dc glow discharge, Penning ionization, and laser induced acoustic desorption techniques to produce ions for the SIFT. Ions pertaining to the studies herein were generated using electron ionization and electrospray ionization. This thesis reports the design and implementation of a new electrospray ion source; this source will be discussed in detail.

2.1.1.1 Electron Ionization

The housing for the electron ionization (EI) source (Figure 2.2) consists of a stainless steel flow tube with an inner diameter of 4.75 cm. The EI source is mounted on a hollow stainless steel rod that can be axially moved within the flow tube. Helium is introduced upstream of the EI filament through a metering valve. The helium gas serves as both a discharge medium and a carrier gas. Precursor gases are introduced through either stationary inlets located axially along the flow tube or one of two axially adjustable ring inlets. The ring inlets contain 24 equally spaced holes that promote even mixing of the precursor gas. The absolute pressure of the helium and precursor gases is maintained at ~0.3 Torr by a Stokes roots pump (190 L s^{-1}). The gases are continuously pumped away generating a flow of helium over the EI filament. About ~2-5V with 2.5A of current is applied across the yttrium oxide coated iridium filament. The electrons are extracted from the filament using a repeller plate and an extraction grid. The grid is biased with an attractive potential ~70V more positive than the filament voltage. The current on the extraction grid is maintained at ~25 μA by a feedback loop. The EI source is floated at the potential applied to the stainless steel flow tube.

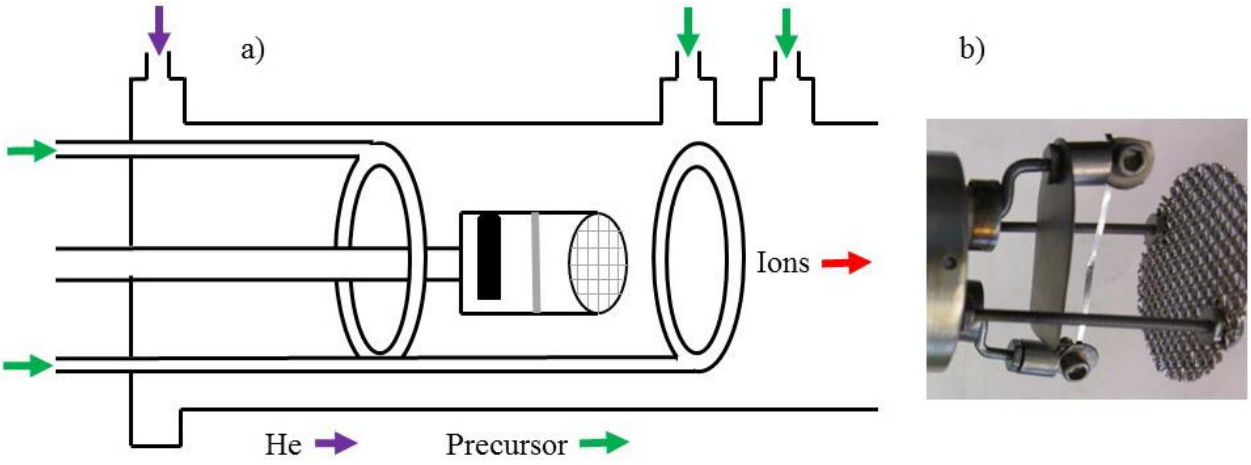

Figure 2.2 Electron Ionization (EI) source diagram (a) and photograph (b).

The EI source may be used to generate a wide variety of ions; it contains several precursor inlets permitting ion synthesis. One example is the production of hydrated methoxide, $CH_3O^-[H_2O]_n$. This is achieved through a multistep ion synthesis. First, O^- is generated from electron ionization of N_2O, equation 2.1.

$$N_2O + e^- \rightarrow O^- + N_2 \qquad \textbf{2.1}$$

Next, O^- extracts a hydrogen from methane to make hydroxide, equation 2.2.

$$O^- + CH_4 \rightarrow OH^- + CH_3 \qquad \textbf{2.2}$$

OH^- subsequently abstracts a proton from methanol to generate methoxide, equation 2.3.

$$OH^- + CH_3OH \rightarrow H_2O + CH_3O^- \qquad \textbf{2.3}$$

Further downstream, water may be introduced to hydrate methoxide, equation 2.4. The methoxide-water cluster is stabilized by collisions with He.

$$CH_3O^- + H_2O + He \rightarrow CH_3O^-[H_2O] + He \qquad \textbf{2.4}$$

Hydroxide, OH^-, is used to make a wide variety of deprotonated species. Amide, NH_2^-, may also be used for deprotonation synthesis; it is formed directly through electron ionization of ammonia, NH_3. However, the EI source is not limited to anions; it can generate a rich variety of cations as well. In particular, the EI source was used to generate the oxygen radical cation, $O^{\bullet+}$, which will be discussed later in this thesis.

2.1.1.2 Electrospray Ionization

The electrospray ionization (ESI) source for the SIFT apparatus (Figure 2.3) is based on Moision and Armentrout's design for their guided ion beam apparatus.[5] Ions are generated at ambient pressure by pushing a solution through a conductive union biased at 2-3 kV. The flow rate of the solution is maintained by a syringe pump; typical flow rates are 0.2-50 μL min^{-1}. The charged solution exits through a silica carbide capillary, which has an inner diameter of ≤ 50 μm. This 'emitter' is mounted to an X-Y-Z stage (not shown in Figure 2.3) and positioned in front of a stainless-steel capillary inlet that leads into the vacuum chamber. The capillary inlet is interchangeable, but for the experiments reported in this thesis, a capillary with an inner diameter of 0.76 mm and a length of 98 mm was used. While these exact dimensions are somewhat arbitrary, using a shorter capillary increased the ion signal intensity. The capillary inlet is seated in an aluminum block that can be heated from 50 °C to 200 °C using heater cartridges and a temperature controller. The entrance capillary is typically biased at 100–300 V.

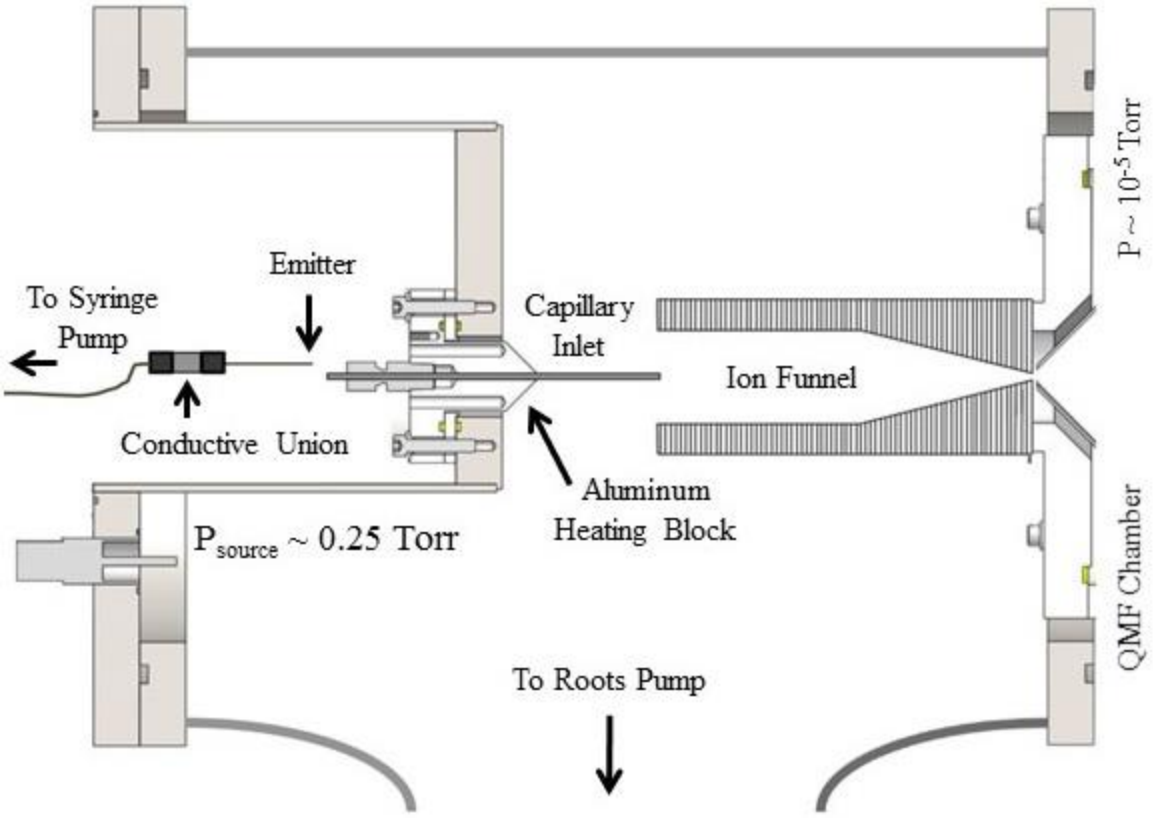

Figure 2.3 Electrospray ionization (ESI) source diagram.

The ions enter the vacuum chamber maintained at ~0.25 Torr by a high-capacity roots-blower pump where they are then concentrated by an ion funnel. The ion funnel is based on the design of Smith and coworkers.[6] The ion funnel consists of 101 electrodes, but does not contain a 'jet disruptor.' The first 100 lenses have both RF and DC potentials applied to them. The RF amplitude is approximately 25 V peak-to-peak and oscillates at a frequency that can be adjusted; for these experiments, a frequency of 1.5–2.8 MHz was used. The RF potential applied to each adjacent electrode is 180 degrees out-of-phase. The RF potentials focus the ions near the center axis of the funnel. The applied DC voltages create a potential gradient along the ion funnel. Both the entrance and exit DC potentials are adjustable, and the DC potential applied across the ion funnel is typically 10–150 V. The potential gradient transmits the ions towards the differentially pumped mass-selection region. The 101st electrostatic lens of the funnel is

supplied with an independently adjustable DC potential. A photograph of the ion funnel is provided in Figure 2.4. Note that each of the potentials listed are referenced to a common ground (Figure 2.5).

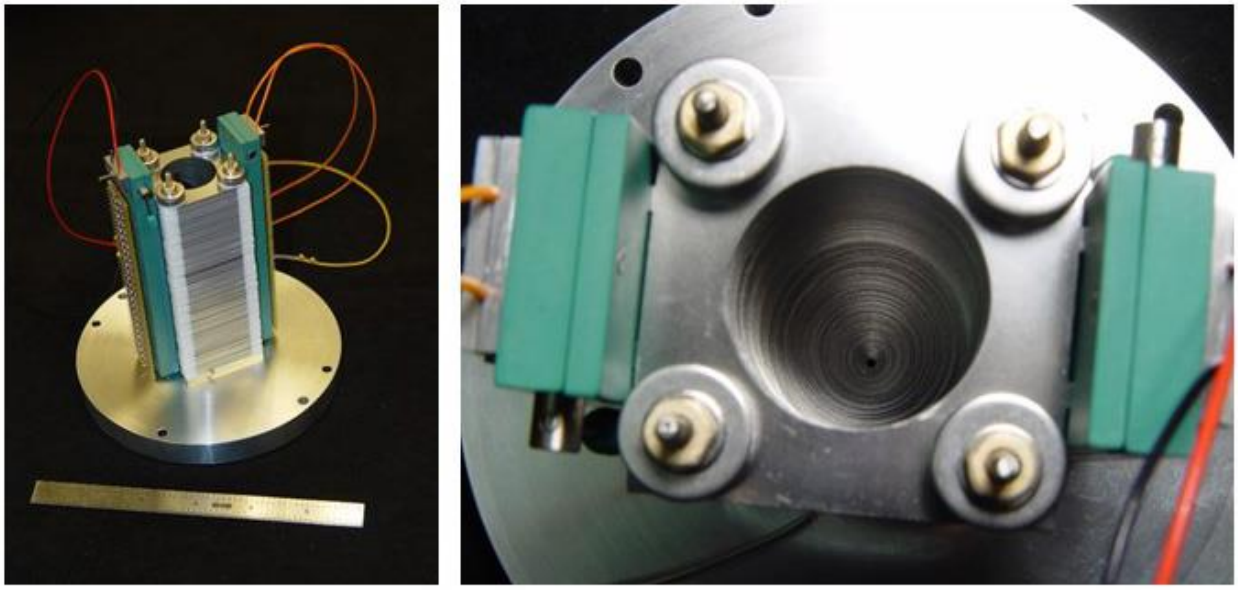

Figure 2.4 Ion funnel photograph

Figure 2.5 shows the wiring layout for the ESI source; the common ground is the source housing. The ion funnel requires five electrical inputs. Two of the inputs provide RF potentials to the lenses of the ion funnel; the remaining electrical inputs provide DC potentials to the entrance, exit, and final lens of the ion funnel. The final, or 101st, lens of the ion funnel is capacitively coupled to ground to remove RF noise. A 100 nF capacitor is used for this purpose.

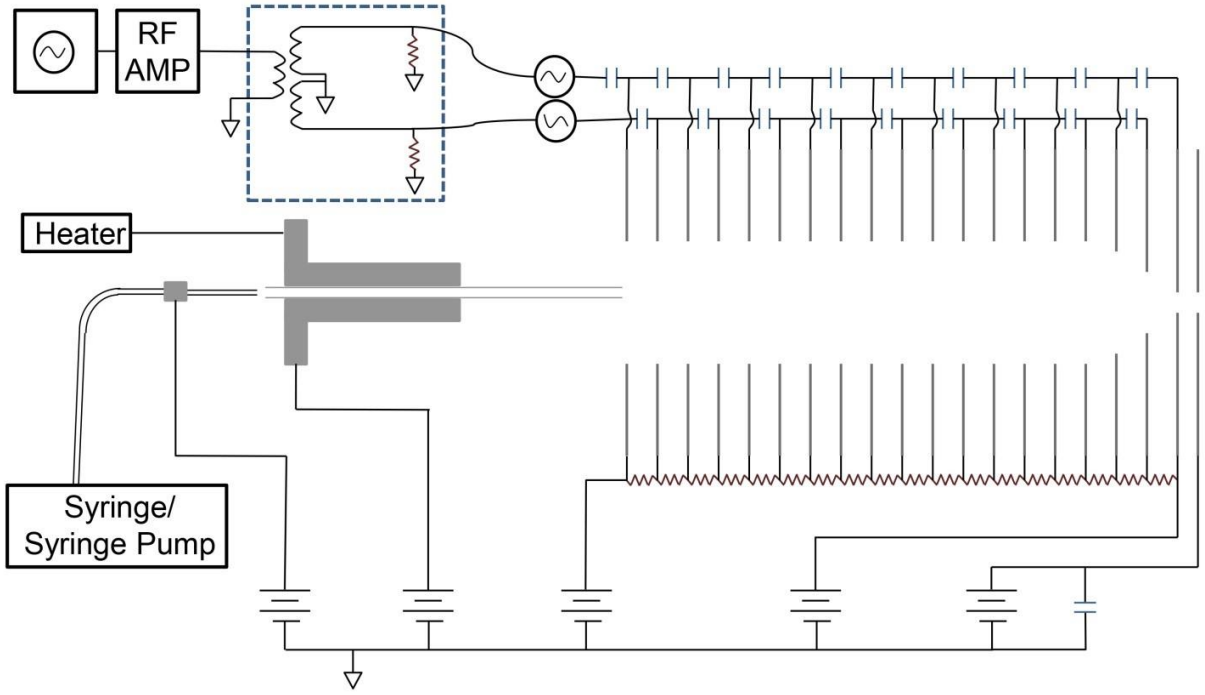

Figure 2.5 Electrospray ionization source wiring schematic

A signal generator (BK Precision, model 4040A) is used to provide a sine wave of tunable frequency. The sine wave is then sent through an RF amplifier (Electronics & Innovation, model 240L), which increases the amplitude from ~1 to ~25 V_{p2p}. The amplified wave then enters an RF balun (indicated by a square of dashed lines in Figure 2.5) that sends out two RF signals, which are 180° out of phase. For instructions on building the RF balun, as well as dimensions on the ion funnel electrodes and spacers, please see Appendix A.

The aluminum heating block is electrically isolated from the chamber housing. The heating block is biased at the same potential as the 'entrance capillary' that sits within it. It uses three heater cartridges (Omega, model CCS-01115/120) that are connected externally, and the temperature is regulated by a thermal controller (Love Controls, series 16A). The temperature heating range is 30-175 °C. The entrance capillary (1.6 mm O.D.) is seated within the heating block using an NPT to Swagelok union. The entrance capillary is removable, which facilitates cleaning and replacement.

The emitter assembly includes a syringe pump (Harvard Apparatus, model Pump11Elite), which depresses a syringe (Hamilton, Model 1750 RN SYR) connected to fused silica capillary tubing (Polymicro technologies; 75 μm I.D., 360 μm O.D.) using a microunion assay (Idex, model P-720) and a tubing sleeve (Idex, model F-185X). Downstream, the fused silica carbide tubing is connected to a conductive union (Idex, model M-572) that is connected to a thinner silica carbide tube (Polymicro technologies; 50 μm I.D., 180 μm O.D.). The emitter tip I.D. is drawn thinner by heating and stretching. The emitter tips are cut with a fused silica carbide tubing cutter (Idex, model FS-311). The newly formed tips are inspected with a microscope to ensure that they are not malformed. Using pre-manufactured emitter tips is also an excellent option.

The ESI source can transmit ions from *solution* into the gas-phase. Therefore any ion that can be generated in solution can, in principle, be transferred into the gas-phase. Typical solution concentrations range from 1×10^{-5} to 4×10^{-4} M. Several solvents, i.e., water, methanol, acetonitrile, etc., can be used with the electrospray. Most ESI experiments performed with the SIFT employ acetonitrile as the solvent. Furthermore, the pH of the solution can be adjusted to form protonated or deprotonated species.

The ESI source performs extremely well. Stable ions can be generated with high intensities comparable to the EI source. Figure 2.6a shows a spectrum of 1-butyl-2,3-dimethylimidazolium cation that was generated from a 2.4×10^{-4} M solution of 1-butyl-2,3-dimethylimidazolium tetrafluoroborate in methanol (99.8%, EMD Millipore). This ion was mass-selected, injected into the flow tube, and detected. Figure 2.6b shows a spectrum of dicyanamide anion that was generated from a 6×10^{-5} M solution of sodium dicyanamide in acetonitrile (99.8%, Sigma-Aldrich). In this case, all negative ions were injected and detected, but the desired dicyanamide anion dominates the mass spectrum.

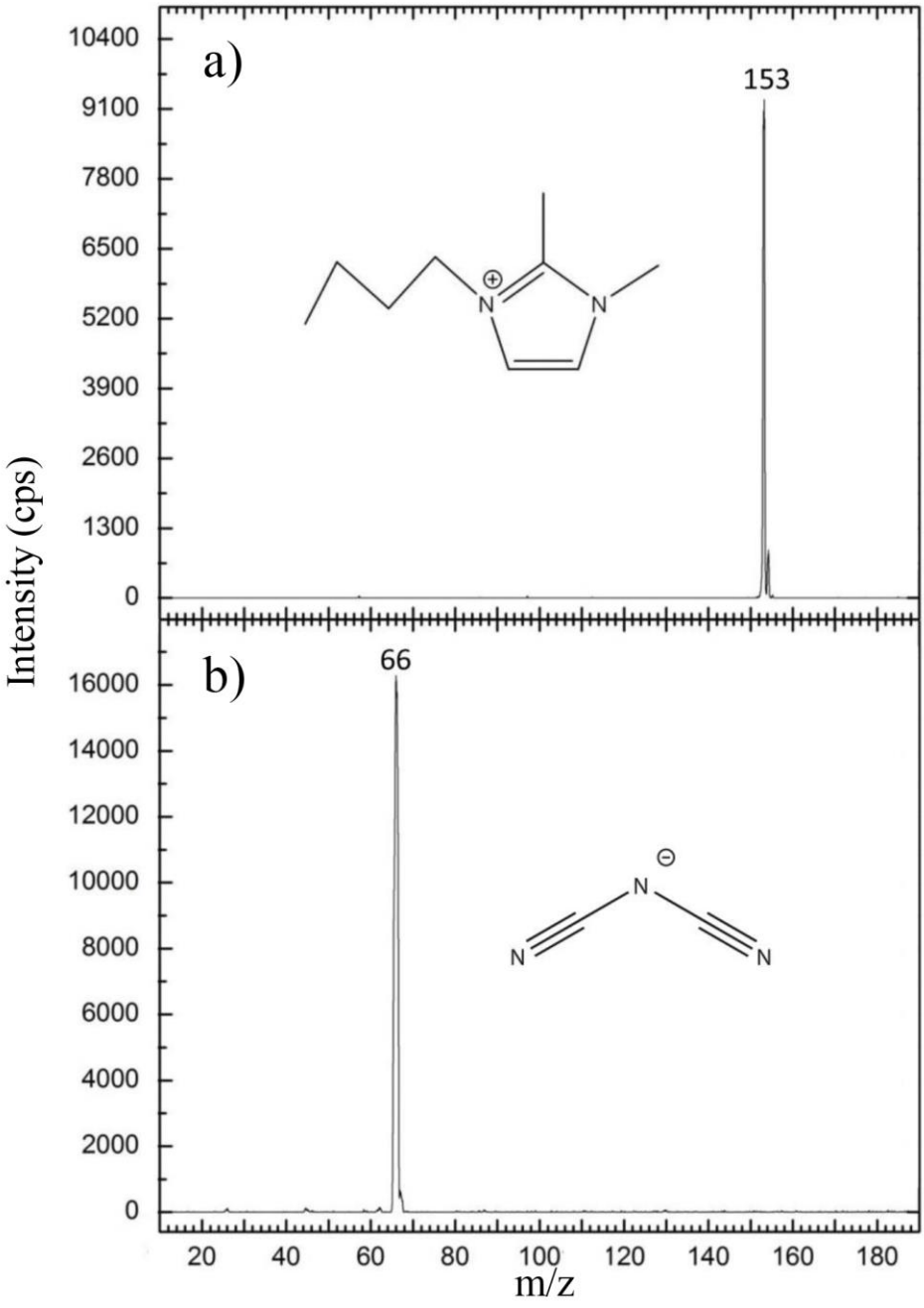

Figure 2.6 Electrospray ionization source spectra
The cation (a) 1-butyl-2,3-dimethylimidazolium and anion (b) dicyanamide are generated in high abundance with the ESI source.

2.1.2 Ion Selection Region

The ion selection region designates the experiment a *selected ion* flow tube; it differentiates FA from SIFT techniques. The ions exit the source region through either an electrostatic nose cone (for EI) or an electrodynamic ion funnel (for ESI) and enter a differentially pumped region maintained at ~10^{-5} Torr by a 10-inch diffusion pump (Edwards Diffstak, 2300 L s^{-1}) backed by a mechanical pump (Welch 1374, 650 L min^{-1}). The ions pass through six focusing lenses directing them into a quadrupole mass filter (Extrel # 4-270-9, four rods 16 mm O.D. × 220 mm). The quadrupole is housed in a smaller chamber differentially pumped to ~10^{-6} Torr by a 6-inch diffusion pump (Edwards Diffstak, 805 L s^{-1}) and backed by a mechanical pump (Welch 1397, 500 L min^{-1}). RF and DC potentials are applied to the quadrupole by an Extrel power supply (# 011-1, #011-14) with a resonant frequency of ~1.5 MHz. The quadrupole is used to mass select (or SIFT) ions of a single m/z with unit resolution. The quadrupole may transmit ions up to ~400 m/z. The mass selected ion current is focused by three electrostatic lenses into an ion injection orifice. The injection orifice contains a Venturi gas-inlet consisting of two concentric annuli. Helium is forced through the concentric circular inlets, and the ratio of flow between the two annuli is adjusted to minimize back streaming of helium into the ion selection region. The Venturi inlet is discussed in detail in the original report of the SIFT apparatus.[4]

Carbon monoxide (CO) is the precursor gas used to generate the positive ion spectra in Figure 2.7. Figure 2.7a illustrates that the EI source produces many ions even when a single precursor gas (CO) is used. Figure 2.7b shows the EI source of mass selected and optimized m/z 16 ($O^{\bullet+}$).

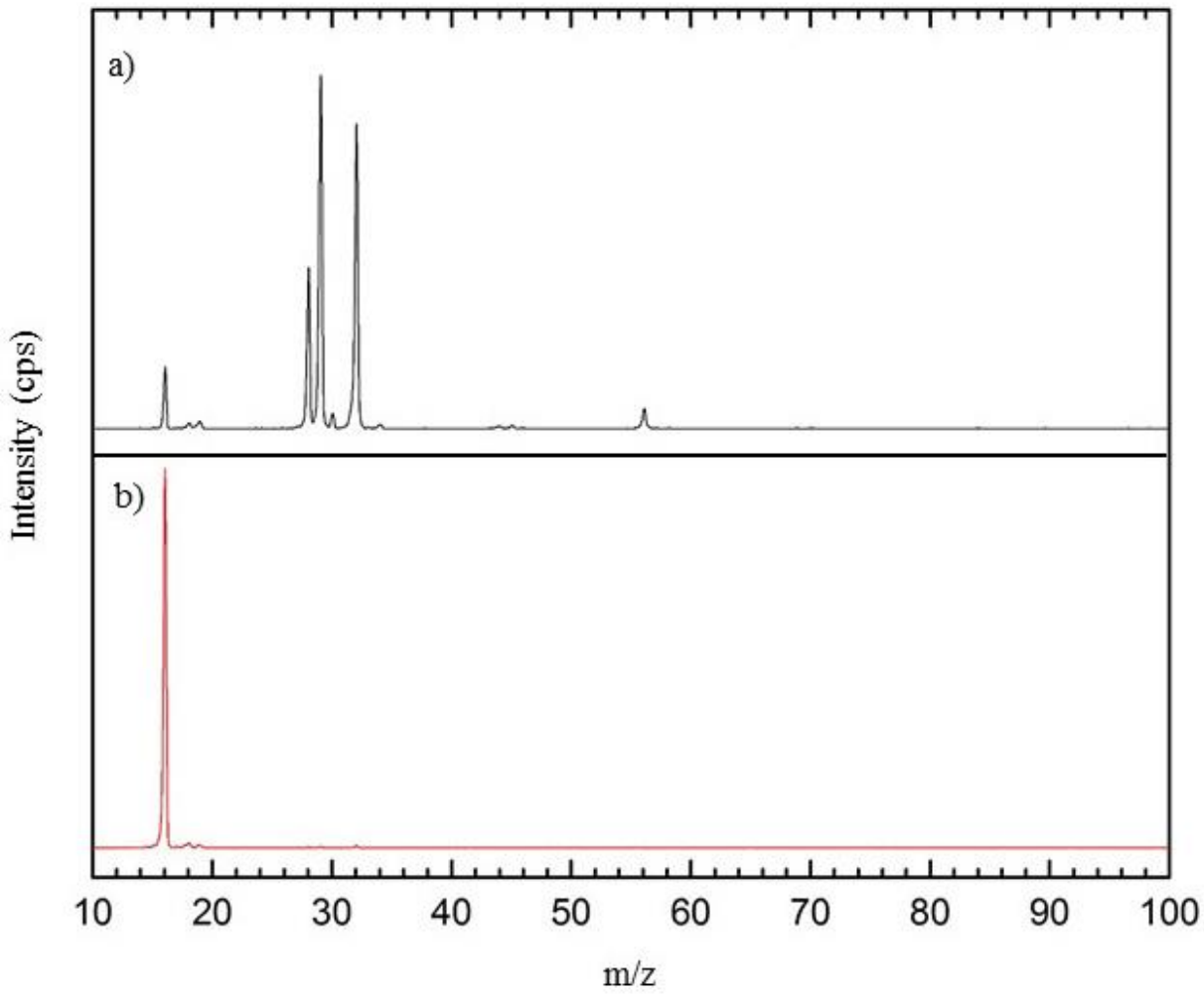

Figure 2.7 EI source positive ion spectra of CO: (a) no mass selection (b) m/z 16 mass selected

2.1.3 Reaction Flow Tube

After mass selection, the ions are injected into the reaction flow tube. The ions are entrained in helium as they pass through the Venturi inlet; the ions are quickly thermalized through multiple collisions with the helium carrier gas (~10^6 collisions s^{-1}). The flow tube is a long (117 cm), field-free stainless steel cylinder with an inner diameter of 7.3 cm. The ions in the flow tube are not transferred by electrostatic lensing, but instead are carried by a ~170 std cm^3 s^{-1} flow of helium maintained at a pressure of ~0.45 Torr by a high-capacity Stokes roots pump (755 L s^{-1}). The ions take ~10 ms to travel the flow tube (v_{ion} ~ 10^4 cm/s). The first ~45 cm of the flow tube is used to establish laminar flow. The remaining ~70 cm of

the flow tube is used to study ion-neutral reactions. Neutral reactants are introduced through seven evenly-spaced ring inlets (section 2.1.5.1), a microwave discharge apparatus (section 2.1.5.2), or a low-volatility neutral reagent source (Chapter 5).

2.1.4 Ion Detection Region

When the product ions and remaining reactant ions reach the end of the reaction flow tube, they are guided into the ion detection region through an electrostatic nose cone with an orifice of 0.5 mm. The nose cone is mounted onto a carrier plate biased with an independent electrostatic potential. Upon exiting the nose cone lens, the ions enter a region containing five electrostatic focusing lenses that is differentially pumped by a 6-inch diffusion pump (Edwards Diffstak, 805 L s^{-1}) backed by a mechanical pump (Welch 1397, 500 L min^{-1}). Next, the ions enter a triple quadrupole mass spectrometer (TQMS; Extrel, Model 5221 C50 TQMS: 1.2 MHz, 300W for Q1 and Q3, 200W for Q2, 19 mm O.D. rods). The triple quadrupole assembly lays across two chambers each differentially pumped by 10-inch diffusion pumps (Edwards Diffstak, 2300 L s^{-1}) and backed by mechanical pumps (Welch 1374, 650 L min^{-1}); the TQMS chambers have pressures of 10^{-6} and 10^{-7} Torr, respectively. The TQMS is coupled to an electron multiplier (DeTech, 402A-H) with a gain of ~10^8. The ion pulses are processed by Extrel Software (Merlin Automation System, version 3.0). The reported SIFT experiments use the TQMS for single MS experiments only. To perform collision induced dissociation experiments reported in this thesis, a commercial instrument is employed (section 2.2).

2.1.5 Ion-Neutral Reaction Rate Constant

Both the FA and SIFT are used to measure ion-neutral reaction rate constants. To understand this process, consider the generalized ion-neutral reaction:

$$I^{\pm} + B \rightarrow \text{Products} \qquad \textbf{2.5}$$

$I^{\pm}$ represents an ion (cation or anion), and B represents a neutral reactant. B may be a molecule or an atom. Bimolecular reactions are defined as second-order because their rate depends on the concentration of *two* reacting species. Consequently, ion-neutral reactions follow the kinetic rate equation:

$$\frac{d[I^{\pm}]}{dt} = -k_{exp}[I^{\pm}][B] \qquad \textbf{2.6}$$

The reaction rate depends on both $[I^{\pm}]$ and [B], but the experiments within this thesis follow pseudo–first-order reaction kinetics because $[I^{\pm}]$ <<< [B] by at least four orders of magnitude. $[I^{\pm}]$ is on the order of ~10^5 ions cm^{-3}; [B] ~ 10^{11} particles cm^{-3}. Rearranging equation 2.6:

$$\int_0^t \frac{1}{[I^{\pm}]} d[I^{\pm}] = -k_{exp}[B] \int_0^t dt \qquad \textbf{2.7}$$

Equation 2.7 is integrated over the reaction time, t; k_{exp} and [B] are removed from the integral because they are constant under pseudo–first-order reaction kinetics. Evaluating the integral yields the pseudo–-first-order reaction rate law:

$$ln\frac{[I^{\pm}]_t}{[I^{\pm}]_0} = -k_{exp}[B]t \qquad \textbf{2.8}$$

Equation 2.8 reveals k_{exp} can be experimentally determined by monitoring the change in $[I^{\pm}]$ with respect to varying the reaction time, t, or varying the neutral concentration, [B].

2.1.5.1 Reaction Rate Constant: Seven-Inlet Method

Volatile neutral reactants are introduced into the flow tube through seven evenly-spaced ring inlets. The first ring inlet lies 13.5 cm upstream from the ion-detection region, and the remaining ring inlets are spaced by 9.7 cm. Each ring inlet contains seventeen radially spaced holes promoting even mixing. The inlets are coupled to a glass-rack by solenoid valves. The neutral-reagent flow rate is established with a

metering valve and measured by monitoring the change in pressure in the glass rack (of known volume) with respect to time ($\Delta P/\Delta t$.)

Due to their axial distribution along the reaction flow tube, each neutral ring-inlet corresponds to a different reaction distance. Furthermore, the SIFT is a constant flow system where the velocity of helium carrier gas, and therefore the velocity of the ion (v_{ion}), is constant. Thus, the distance of the ring-inlet from the ion-detection chamber renders a temporal relationship to the reaction kinetics, and reaction rate constants are measured by monitoring the parent ion signal, $[I^{\pm}]$, as a function of reaction distance.

To formulate the experimental rate constant, equation 2.8 is rearranged to yield the relationship:

$$\ln[I^{\pm}]_t = -k_{exp}[B]t + \ln[I^{\pm}]_0 \qquad \textbf{2.9}$$

Incorporating the relationship between velocity and time into equation 2.9 yields the expression:

$$\ln[I^{\pm}]_t = \frac{-k_{exp}[B]z}{v_{ion}} + \ln[I^{\pm}]_0 \qquad \textbf{2.10}$$

Where z is the reaction distance, or axial–flow tube distance between the ion-detection chamber and the ring-inlet. This parallels the equation y = mx + b where $m = -k_{exp} \times [B]/v_{ion}$. The ion-neutral reaction rate constant, k_{exp}, for reaction 2.5 is determined by plotting $\ln[I^{\pm}]$ vs. reaction distance. Figure 2.8 shows an example for the reaction of $O^{\bullet+}$ with CH_3F.

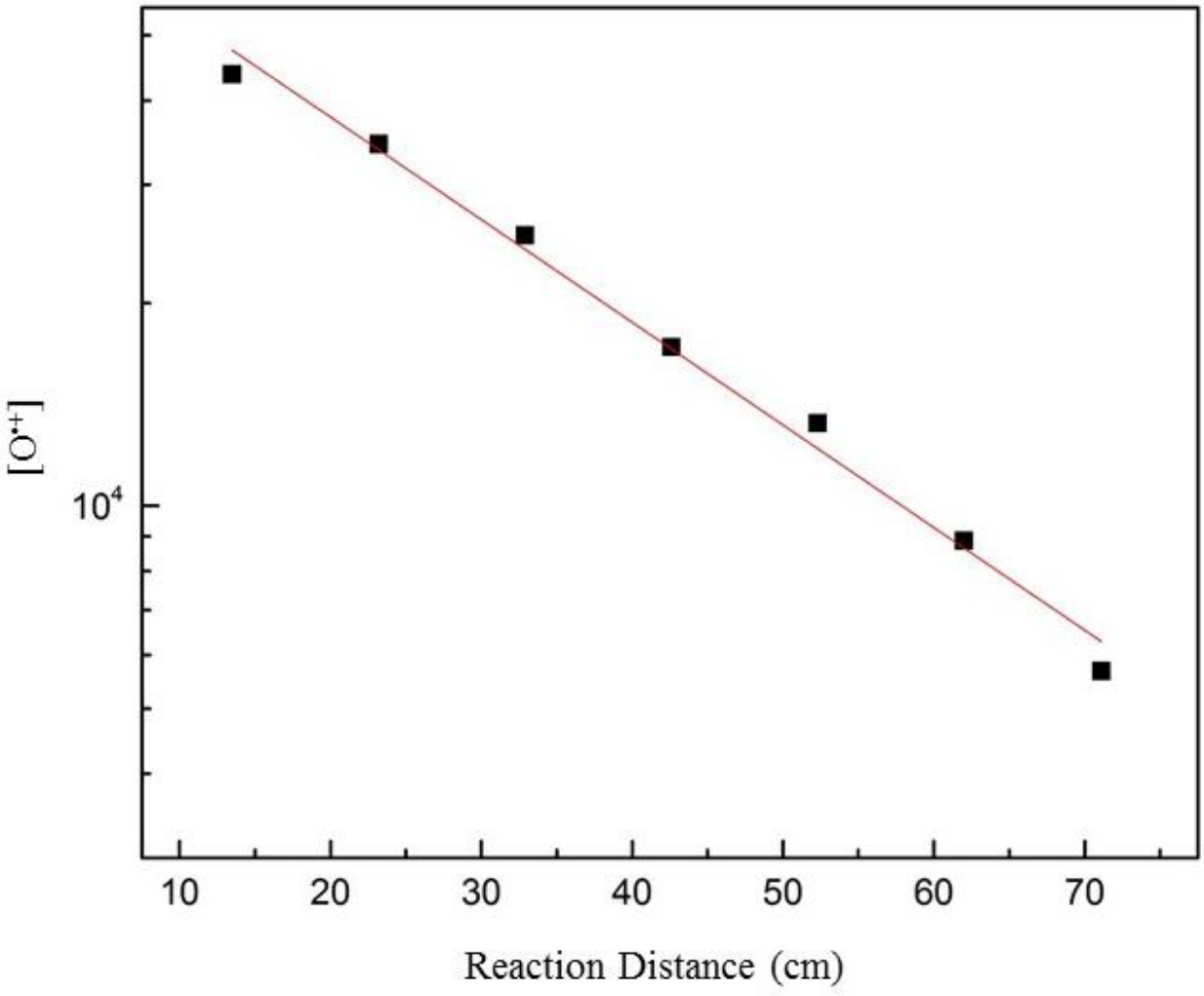

Figure 2.8 [$O^{\bullet+}$] vs. reaction distance for the $O^{\bullet+}$ + CH_3F reaction

For Figure 2.8, each of the data points represents one of the seven neutral reagent ring-inlets. Because [CH_3F] and v_{ion} are known, the reaction rate constant, k_{exp}[$O^{\bullet+}$ + CH_3F], can be determined from the slope in Figure 2.8.

2.1.5.2 Reaction Rate Constant: Microwave Discharge

N(^{4}S) and O(^{3}P) are introduced as neutral reagents by using a microwave discharge connected to the reaction flow tube.[7] The experimental setup is shown in Figure 2.9. A microwave power supply (Opthos

MPG-4) provides ~40-50W of microwave radiation to the Evenson cavity. Molecular nitrogen is passed through the Evenson cavity generating N atoms, equation 2.11.

$$N_2 + h\nu \rightarrow 2N \qquad \textbf{2.11}$$

The dominant active species released into the flow tube from the microwave discharge of N_2 is $N(^4S)$. While concentrations of metastable excited species, $N(^2D)$, $N(^2P)$, and $N_2(^3\Sigma_u^+)$ are considerable near the discharge plasma, these excited species are destroyed within a few milliseconds and will not survive the path to the flow tube.[8-11]

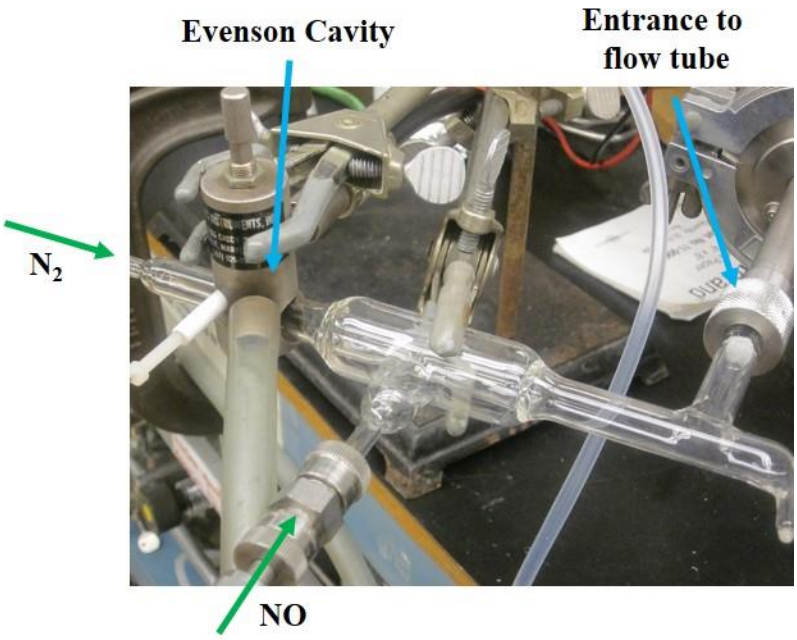

Figure 2.9 Microwave discharge apparatus

O atoms are generated by titrating [N] with NO, equation 2.12.

$$N + NO \rightarrow N_2 + O \qquad \textbf{2.12}$$

To determine [N] and [O] for kinetic formulation, a titration plot is generated by monitoring the log of the intensity of the parent ion as a function of NO flow, Figure 2.10.

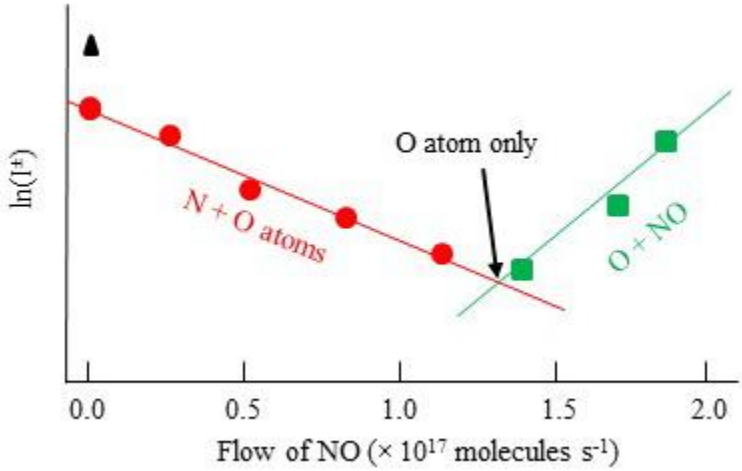

Figure 2.10 Microwave discharge titration plot

The black triangle represents the intensity of the parent ion signal before the microwave discharge is ignited. The depletion in ion signal between the black triangle and the red circle occurs due to the reaction of the ion with N atom. The first red circle represents $[N]_0$. The flow of NO is established using a metering valve, and monitored using a Tylan flow meter. As the flow of NO is increased, [N] is converted to [O]. The lowest point in the titration plot occurs where [O] is at a maximum. At this point, $[NO]_{added} = [N]_0 = [O]_{titration\ point}$. After the titration plot is obtained, a reaction rate constant for equations 2.13 and 2.14 can be determined.

$$I^{\pm} + N \rightarrow \text{Products} \qquad \textbf{2.13}$$

$$I^{\pm} + O \rightarrow \text{Products} \qquad \textbf{2.14}$$

While the seven inlet method monitors reactant ion falloff vs. reaction distance and determines the rate constant by evaluating the slope, the microwave discharge method determines the reaction rate constant from a single experimental reaction distance (distance $\propto$ t), equation 2.15.

$$-k_{exp} = \left. ln\frac{[I^{\pm}]_t}{[I^{\pm}]_0} \right/ [B]t \qquad \textbf{2.15}$$

Equation 2.15 arrives from the rearrangement of equation 2.8, where [B] represents either [N] or [O], both of which are determined from the titration plot.

2.1.5.3 Determination of Variables

The velocity of the helium carrier gas (v_{He}) is determined from the helium flow rate (F_{He}), pressure (P_{He}), and the cross sectional area of the reaction flow tube (πr^2), equation 2.16.

$$v_{He}\left(\frac{cm}{s}\right) = \frac{F_{He}(STP\,\frac{cm^3}{s})}{\pi r^2(cm^2)P_{He}(Torr)} \times \frac{760(Torr)}{atm} \times \frac{T(K)}{273.16(K)} \qquad \textbf{2.16}$$

The velocity of the ions relative to the velocity of helium was determined experimentally. In fact, the ions move through the flow tube slightly faster than the carrier gas. A correction constant (α), determined both computationally and empirically, is multiplied by v_{He} to determine v_{ion}, equation 2.17.

$$v_{ion}\left(\frac{cm}{s}\right) = \alpha \times v_{He}\left(\frac{cm}{s}\right) = 1.6 \times v_{He}\left(\frac{cm}{s}\right) \qquad \textbf{2.17}$$

The flow of the neutral reagent, F_B, may be directly measured with a flow meter. Otherwise, F_B is determined experimentally by monitoring the change in pressure within a known volume with respect to time, equation 2.18.

$$F_B\left(Torr\,\frac{cm^3}{s}\right) = V_{known}(cm^3) \times \frac{\Delta P(Torr)}{\Delta t(s)} \qquad \textbf{2.18}$$

The concentration of the neutral reagent, [B], in the flow tube is determined using the flow of the neutral reagent (F_B), helium velocity (v_{He}), and the cross sectional area of the reaction flow tube (πr^2), equation 2.19.

$$[B]\left(\frac{particles}{cm^3}\right) = \frac{F_B\left(Torr\frac{cm^3}{s}\right)}{\pi r^2(cm^2)v_{He}\left(\frac{cm}{s}\right)} \times 3.535 \cdot 10^{16}\left(\frac{particles}{cm^3 \cdot Torr}\right) \quad \textbf{2.19}$$

'Particles' is a unitless quantity, and may represent atoms or molecules. The reaction rate constant will now be considered. Rearrangement of equation 2.10 yields equation 2.20.

$$k_{[I^{\pm}+B]}\left(\frac{particles \cdot cm^3}{s}\right) = \frac{-dln[I^{\pm}]}{dz} \times \frac{v_{ion}}{[B]} \quad \textbf{2.20}$$

Substituting for [B] and v_{ion} yields equation 2.21.

$$k_{[I^{\pm}+B]} = \frac{-\Delta ln[I^{\pm}]}{\Delta z} \times \frac{\alpha F_{He}^2}{F_B P_{He}^2 \pi r^2} \quad \textbf{2.21}$$

Equation 2.21 formulates the rate constant in terms of experimentally measurable variables.

2.1.6 Product Fraction

Rate constants in the SIFT are measured by monitoring $\Delta ln[I^{\pm}]$, but how are products measured/reported? Indeed, ion-neutral reactions will often generate various products through competing product generation channels. When this occurs the product fraction must also be reported. Consider the ion-neutral reaction shown in Scheme 2.1. While this scheme considers a real example using cations the principles illustrated also apply to anions.

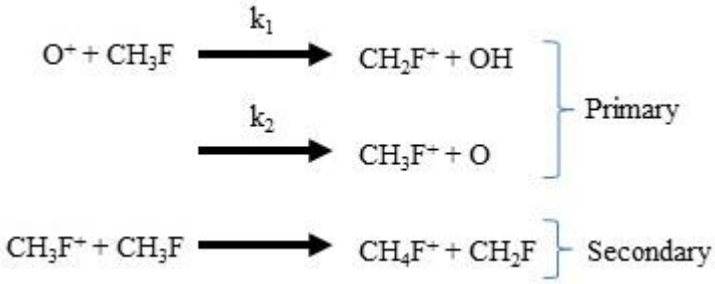

Scheme 2.1

As indicated in Scheme 2.1, the total ion spectra would show peaks corresponding to O^+, CH_2F^+, CH_3F^+, and CH_4F^+. The primary and secondary reactions need to be disentangled. This can be accomplished by monitoring the product ion intensities, $[CH_2F^+]$, $[CH_3F^+]$, and $[CH_4F^+]$, as a function of reaction (or inlet) distance, and extrapolating to 'zero' reaction distance. At 'zero' reaction distance, the concentration of the secondary product ions will approach zero. The ratio of the primary product ions at 'zero' reaction distance is reported as the product fraction (PF). Figure 2.11 shows a product fraction plot for the reaction of $O^{\bullet+}$ + CH_3F. The PF is reported as the y-intercept for the linear curves. CH_4F^+ is a secondary product since its intensity extrapolates to zero.

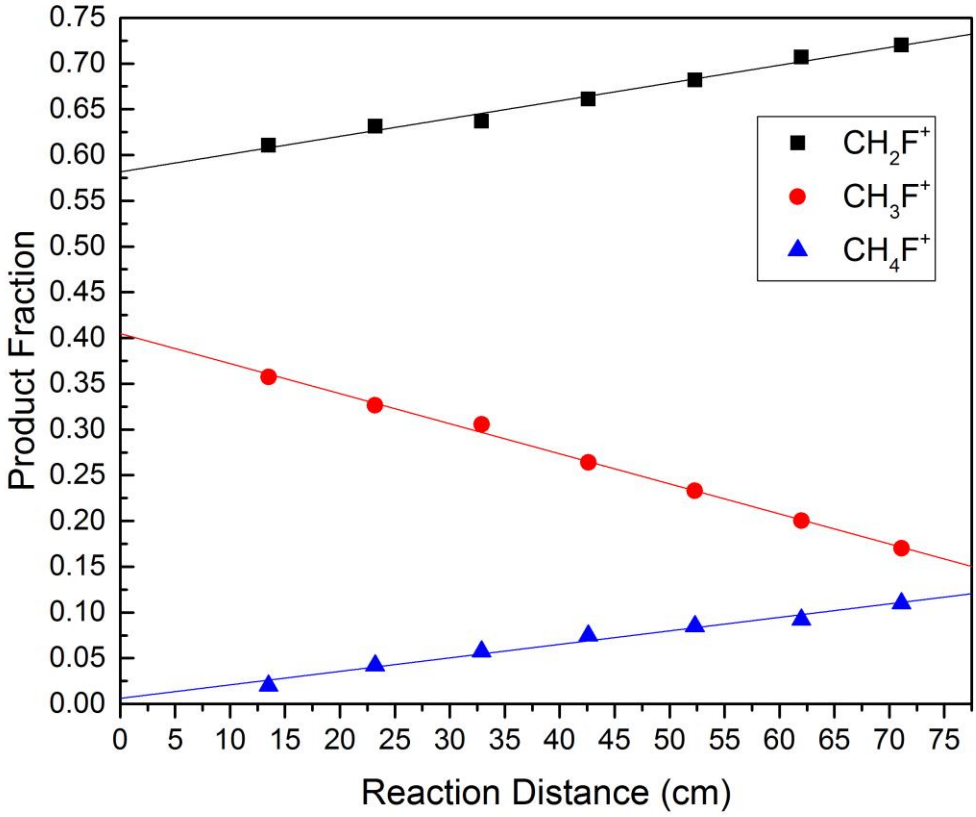

Figure 2.11 Product Fraction plot for $O^{\bullet+}$ + CH_3F

The PF may also be determined as a function of reactant ion depletion. Furthermore, the PF may be used for determining the relative reaction rate constants because $k_{total} = k_1 + k_2$. The relative reaction rate constants are directly proportional to the relative abundance of the primary products, equations 2.22 and 2.23.

$$PF_{CH_2F^+} = \frac{[CH_2F^+]}{[CH_2F^+] + [CH_3F^+]} = \frac{k_1}{k_1 + k_2} \quad \textbf{2.22}$$

$$PF_{CH_3F^+} = \frac{[CH_3F^+]}{[CH_2F^+] + [CH_3F^+]} = \frac{k_2}{k_1 + k_2} \quad \textbf{2.23}$$

2.2 Triple Quadrupole Mass Spectrometer

In addition to the SIFT technique, collision induced dissociation experiments were performed on a commercial triple quadrupole mass spectrometer (AB Sciex, 4000 QTrap).[12] This apparatus is located at the University of Colorado's core mass spectrometry facility on east campus. While the detection region of the SIFT contains a triple quadrupole, the collision energies are not well defined, and ion intensities are more difficult to optimize. Figure 2.12 provides a schematic for the QTrap.

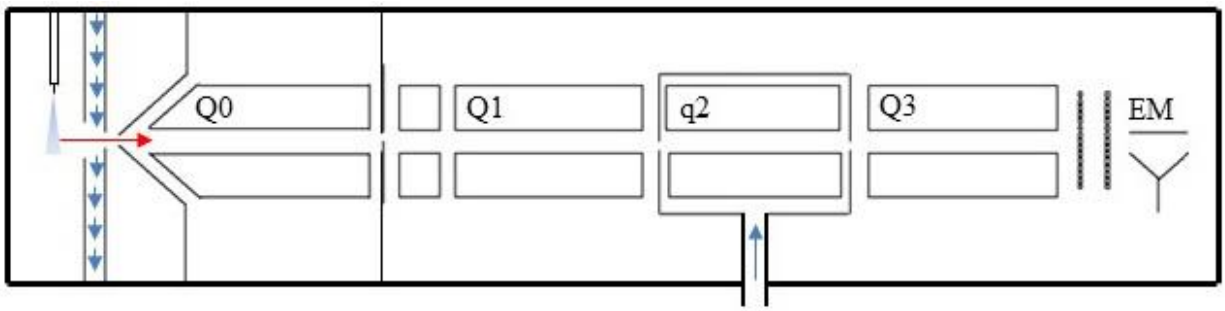

Figure 2.12 4000 QTrap triple quadrupole mass spectrometer

Ions are generated using a 'turbo spray' electrospray ionization source; the spray trajectory is off axis relative to the path of the ions. Due to the high sensitivity of the QTrap, dilute solutions with analyte

concentrations of 7.5 μM or smaller in methanol were used to generate ions. Infusion rates were controlled by a syringe pump, and typical flow rates varied from 5 to 40 μL/min. After generation, the ions are extracted from the spray by attractive potentials. The ions pass through a 'curtain' of N_2 gas (represented by blue arrows). The curtain gas flow, which is tunable in the software, desolvates the ions. Beyond the curtain gas is a differentially pumped region maintained at approximately 2 Torr. The entrance region is separated from the next differentially pumped region by a skimmer. The skimmer chamber contains a radio frequency (RF)-only quadrupole ion guide, Q0, and is maintained at ~3×10^{-3} Torr. An aperture separates the next differentially pumped chamber which contains a Brubaker lens and Q1; this chamber is maintained ~1×10^{-6} Torr. Q0, Q1, and the Brubaker lens are capacitively coupled to one another by an RF drive voltage. Q1 is used to mass-select the precursor ion of interest by applying a DC potential offset. The collision cell, q2, is placed in an isolated enclosure containing 3 mm entrance and exit apertures. N_2 gas (blue arrow) can be introduced into the q2 enclosure to perform collision induced dissociation. For the experiments reported in this thesis, the collision gas pressure is maintained as low as possible (~6×10^{-3} Torr) in order to approach single collision conditions. The collision energy for the QTrap is defined by the DC potential differences between Q0 and q2. The third quadrupole, Q3, is used to analyze the collision induced dissociation fragment ions. Q3 is coupled to an electron multiplier.

The QTrap was utilized to study the gas-phase acidities of the nitrated-azoles using Cook's kinetic method. This technique will be discussed in detail in Chapter 5.

2.3 Computational Methods

Throughout this thesis, computational methods are used to theoretically examine the experimental systems under investigation. Many *ab initio* methods have been employed. The methods employed are Becke-Lee-Yang-Parr exchange-correlation functional (B3LYP), coupled cluster (CCSD), and Møller-Plesset perturbation theory (MP2) in conjunction with either Pople or Dunning basis sets. Most of the

theoretical computations reported within this work were carried out using the *Gaussian 09* software suite.[13]

Computational methods are employed to optimize geometries for global minima of reactants, products, and intermediates. The energies of the optimized geometries are then obtained. Frequency calculations are then carried out to establish the optimized structure as either a transition state (characterized by one imaginary frequency) or intermediate (no imaginary frequencies).

Structures of transition states are important for explaining the kinetics and dynamics of a reaction system. Transition state optimization can sometimes be challenging. However, using the relaxed potential energy surface scans along a fixed reaction coordinate (i.e., the elongation of a bond or the rotation about an angle) can help to find the transition state by revealing a first-order saddle point. The geometry of the saddle point can be used for further optimization, and the frequency calculation will determine if the structure is a true transition state with only one imaginary frequency. As a proper transition state, the imaginary vibrational frequency should be consistent with the reaction coordinate of interest. Transition states are further confirmed by employing the intrinsic reaction coordinate (IRC) analysis.

For each of the studies presented in this thesis, appropriate computational details will be discussed in the relevant chapters.

2.4 References

[1] E.E. Ferguson, F.C. Fehsenfeld, A.L. Schmeltekopf, *Flowing afterglow measurements of ion-neutral reactions*, Adv. in Atom. Mol. Phys., 5 (1969) 1-56.

[2] V.M. Bierbaum, *Go with the flow: Fifty years of innovation and ion chemistry using the flowing afterglow*, Int. J. Mass Spectrom., 377 (2015) 456-466.

[3] N.G. Adams, D. Smith, *The selected ion flow tube: A technique for studying ion-neutral reactions*, Int. J. Mass Spectrom. Ion Phys., 21 (1976) 349-359.

[4] J.M. Van Doren, S.E. Barlow, C.H. DePuy, V.M. Bierbaum, *The tandem Flowing Afterglow-SIFT-DRIFT*, Int. J. Mass Spectrom. Ion Process., 81 (1987) 85-100.

[5] R.M. Moision, P.B. Armentrout, *An electrospray ionization source for thermochemical investigation with the guided ion beam mass spectrometer*, J. Am. Soc. Mass Spectrom., 18 (2007) 1124-1134.

[6] R.T. Kelly, A.V. Tolmachev, J.S. Page, K.Q. Tang, R.D. Smith, *The ion funnel: Theory, implementations, and applications*, Mass Spectrom. Rev., 29 (2010) 294-312.

[7] Z.C. Wang, C.A. Cole, N.J. Demarais, T.P. Snow, V.M. Bierbaum, *Reactions of azine anions with nitrogen and oxygen atoms: Implications for Titan's upper atmosphere and interstellar chemistry*, J. Am. Chem. Soc., 137 (2015) 10700-10709.

[8] S.N. Foner, R.L. Hudson, *Mass spectrometric studies of metastable nitrogen atoms and molecules in active nitrogen*, J. Chem. Phys., 37 (1962) 1662-1667.

[9] C.L. Lin, F. Kaufman, *Reactions of metastable nitrogen atoms*, J. Chem. Phys., 55 (1971) 3760-3770.

[10] J.A. Meyer, D.W. Setser, D.H. Stedman, *Energy transfer reactions of $N_2(A^3\Sigma_u^+)$. II. Quenching and emission by oxygen and nitrogen atoms*, J. Phys. Chem., 74 (1970) 2238-2240.

[11] R.A. Young, G.A. St. John, *Experiments on $N_2(A^3\Sigma_u^+)$. I. Reaction with N*, J. Chem. Phys., 48 (1968) 895-897.

[12] J.W. Hager, *A new linear ion trap mass spectrometer*, Rapid Commun. Mass Spectrom., 16 (2002) 512-526.

[13] M.J. Frisch, G.W. Trucks, H.B. Schlegel, G.E. Scuseria, M.A. Robb, J.R. Cheeseman, G. Scalmani, V. Barone, B. Mennucci, G.A. Peterson, H. Nakatsuji, M. Caricato, X. Li, H.P. Hratchian, A.F. Izmaylov, J. Bloino, G. Zheng, J.L. Sonnenberg, M. Hada, M. Ehara, K. Toyota, R. Fukuda, J. Hasegawa, T. Nakajima, Y. Honda, O. Kitao, H. Nakai, T. Vreven, J.A. Montgomery Jr., J.E. Peralta, F. Ogliaro, M. Bearpark, J.J. Heyd, E. Brothers, K.N. Kudin, V.N. Staroverov, R. Kobayashi, J. Normand, K. Raghavachari, A. Rendell, J.C. Burant, S.S. Iyengar, J. Tomasi, M. Cossi, N. Rega, J.M. Millam, M. Klene, J.E. Knox, J.B. Cross, V. Bakken, C. Adamo, J. Jaramillo, R. Gomperts, R.E. Stratmann, O. Yazyev, A.J. Austin, R. Cammi, C. Pomelli, J.W. Ochterski, R.L. Martin, K. Morokuma, V.G. Zakrzewski, G.A. Voth, P. Salvador, J.J. Dannenberg, S. Dapprich, A.D. Daniels, Ö. Farkas, J.B. Foresman, J.V. Ortiz, J. Cioslowski, D.J. Fox, *Gaussian 09*, Gaussian, Inc., Wallingford CT, 2009.

3 Gas-Phase Reactions of the Oxygen Radical Cation, $O^{\bullet+}$

3.1 Introduction

The oxygen radical cation, $O^{\bullet+}$, is abundant in many regions of the Universe. In the Earth's atmosphere, this ion dominates the ionic constituents in the F-region of the ionosphere, reaching concentrations of 4×10^5 particles cm^{-3}. $O^{\bullet+}$ is commonly generated by photoionization from UV radiation, but it may also be generated by charge exchange with H^+.[1, 2] These phenomena also account for the existence of $O^{\bullet+}$ in the diffuse clouds of the interstellar medium (ISM) and other non-terrestrial atmospheres.[3] Furthermore, $O^{\bullet+}$ has been detected in flames[4] and in industrial plasma-etching processes using O_2.[5, 6]

This chapter investigates the reactivity of $O^{\bullet+}$ with a variety of neutral molecules. It summarizes two research publications. The first publication explored the reactions of $O^{\bullet+}$ with the perfluorinated compounds CF_4, SF_6, and SF_5CF_3, as well as the methyl halides CH_3F, CH_3Cl, CH_3Br, and CH_3I to examine trends in reactivity.[7] The second $O^{\bullet+}$ publication explored reactivity of organic compounds with various functional groups including methanol, acetaldehyde, acetic acid, methyl formate, dimethyl ether, and acetone.[8] The majority of these reactions are reported here for the first time. While these studies contribute to the general knowledge of gas-phase reactions, they also taught me how to investigate ion-neutral reactions both experimentally and theoretically. Furthermore, the wide range of neutral molecules investigated (from perfluorinated compounds to organic molecules) permits some profound insight into the overall reactivity of $O^{\bullet+}$.

All in all, the chemical reactivity of $O^{\bullet+}$ is quite interesting! With its large recombination energy (RE) of 13.62 eV, $O^{\bullet+}$ can ionize every carbon-containing molecule except carbon monoxide/dioxide. Furthermore, $O^{\bullet+}$ will sometimes undergo electron-spin conversion processes, an occurrence that is often

described as forbidden. Even in situations where spin-conserved reaction channels generate highly exothermic products, the spin-conversion reactions channels are likely in competition.

3.2 Experimental Methods

For the following experiments, electron ionization (EI) was used to produce the atomic oxygen radical cation, $O^{\bullet+}$. The selected ion flow tube (SIFT) apparatus and the EI ion source are described in detail in Chapter 2. Chapter 2 also presents a mass-selected spectrum of $O^{\bullet+}$.

When generating $O^{\bullet+}$ to study ion-neutral reactions, it is important to ensure that only a single electronic-state is present. Using the methods of Smith et al.,[9] a high percentage of ground-state, $O^{\bullet+}(^4S)$, ions are produced. In the EI source, a mixture of 0.10 Torr CO (Airgas, CP grade; ionization energy = 14.01 eV) and 0.30 Torr He (Airgas, 99.999%) undergoes electron ionization to form both ground- and excited-state $O^{\bullet+}$. Since the ionization energy of CO is between the recombination energies of the ground- and excited-state $O^{\bullet+}$ ions, the excited-state ions, $O^{\bullet+}(^2D)$, $O^{\bullet+}(^2P)$, etc., are rapidly destroyed in the ion source by charge-transfer reactions with CO ($k_{exp} = 1.3 \times 10^{-9}$ cm^3 s^{-1}) [10], while the ground state, $O^{\bullet+}(^4S)$, does not react. Therefore, by introducing a large concentration of CO in the source, the excited-state $O^{\bullet+}$ ions are quenched. To confirm the absence of excited states in the experiments, $O^{+\cdot}$ is injected into the reaction flow tube, and CO was introduced downstream. The observed rate constant, $< 3.3 \times 10^{-12}$ cm^3 s^{-1}, indicates that less than 0.25% of $O^{\bullet+}$ introduced into the reaction flow tube is electronically excited.

The chemical compounds used in this study were obtained from commercial vendors: helium, Airgas, 99.999%; CF_4, Airgas, 99.99%; SF_6, Airgas, 99.99%; SF_5CF_3, SynQuest, 99%; CH_3F, Matheson, 99%; CH_3Cl, Matheson, 99.9%; CH_3Br, Matheson, 99%; CH_3I, Sigma, 99%; acetaldehyde, Sigma, ≥99.5%; acetic acid, Mallinckrodt, 99.9%; acetone, Fischer, 99.5%; dimethyl ether, Sigma, ≥99%; methanol, Sigma, ≥99.9%; methyl formate, Sigma, 99%. Several compounds employed as neutral reactants exist as liquids. For these compounds, the vapor pressures of the liquids are high enough to establish a stable

gaseous flow rate; each liquid sample is submerged in a room-temperature water bath to ensure flow stability.

3.3 Computational Methods

Energy diagrams for the reaction of $O^{\bullet+}$ with methyl chloride and acetaldehyde were calculated at the CCSD(T)/aug-cc-pVDZ//B3LYP/aug-cc-pVDZ level of theory using *Gaussian 09*.[11] The product fractions for the unimolecular dissociation of acetaldehyde ionized by charge transfer with $O^{\bullet+}$ were determined using RRKM theory implemented by the CRUNCH program.[12-14]

3.4 Results and Discussion

The gas-phase ion-neutral reactions of $O^{\bullet+}$ (^4S) with CF_4, SF_6, SF_5CF_3, CH_3F, CH_3Cl, CH_3Br, CH_3I, CH_3COH (acetaldehyde), CH_3COOH (acetic acid), CH_3COCH_3 (acetone), CH_3OH (methanol), and CH_3OCOH (methyl formate) have been studied; rate constants and product fractions are reported. The results are discussed in three sections: perfluorinated compounds, methyl halides, and organic molecules. Using this diverse set of neutral reagents, some interesting trends in the reactivity of $O^{\bullet+}$ are reported.

3.4.1 $O^{\bullet+}$ + Perfluorinated Compounds

The perfluorinated compounds are characterized by large ionization energies (IE) comparable to the recombination energy of $O^{\bullet+}$. Rate constants and product fractions for the reaction of $O^{\bullet+}$ with CF_4, SF_6, and SF_5CF_3, which have been determined in this study, are reported in Table 3.1.

Table 3.1 Reaction rate constants and product fractions for $O^{\bullet+}$ with perfluorinated compounds

Reactant [IE (eV)][a]	Ionic Product Fraction[b]	Products[c]	Rxn. #	ΔH_{rxn}[d] (kcal mol^{-1})	$k_{exp.}$[e] ($\times10^{-9}$ cm^3 s^{-1})	Efficiency[f] ($k_{exp.}/k_{col.}$)
CF_4 [≤14.7]	1.00	CF_3^+[S] + OF[Q]	3.1a	9.4	1.0(±0.3)[g]	0.78
		CF_3^+[T] + OF[D]	3.1b	132.3		
		CF_3^+[S] + O[T] + F[D]	3.1c	123.4		
		CF_3^+ [S] + OF[D]	3.1d	–10.6		
SF_6 [15.3]	1.00	SF_5^+[S] + OF[D]	3.2	–30.6	1.3(±0.4)[h]	0.82
SF_5CF_3 [12.9]	0.07(±0.05)	CF_3^+[S] + SF_5[D]+O[T]	3.3	–30.1	1.4(±0.4)[i]	0.60
	0.88(±0.05)	SF_3^+[S] + CF_4[S] + F[D] + O[T]	3.4a	–30.0		
		SF_3^+[S] + CF_4[S] + FO[D]	3.4b	–91.1		
	0.05(±0.01)	SF_5^+[S] + CF_3[D] + O[T]	3.5	–16.5		

[a]Ionization energies from Lias *et al.* (Ref. 22). [b]Product Fraction error reported as 1σ of the data sets. [c]S,D,T, and Q denote the multiplicity. [d]The enthalpies of reaction from Lias *et al.* (Ref. 22) and Afeefy *et al.* (Ref. 23). [e]Rate constants determined in this study; Error bars reported as total error (±30%). [f]Su and Chesnavich (Ref. 24). [g]Previous values ($\times10^{-9}$ cm^3 s^{-1}): k=1, Richter and Lindinger (Ref. 6); k=1.3(±0.4), Fisher and Armentrout (Ref. 5); k=1.4(±0.4), Morris et al. (Ref. 27). [h]Previous values ($\times10^{-9}$ cm^3 s^{-1}): k=1.8(±0.5), Morris et al. (Ref. 27); k=1.5(±0.5), Fehsenfeld (Ref. 25). [i]Previous value k=1.9(±0.4) $\times10^{-9}$ cm^3 s^{-1}, Atterbury et al. (Ref. 26).

The reactions of $O^{\bullet+}$ with the three fully fluorinated compounds, CF_4, SF_6, and SF_5CF_3 have been studied previously.[5, 6, 18-20] Our rate constants agree with previous studies within reported error.

It is well documented that reactions involving atomic species with high spin states often undergo spin-conversion processes,[21, 22] i.e., they break the spin selection rule, $\Delta S=0$. Previous studies of the $O^{\bullet+}$ + CF_4 reaction report CF_3^+ and OF as the products at thermal energies.[5, 6, 20] The ground state multiplicities of OF and CF_3^+ are a doublet and a singlet, respectively. To gain insight into the electron-spin dynamics, this reaction is examined computationally. In Table 3.1, the multiplicity of each product is indicated in brackets (neutral *reagents* are singlets). The total spin of the reactants, $O^{\bullet+}$ and CF_4, is S=3/2, and reactions 3.1a-3.1c in Table 3.1 present the three spin conserved reaction channels for generation of CF_3^+. Interestingly, these channels are all endothermic by at least 9 kcal/mol. The only exothermic product channel, reaction 3.1d, follows a spin-forbidden process. Therefore, the total spin of the system has changed from 3/2 to 1/2. Despite the necessity for spin-conversion, the reaction of $O^{\bullet+}$ and CF_4 occurs with an efficiency that approaches the collision limit.

Reaction 3.2 between $O^{\bullet+}$ (^4S) and SF_6 likely occurs by a similar mechanism to the CF_4 reaction, i.e., it likely undergoes spin-conversion. The ground state products of SF_5^+ and OF are a singlet and doublet, respectively; their enthalpies of formation were taken from the literature. The energies of the excited states of SF_5^+ and OF were not reported, nor were they computed due to limited computational resources. However, noting that the computational difference in energy between CF_3^+[S] and CF_3^+[T] is ~140 kcal/mol, the spin-conserved products for the reaction between $O^{\bullet+}$ (^4S) and SF_6 would likely be highly endothermic. Therefore, it is expected that the reaction with SF_6 occurs through a spin-conversion process.

In addition, the reaction of $O^{\bullet+}$ with SF_5CF_3 has been investigated. This process differs from the reactions with CF_4 and SF_6 because the ionization energy of SF_5CF_3 (12.9 eV) is low enough to permit charge transfer with $O^{\bullet+}$. Because the ground state of $SF_5CF_3^+$ is repulsive in the Franck-Condon region, the radical cation rapidly dissociates.[23] Three major ionic products, CF_3^+, SF_3^+, and SF_5^+, were observed, and trace amounts of the ion SF_4^+ were also observed. Previous results suggest that this reaction occurs only by charge transfer.[19] While the reaction of $O^{\bullet+}$ with SF_5CF_3 is rapid, it does not occur at the collision rate, suggesting that some of the ion-neutral complexes dissociate before a reaction takes place. Since charge transfer does not occur upon every collision, fluoride abstraction may occur in addition to charge transfer as it yields more exothermic products. If the product SF_3^+ is formed by fluoride abstraction as shown in reaction (3.4b), the generation of this ion is three times more exothermic. Reactions (3.3) and (3.5) are likely the result of charge transfer processes. Because the HOMO of SF_5CF_3 most closely resembles the single bond between the carbon and sulfur atom,[24] removing an electron from this orbital will cause the molecule to fragment. Products of reaction 3.3 and 3.5 differ only in the location of the charge.

Our product fraction for the reaction with SF_5CF_3 disagrees sharply with the previous study.[19] Earlier experiments report that the product fraction is dominated by the formation of CF_3^+ at 0.83, while SF_3^+ constituted only 0.16. However, the dominant product in our studies is SF_3^+ with a product fraction of

0.88; both spin-allowed and spin-forbidden channels are likely in competition to generate SF_3^+. The origin of the differences in product branching fractions is unknown; our experiments carefully excluded excited states of $O^{\bullet+}$, determined initial product fractions, and minimized mass discrimination. All of these factors can affect product ratios. There is no reason to doubt the present result; this is the recommended product fraction.

3.4.2 $O^{\bullet+}$ + Methyl Halides

Rate constants and product fractions for the reaction of $O^{\bullet+}$ with CH_3F, CH_3Cl, CH_3Br, and CH_3I are reported in Table 3.2.

Table 3.2 Reaction rate constants and product fractions for $O^{\bullet+}$ with methyl halides

Reactant [IE (eV)][a]	Product Fraction[b]	Products [c]	Rxn. #	ΔH_{rxn} (kcal mol^{-1})[d]	kexp. ($\times 10^{-9}$ cm^3 s^{-1})[e]	Efficiency ($k_{exp.}/k_{col.}$)[f]
CH_3F [12.50]	0.57(±0.06)	CH_2F^+[S] + H[D] + O[T]	3.6a	–4.7	2.7(±0.8)	0.92
		CH_2F^+[S] + HO[D]	3.6b	–111.6		
	0.43(±0.06)	CH_3F^+[D] + O[T]	3.7	–29.6		
CH_3Cl [11.26]	0.88(±0.03)	CH_3^+[S] + Cl[D] + O[T]	3.8a	–3.8	2.2(±0.7)	0.72
		CH_3^+[S] + ClO[D]	3.8b	–68.1		
	0.08(±0.02)	HCO^+[T] + H[D] + HCl[S]	3.9	–126.3		
	0.04(±0.02)	H_2CO^+[D] + HCl[S]	3.10	–149.9		
CH_3Br [10.54]	1.00	CH_3^+[S] + Br[D] + O[T]	3.11a	–17.8	2.2(±0.7)	0.77
		CH_3^+[S] + BrO[D]	3.11b	–74.1		
CH_3I [9.61]	0.94(±0.04)	CH_3^+[S] + I[D] + O[T]	3.12a	–30.7	1.4(±0.3)	0.51
		CH_3^+[S] + IO[D]	3.12b	–170.1		
	0.06(±0.04)	I^+[T] + CH_3[D] + O[T]	3.13	–16.0		

[a]Ionization energies from Lias *et al.* (Ref. 22). [b]Product Fraction error reported as 1σ of the data sets. [c]S,D,T, and Q denote the multiplicity. [d]The enthalpies of reaction from Lias *et al.* (Ref. 22) and Afeefy *et al.* (Ref. 23). [e]Error bars reported as total error (±30%). [f]Su and Chesnavich (Ref. 24).

This study reports for the first time the reactivity of $O^{\bullet+}$ with CH_3F, CH_3Cl, CH_3Br, and CH_3I. The adiabatic ionization energies (AIEs) of the methyl halides are all below the RE of $O^{\bullet+}$; the exothermicity for charge transfer increases as the halides become larger. Each reaction proceeds at 50% or more of the collision rate with the CH_3F reaction being the most efficient.

For CH_3Cl, CH_3Br, and CH_3I, the dominant product ion is CH_3^+. In contrast, the dominant product of the CH_3F reaction is CH_2F^+. The relevant bond energies for the methyl halides are provided in Table 3.3.[25]

Table 3.3 Bond dissociation energies of methyl halides

Bond	BDE_{298}[a] (kcal mol^{-1})
CH_3–F	110.0
CH_3–Cl	83.7
CH_3–Br	70.3
CH_3–I	54.0
H–CH_2F	101.3
H–CH_2Cl	100.1
H–CH_2Br	102.1
H–CH_2I	103.2

[a]Ref. 32

Since the carbon-fluorine bond is the only carbon-halogen bond that is stronger than the carbon-hydrogen bond, cleavage of the carbon-hydrogen bond is more favorable for reaction (3.6). The major product ions of these reactions can be formed by the spin-allowed process (charge transfer followed by bond cleavage [(3.6a), (3.8a), (3.11a), (3.12a)]) or the spin-forbidden process (atom abstraction [(3.6b), (3.8b), (3.11b), (3.12b)].) It is possible that these mechanisms are competing, but the spin-forbidden pathway may dominate since it is more exothermic in every case.

Although charge transfer is energetically feasible for all methyl halide reactions, the charge transfer product is only observed for CH_3F (reaction 3.7). Charge transfer is facilitated by good energy resonance between the RE of the cation and the AIE of the neutral molecule, and the existence of nonzero Franck-Condon factors.[26] For reactions of $O^{\bullet+}$ with the methyl halides, the best energy resonance occurs for CH_3F; therefore charge transfer deposits the smallest amount of energy into the internal modes of CH_3F^+. The lack of energy resonance during charge transfer of $O^{\bullet+}$ with the heavier methyl halides, and the weaker carbon-halogen bonds leads to their fragmentation upon production. The richness of product

channels in the reaction of $O^{\bullet+}$ with CH_3Cl warrants a deeper investigation of the energy landscape in the following section.

3.4.2.1 Stationary Points for the $O^{\bullet+}$ + CH_3Cl Reaction

CCSD(T)/aug-cc-pVDZ level calculations were used to develop two reaction coordinate plots for the reaction of $O^{\bullet+}$ with CH_3Cl. For Figure 3.1 and Figure 3.2, the total spin for each point on the potential energy surface is 3/2 and 1/2, respectively.

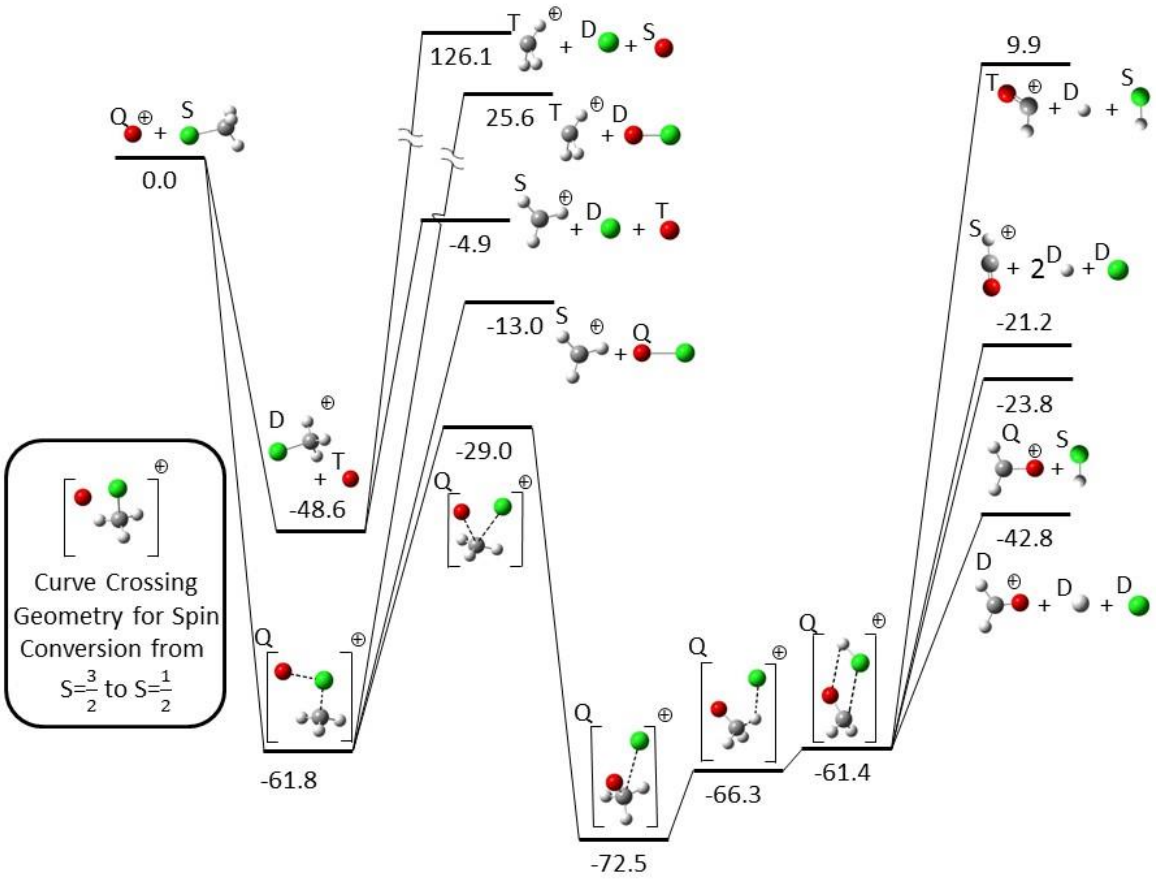

Figure 3.1 Stationary points for the reaction of $O^{\bullet+}$ + CH_3Cl; S=3/2
Values on the potential energy surface are in kcal mol^{-1}. The energies were determined at the CCSD(T)/aug-cc-pVDZ//B3LYP/aug-cc-pVDZ level of theory, they are corrected for zero point energy using the harmonic-oscillator approximation, and reported at 0 K. At each stationary point, S=3/2. The symbols S, D, T, and Q denote the multiplicity. The caption on the left side of the plot represents the curve crossing geometry.

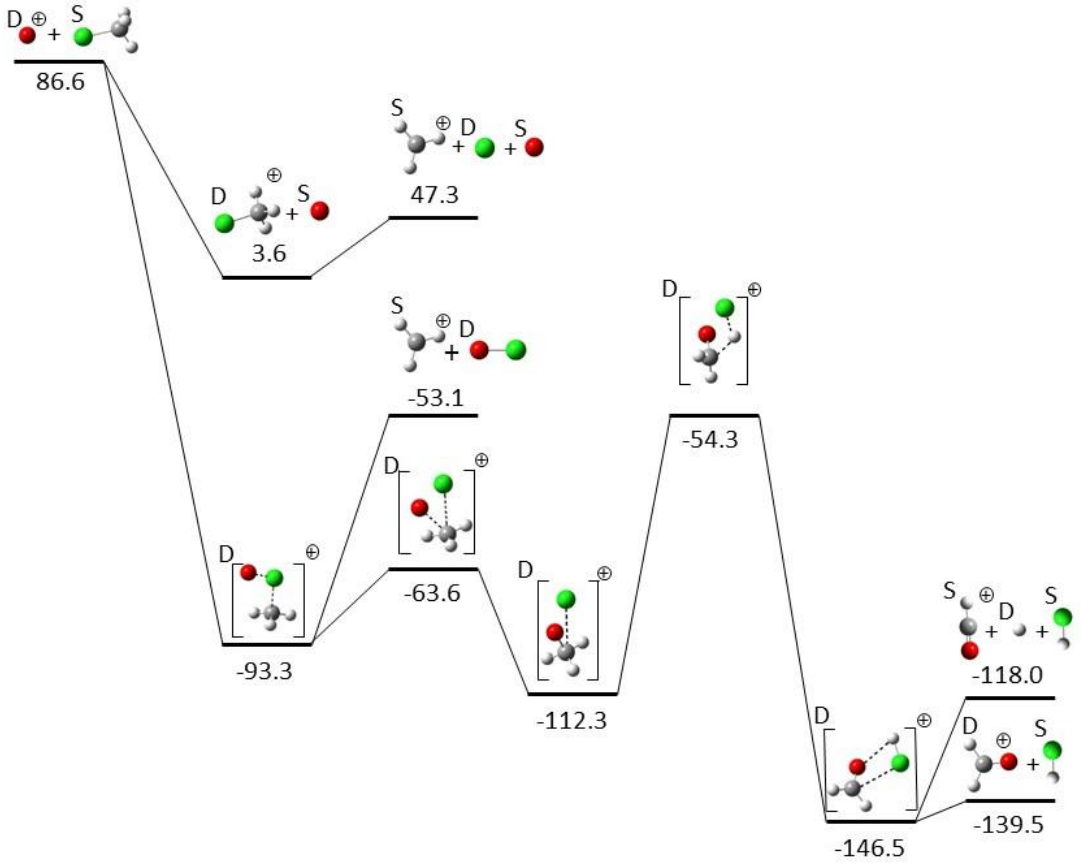

Figure 3.2 Stationary points for the reaction of $O^{\bullet+}$ + CH_3Cl; S=1/2
Values on the potential energy surface are in kcal mol^{-1}. The energies were determined at the CCSD(T)/aug-cc-pVDZ//B3LYP/aug-cc-pVDZ level of theory, they are corrected for zero point energy using the harmonic-oscillator approximation, and reported at 0 K. At each stationary point, S=1/2. The symbols S and D denote the multiplicity.

In each case, all possible spin allowed product combinations, even those which are endothermic and thus not energetically feasible, are included. The major product of the CH_3Cl reaction is the ion CH_3^+. Formation of this ion occurs by either dissociative charge transfer, or chloride abstraction as illustrated on the two reaction coordinate plots. It is the only possible experimentally observed product from the charge transfer channel of reactivity. However, we have shown with the $O^{\bullet+}$ + CF_4 reaction that spin-forbidden

atom abstraction processes are feasible. It is possible that this product is generated through the spin-forbidden chloride abstraction process, as this process is more exothermic by an order of magnitude. This would proceed via curve crossing between the two spin states; this crossing would likely occur during the formation of a primary complex as the energies overlap for the reactants and primary complexes in both plots. An ion complex geometry for spin conversion, or curve crossing, was calculated and is included on the left side of Figure 3.1. This geometry embodies a minor perturbation between the primary complexes of each reaction coordinate plot. It represents a point in which the two spin states are energetically equivalent.

Formation of the CH_3^+ ion likely dominates the product distribution of the CH_3Cl reaction because the minor product ions, H_2CO^+ and HCO^+, are formed through complex rearrangement processes. If the complex is short-lived, these products are unlikely to be generated. The product ions H_2CO^+ and HCO^+ were not observed in reactions involving CH_3Br and CH_3I because more energy is transferred during the reactions, and the complexes dissociate even more rapidly.

3.4.3 $O^{\bullet+}$ + Small Organic Molecules

Reaction rate constants and product fractions were determined for each reaction. The results of these experiments as well as pertinent thermochemical data (ionization energies, appearance energies, reaction enthalpies, etc.) are presented in Table 3.4.[9, 17, 27-38]

Table 3.4 Reaction rate constants and product fractions for $O^{\bullet+}$ with small organic molecules

Reactant [I.E. (eV)][a]	A.E. (eV)	Products	Rxn. #	Product Fraction	ΔH_{rxn} (kcal mol^{-1}) Calc.[b]	ΔH_{rxn} (kcal mol^{-1}) Lit.[a]	$k_{exp.}$[c] ($\times 10^{-9}$ cm^3 s^{-1})	Efficiency ($k_{exp.}/k_{col.}$)
Acetaldehyde CH_3COH [10.23]	11.78	$CHO^+[S] + CH_3[D] + O[T]$	3.14	0.99(±0.01)	–40.0	–41.1	2.9(±0.9)	0.82
	10.67	$CH_3CO^+[S] + H[D] + O[T]$	3.15	0.01(±0.01)	–60.4	–68.1		
Acetic Acid CH_3COOH [10.65]	12.05	$CH_2OH^+[S] + CHO[D] + O[T]$	3.16	0.03(±0.01)	–28.8	–32.2	3.0(±0.9)	1.09
	11.54	$CH_3CO^+[S] + OH[D] + O[T]$	3.17	0.06(±0.02)	–43.4	–48.2		
	12.3	$COOH^+[S] + CH_3[D] + O[T]$	3.18	0.05(±0.02)	–28.6	–34.7		
	10.65	$CH_3COOH^+[D] + O[T]$	3.19	0.24(±0.09)	–63.1	–68.5		
	–	$CO_3H^+[S] + CH_3[D]$	3.20	0.62(±0.10)	–34.0	–		
Acetone CH_3COCH_3 [9.70]	–	$CHO^+[S] + 2H[D] + CH_3CO[D]$	3.21	0.06(±0.02)	–17.3	–22.8	2.8(±0.8)[d]	0.67
	10.38	$CH_3CO^+[S] + CH_3[D] + O[T]$	3.22	0.18(±0.14)	–65.1	–74.0		
	9.70	$CH_3COCH_3^+[D] + O[T]$	3.23	0.09(±0.05)	–89.4	–84.4		
	–	$CH_3CO_2^+[S] + CH_3[D]$	3.24	0.67(±0.20)	–55.6	–		
Dimethyl Ether CH_3OCH_3 [10.02]	≤12.85	$CHO^+[S] + H_2[S] + CH_3[D] + O[T]$	3.25	0.31(±0.12)	–37.4	–37.9	1.7(±0.5)	0.69
	≤11.85	$CH_2OH^+[S] + CH_3[D] + O[T]$	3.26	0.34(±0.04)	–61.8	–67.2		
	11.12	$CH_3OCH_2^+[S] + H[D] + O[T]$	3.27	0.35(±0.11)	–53.6	–61.0		
Methanol CH_3OH [10.84]	13.06	$CHO^+[S] + H_2[S] + H[D] + O[T]$	3.28	0.06(±0.02)	–16.0	–15.6	2.2(±0.6)[e]	0.76
	12.05	$CH_2O^+[D] + H_2[S] + O[T]$	3.29	0.13(±0.04)	–37.6	–40.2		
	11.55	$CH_2OH^+[S] + H[D] + O[T]$	3.30	0.73(±0.02)	–40.4	–44.9		
	10.84	$CH_3OH^+[D] + O[T]$	3.31	0.08(±0.01)	–57.1	–64.0		
Methyl Formate CH_3OCOH [10.84]	12.91	$CHO^+[S] + CH_3O[D] + O[T]$	3.32	0.04(±0.01)	–25.9	–32.1	2.3(±0.7)	0.80
	13.6	$CH_2O^+[D] + H_2[S] + CO[S] + O[T]$	3.33	0.02(±0.01)	–31.3	–35.1		
	12.4	$CH_2OH^+[S] + H[D] + CO[S] + O[T]$	3.34	0.94(±0.01)	–34.0	–39.8		

[a]Ref. 22. [b]Reaction enthalpies are calculated using CCSD(T)/aug-cc-pVDZ//B3LYP/aug-cc-pVDZ level of theory and reported at 0 K. [c]Error reported as total error, ±30%. [d]Previously measured rate constant is 7.1×10^{-9} cm^3 s^{-1} (Ref. 44). [e]Previously measured rate constant is 1.9×10^{-9} cm^3 s^{-1} (Ref. 45) and 2.7×10^{-9} cm^3 s^{-1} (Ref. 20).

The RE of $O^{\bullet+}$ is well above the ionization energy of each of the organic neutrals. As a result, each reaction reported proceeds rapidly, and charge transfer is a common process within these reactions. The efficiency of each reaction is over 50% of the collision rate. The most efficient reaction is that of $O^{\bullet+}$ with acetic acid, which occurs at unit efficiency.

When dealing with ion-molecule reactions involving high energy ions, such as $O^{\bullet+}$, it can be useful to compare the experimental results to experimental appearance energy data. The high RE of $O^{\bullet+}$ allows it to remove an electron from the neutral molecules, and therefore its reactivity can be compared to different ionization experiments. Although investigating the difference in appearance energy of the product ions

and the recombination energy of $O^{\bullet+}$ provides similar information as investigating ΔH_{rxn} values, the results of ionization experiments can be used to guide the analysis of exothermic ion-neutral reactions. When certain products are not observed in ionization experiments, it suggests that these products are the result of some ion-molecule interaction and rearrangement. Therefore, we have included appearance energy data in Table 3.4.

3.4.3.1 $O^{\bullet+}$ + Acetaldehyde

The reaction of $O^{\bullet+}$ with acetaldehyde generates two products ions of m/z 29 and 43, the formyl and acetyl cations, respectively. The appearance energies of both ions were determined previously by photoionization experiments, and are 11.78 and 10.67 eV, respectively.[28, 29] Therefore both reactions 3.14 and 3.15 likely occur through dissociative charge transfer processes. Reaction 3.14 and 3.15 show cleavage of the C-C and C-H bonds, respectively. The distribution favors reaction pathway 3.14 (99%) although it is less exothermic than reaction pathway 3.15 (1%) by 27 kcal mol^{-1}. For this reaction, RRKM theory provides some insight into this preference in reactivity.

Calculated stationary points along a multi-dimensional potential energy surface for the reaction of $O^{\bullet+}$ with acetaldehyde are shown in Figure 3.3. The relaxed potential energy scan along the C-C bond in the reaction intermediate (CH_3COH^+) indicates that reaction 3.14 occurs through a loose transition state. If these reactions proceed by charge transfer, fragmentation of the acetaldehyde cation can be treated by RRKM unimolecular dissociation theory where the energy available to the acetaldehyde ion is the difference between the ionization energy of acetaldehyde and atomic oxygen (72.3 kcal mol^{-1}, Figure 3.3). The energy then available to each fragmentation channel, E_{aval}, is the difference between the charge transfer energy and the zero point energy of the products, or transition state for reaction 3.14 and 3.15, respectively; these values are 40.0 and 55.0 kcal mol^{-1} as shown in Figure 3.3. Based on these energies, RRKM predicts a branching ratio of 99.6% and 0.4% for the two reactions, respectively.[12-14] These values are in excellent agreement with the experimental results.

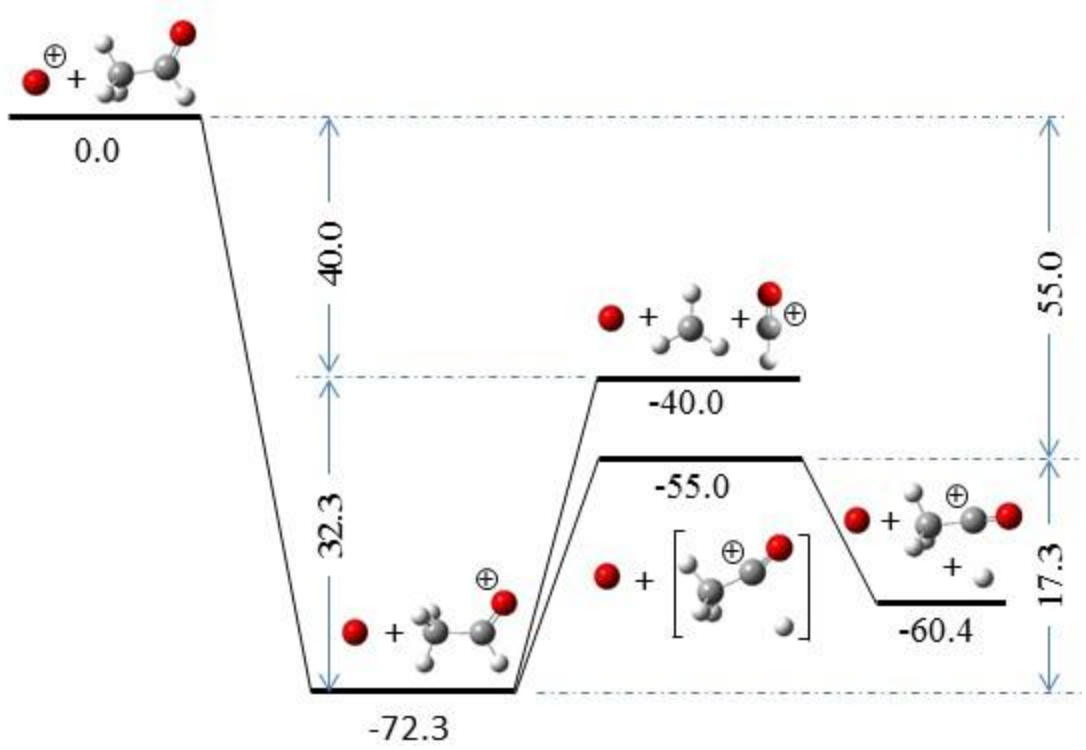

Figure 3.3 Stationary points for the reaction of $O^{\bullet+}$ with acetaldehyde
Units are in kcal/mol. The unimolecular product distribution (RRKM theory) for the acetaldehyde cation is determined with an excitation energy of 72.3 kcal/mol.

3.4.3.2 $O^{\bullet+}$ + Acetic Acid

The reaction of $O^{\bullet+}$ with acetic acid generates five ionic products with m/z 31 (CH_2OH^+), 43 (CH_3CO^+), 45 ($COOH^+$), 60 (CH_3COOH^+), and 61 (CO_3H^+). All but one of these products, m/z 61, are the result of charge transfer reactions. The appearance energies of the first four molecular ions are below the recombination energy of $O^{\bullet+}$; they are 12.05, 11.54, 12.3, and 10.65 eV, respectively.[27, 29-31] Selim and Helal have determined that the m/z 31 ion forms as the hydroxylmethyl cation, CH_2OH^+, and not the methoxy cation, CH_3O^+, based on heats of formation.[30] The heats of formation of the two ions are 168 and 201 kcal mol^{-1}, respectively.[36] The hydroxylmethyl cation is therefore formed by fragmentation followed by hydrogen atom rearrangement, a common process in ion fragmentation.[34, 39] Reaction 3.17 produces m/z 43, the acetyl cation. This ion is formed by fragmentation of the C-OH bond upon ionization.

Reaction 3.18 forms the m/z 45, protonated carbon dioxide. This occurs through dissociative charge transfer where the C-C bond is broken upon ionization. Shuman et al. observed m/z 43 and 45 ions in their threshold photoelectron-photoion coincidence (TPEPICO) spectroscopy experiment,[40] which examined the unimolecular dissociation of energy selected acetic acid cations. Their results confirm that these products are the result of charge transfer, and that the neutral fragments for reaction 3.17 and 3.18 are hydroxyl and methyl radical, respectively. Reaction 3.19 shows charge transfer where there is no fragmentation after ionization. These four charge transfer reactions together account for about one third of the product fraction, where reaction 3.19 alone represents 24%.

The final product channel, reaction 3.20, produces the ion m/z 61, and represents 62% of the product fraction. The m/z 61 ion is especially intriguing, and no information appears to be available in the literature. Our product fraction studies indicate that m/z 61 is not a secondary product. This product instead is formed from an interesting reaction in which a methyl radical is replaced by $O^{\bullet+}$. There are no literature values for the enthalpy of formation of the CO_3H^+ ion, but we have determined this reaction channel to be exothermic based on theoretical calculations. The lowest energy geometry of this ion is shown in Figure 3.4; it is a singlet with the three oxygen atoms bound directly to the carbon. The molecule is completely planar. A similar mechanism and product is observed in the $O^{\bullet+}$ + acetone reaction.

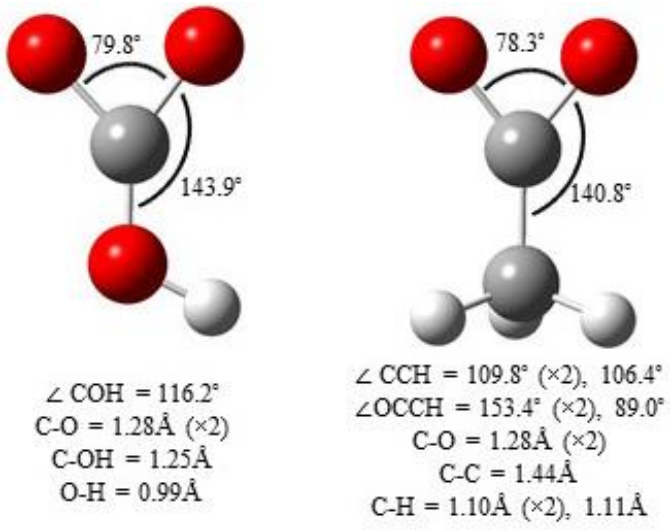

Figure 3.4 Lowest energy ionic products for reaction 3.20 and 3.24
Optimized at B3LYP/aug-cc-pVDZ level. For each reaction, $O^{\bullet+}$ has replaced $^{\bullet}CH_3$.

3.4.3.3 $O^{\bullet+}$ + Acetone

The reaction of $O^{\bullet+}$ with acetone generates four products of m/z 29, 43, 58, and 59. The formyl cation (m/z 29, reaction 3.21) is not observed in any appearance energy experiments for acetone. We suggest an addition elimination reaction in which the oxygen cation attacks the methyl group, causing fragmentation of the C-C bond, and a release of two hydrogen atoms. Because the m/z 29 product is the result of a chemical reaction, this cation could be generated as COH^+, protonated carbon monoxide. However, literature values for the enthalpy of formation of COH^+[36] indicate that this reaction would be endothermic by about 10 kcal mol^{-1}.

Reaction 3.22 generates the acetyl cation, CH_3CO^+, through a dissociative charge transfer reaction in which one of the two equivalent C-C bonds has fragmented. The appearance energy of the acetyl cation is 10.38 eV.[29] Reaction 3.23 is a charge transfer reaction in which the acetone molecule remains intact after ionization.

Reaction 3.24 generates m/z 59, one amu heavier than the acetone molecule. The structure of this product is similar to that observed with the $O^{\bullet+}$ + acetic acid reaction, where $O^{\bullet+}$ replaces a methyl radical. There is no information in the literature about the $CH_3CO_2^+$ ion, but we have provided an optimized geometry for this ion in Figure 3.4. It is a singlet, similar in geometry to the product of reaction 3.20. The ion is nearly planar with respect to the two carbon and two oxygen atoms.

The rate constant for the reaction of $O^{\bullet+}$ with acetone is much lower than the previously measured rate constant which was obtained using a flowing afterglow.[37] The SIFT often provides more reliable rate constants than the flowing afterglow due to the separation of ionization and reaction regions. Moreover, the rate constant previously obtained for the $O^{\bullet+}$ + acetone reaction ($k = 7.1\times10^{-9}$ cm^3 s^{-1}) is almost double the collision rate constant, which is not physically reasonable.[26]

3.4.3.4 $O^{\bullet+}$ + Dimethyl Ether

The reaction of $O^{\bullet+}$ with dimethyl ether generates three products with m/z 29 (CHO^+), 31 (CH_2OH^+), and 45 ($CH_3OCH_2^+$). The appearance energies of these ions were determined by threshold photoelectron-photoion coincidence (TPEPICO) spectroscopy to be ≤12.85, ≤11.85, and 11.12 eV respectively.[32] Therefore, the observed products are likely the results of dissociative charge transfer reactions.

Many studies have focused on the unimolecular dissociation of ionized dimethyl ether.[32, 41, 42] The m/z 31 ion observed during these studies is often the focal point of discussion, for this ion may form as either the methoxy, CH_3O^+, or hydroxyl methyl, CH_2OH^+, cation. Nishimura et al. investigated the dissociation dynamics of energy selected dimethyl ether ions.[41] The identities of the products observed in their TPEPICO breakdown curves at 13.6 eV (the recombination energy of $O^{\bullet+}$) are in agreement with our observations. However, at 13.6 eV they observe a greater fraction of the m/z 45 ion than m/z 29 or 31, while our results generate all products at roughly equal distributions. The authors[41] utilized the non-statistical spectator mechanism of direct dissociation theory (SSD) to determine that, at high energies, the formation of the m/z 31 ion is accompanied by a large kinetic energy release, indicating that at these higher energies, the m/z 31 product is the methoxy cation. However, based on their results, the kinetic

energy release is negligible around the recombination energy of $O^{\bullet+}$, and the m/z 31 ion formed in our study is likely the hydroxyl methyl cation.

3.4.3.5 $O^{\bullet+}$ + Methanol

The reaction of $O^{\bullet+}$ with methanol forms four products of m/z 29 (CHO^+), 30 (CH_2O^+), 31 (CH_2OH^+), and 32 (CH_3OH^+). We propose these ions are formed through charge transfer reactions. The appearance energies of these ions are 13.06, 12.05, 11.55 and 10.84 eV, respectively.[27, 33] The $O^{\bullet+}$ + methanol reaction has been studied previously.[9, 38] The most recently measured reaction rate constant ($k = 2.7\times10^{-9}$ cm^3 s^{-1}) and product branching ratio (m/z 29, 5%; m/z 30, 10%; m/z 31, 80%; m/z 32, 5%)[9] are in good agreement with our rate constant and product fraction results.

3.4.3.6 $O^{\bullet+}$ + Methyl Formate

The reaction of $O^{\bullet+}$ with methyl formate generates three product ions with m/z 29, 30, and 31. We propose these products are formed by dissociative charge transfer reactions; the appearance energy of each product ion is less than the recombination energy of $O^{\bullet+}$. Fragmentation of the methyl formate cation is well studied.[31, 34, 35, 43, 44] Reaction 3.32 produces m/z 29, the formyl cation, CHO^+, by fragmentation of the C-O bond after ionization. Reaction 3.33 forms the formaldehyde cation of m/z 30, likely through a sequential rearrangement/dissociation mechanism.

$$O^{+\cdot} + CH_3OCHO \rightarrow [CH_3OH^+]^* + CO + O \rightarrow CH_2O^+ + H_2 + CO + O \qquad 3.33$$

Experiments show that at the onset of the unimolecular dissociation of the methyl formate cation at about 11.5 eV, the formyl hydrogen will migrate forming a methanol cation, CH_3OH^+.[43, 44] The first step of reaction 3.33 involves ionization and re-arrangement of the methyl formate molecule, forming this methanol cation. The methanol cation will then fragment to form the hydrogen molecule and the formaldehyde cation.

The dominant product ion is m/z 31. This product is formed by the sequential reaction:

$$O^{+\cdot} + CH_3OCHO \rightarrow [CH_3OH^+]^* + CO + O \rightarrow CH_2OH^+ + H + CO + O \quad 3.34$$

Again, the first step of this process involves ionization and formation of the methanol cation through hydrogen migration. The methanol cation then fragments to lose a hydrogen atom, forming the hydroxyl methyl cation, CH_2OH^+.

Because the initial step of the $O^{\bullet+}$ + methyl formate reaction involves generation of the methanol cation, this reaction can be compared to $O^{\bullet+}$ + methanol. The results agree nicely considering that the dominant product of both of these reactions is the hydroxyl methyl cation, with minor contributions of the formyl and formaldehyde cations.

3.5 Conclusion

This study explored reactions of $O^{\bullet+}$ with a wide range of neutral molecules. The perfluorinated compounds CF_4 and SF_6 have large ionization energies of ~14.7 and 15.3 eV, much larger than the RE of $O^{\bullet+}$. Both of these reactions occur through fluoride abstraction, a process that is spin-forbidden. Despite the requirement of spin-conversion, these reactions occur rapidly, near the collision limit.

Each of the subsequent reactions reported in this chapter involve neutral molecules with ionization energies below the recombination energy of $O^{\bullet+}$. Most of these reactions are assumed to occur through dissociative charge transfer product generation channels. In fact, the reaction of $O^{\bullet+}$ with acetaldehyde follows this assumption so well that the fragmentation pattern for the acetaldehyde cation is successfully modeled using RRKM theory where the internal excitation energy is supplied by the excess charge transfer energy (~3.4 eV).

In many cases, the product channels are complex, and dissociative charge transfer appears to compete with atom-abstraction reactions. Although spin-conversion is often required for the atom-abstraction process, this does not appear to limit the reaction efficiency. As a general comment, products accessed

through spin-forbidden reaction channels are typically more exothermic. Whether the reactions undergo spin-conversion or not, the reactions of $O^{\bullet+}$ occur rapidly.

The high reactivity of $O^{\bullet+}$ indicates that ion-molecule chemistry is an important potential loss mechanism for this radical cation in many environments, including the Earth's atmosphere, the ISM, and combustion processes. Inclusion of the rate constants and products observed in this study into models of these environments will provide more accurate characterization of the relevant chemistry.

3.6 References

[1] J.H. Hoffman, *A mass spectrometric determination of the composition of the nighttime topside ionosphere*, J. Geophys. Res., 72 (1967) 1883-1888.

[2] J.H. Hoffman, C.Y. Johnson, J.C. Holmes, J.M. Young, *Daytime midlatitude ion composition measurements*, J. Geophys. Res., 74 (1969) 6281-6290.

[3] D. Smith, *The ion chemistry of interstellar clouds*, Chem. Rev., 92 (1992) 1473-1485.

[4] A.B. Fialkov, K.Y. Kalinich, B.S. Fialkov, *Experimental determination of primary ions in flames*: 24th Symposium (International) on Combustion/The Combustion Institute, 1992, pp. 785-791.

[5] E.R. Fisher, P.B. Armentrout, *Kinetic-energy dependence of the reactions of O^+ and O_2^+ with CF_4 and C_2F_6*, J. Phys. Chem., 95 (1991) 6118-6124.

[6] R. Richter, W. Lindinger, *Ion-molecule-reactions pertaining to etching plasmas*, in: SASP, Symposium on Atomic and Surface Physics,contributions; February 9-15, Obertraun, Austria, 1986, pp. 203-205.

[7] C.M. Nichols, Z. Yang, B.B. Worker, D.R. Hager, N.M.M. Nibbering, V.M. Bierbaum, *Gas-phase reactions of the atomic oxygen radical cation with halogenated compounds*, Phys. Chem. Chem. Phys., 15 (2012) 561-567.

[8] C.M. Nichols, Z. Yang, V.M. Bierbaum, *Gas-phase organic reactions of the atomic oxygen radical cation*, Int. J. Mass Spectrom., 353 (2013) 1-6.

[9] D. Smith, P. Spanel, C.A. Mayhew, *A selected ion-flow tube study of the reactions of O^+, H^+ and HeH^+ with severeal molecular gases at 300 K*, Int. J. Mass Spectrom. Ion Process., 117 (1992) 457-473.

[10] J. Glosik, A.B. Rakshit, N.D. Twiddy, N.G. Adams, D. Smith, *Measurement of the rates of reaction of the ground and metastable excited-states of O_2^+, NO^+ and O^+ with atmospheric gases at thermal-energy*, J. Phys. B-Atom. Mol. and Opt. Phys., 11 (1978) 3365-3379.

[11] M.J. Frisch, G.W. Trucks, H.B. Schlegel, G.E. Scuseria, M.A. Robb, J.R. Cheeseman, G. Scalmani, V. Barone, B. Mennucci, G.A. Peterson, H. Nakatsuji, M. Caricato, X. Li, H.P. Hratchian, A.F. Izmaylov, J. Bloino, G. Zheng, J.L. Sonnenberg, M. Hada, M. Ehara, K. Toyota, R. Fukuda, J. Hasegawa, T. Nakajima, Y. Honda, O. Kitao, H. Nakai, T. Vreven, J.A. Montgomery Jr., J.E. Peralta, F. Ogliaro, M. Bearpark, J.J. Heyd, E. Brothers, K.N. Kudin, V.N. Staroverov, R. Kobayashi, J. Normand, K. Raghavachari, A. Rendell, J.C. Burant, S.S. Iyengar, J. Tomasi, M. Cossi, N. Rega, J.M. Millam, M. Klene, J.E. Knox, J.B. Cross, V. Bakken, C. Adamo, J. Jaramillo, R. Gomperts, R.E. Stratmann, O. Yazyev, A.J. Austin, R. Cammi, C. Pomelli, J.W. Ochterski, R.L. Martin, K. Morokuma, V.G. Zakrzewski, G.A. Voth, P. Salvador, J.J. Dannenberg, S. Dapprich, A.D. Daniels, Ö. Farkas, J.B. Foresman, J.V. Ortiz, J. Cioslowski, D.J. Fox, *Gaussian 09*, Gaussian, Inc., Wallingford CT, 2009.

[12] M.T. Rodgers, K.M. Ervin, P.B. Armentrout, *Statistical modeling of collision-induced dissociation thresholds*, J. Chem. Phys., 106 (1997) 4499-4508.

[13] M.T. Rodgers, P.B. Armentrout, *Statistical modeling of competitive threshold collision-induced dissociation*, J. Chem. Phys., 109 (1998) 1787-1800.

[14] P.B. Armentrout, K.M. Ervin, M.T. Rodgers, *Statistical Rate Theory and Kinetic Energy-Resolved Ion Chemistry: Theory and Applications*, J. Phys. Chem. A, 112 (2008) 10071-10085.

[15] S.G. Lias, J.E. Bartmess, J.F. Liebman, J.L. Holmes, W.G. Mallard, *NIST Chemistry WebBook*, in: P.J. Lindstrom, W.G. Mallard (Eds.) Ion Energetics Data, National Institute of Standards and Technology, Gaithersburg, MD, 2014.

[16] H.Y. Afeefy, J.F. Liebman, S.E. Stein, *Neutral Thermochemical Data, NIST Chemistry WebBook, NIST Standard Reference Database*, in: P.J. Linstrom, W.G. Mallard (Eds.), National Institute of Standards and Technology, Gaithersburg, 2012.

[17] T. Su, W.J. Chesnavich, *Parametrization of the ion-polar molecule collision rate-constant by trajectory calculations*, J. Chem. Phys., 76 (1982) 5183-5185.

[18] F.C. Fehsenfeld, *Ion chemistry of SF_6*, J. Chem. Phys., 54 (1971) 438-439.

[19] C. Atterbury, R.A. Kennedy, C.A. Mayhew, R.P. Tuckett, *A study of the reactions of trifluoromethyl sulfur pentafluoride, SF_5CF_3, with several positive ions of atmospheric interest*, Phys. Chem. Chem. Phys., 3 (2001) 1949-1953.

[20] R.A. Morris, A.A. Viggiano, S.T. Arnold, J.F. Paulson, *Chemistry of atmospheric ions reacting with fully fluorinated compounds*, Int. J. Mass Spectrom. Ion Process., 149 (1995) 287-298.

[21] F.C. Fehsenfeld, E.E. Ferguson, A.L. Schmeltekopf, *Thermal-Energy Ion-Neutral Reaction Rates. III. The Measured Rate Constant for the Reaction $O^+(^4S)+CO_2(^1\Sigma)\rightarrow O_2^+(^2\Pi)+CO(^1\Sigma)$*, J. Chem. Phys., 44 (1966) 3022-3024.

[22] W. Federer, H. Villinger, W. Lindinger, E.E. Ferguson, *Reactions of some hydrocarbon cations with nitrogen atoms*, Chem. Phys. Lett., 123 (1986) 12-16.

[23] R.Y.L. Chim, R.A. Kennedy, R.P. Tuckett, W.D. Zhou, G.K. Jarvis, D.J. Collins, P.A. Hatherly, *Fragmentation of energy-selected $SF_5CF_3^+$ probed by threshold photoelectron photoion coincidence*

spectroscopy: Bond dissociation energy of SF_5-CF_3 and its atmospheric implications, J. Phys. Chem. A, 105 (2001) 8403-8412.

[24] R.P. Tuckett, T. Alain, *Chapter 3: Trifluoromethyl Sulphur Pentafluoride, SF_5CF_3: Atmospheric Chemistry and Its Environmental Importance via the Greenhouse Effect*, in: Adv. Fluorine Sci., Elsevier, 2006, pp. 89-129.

[25] D.R. Lide, *Handbook of Chemistry and Physics*, CRC Press, New York, NY, 2009.

[26] G.K. Jarvis, R.A. Kennedy, C.A. Mayhew, R.P. Tuckett, *Charge transfer from neutral perfluorocarbons to various cations: long-range versus short-range reaction mechanisms*, Int. J. Mass Spectrom., 202 (2000) 323-343.

[27] S.G. Lias, J.E. Bartmess, J.F. Liebman, J.L. Holmes, W.G. Mallard, *NIST Chemistry WebBook*, in: P.J. Lindstrom, W.G. Mallard (Eds.) Ion Energetics Data, National Institute of Standards and Technology, Gaithersburg, MD, 2013.

[28] J.C. Traeger, *Heat of formation for the formyl cation by photoionization mass-spectrometry*, Int. J. Mass Spectrom. Ion Process., 66 (1985) 271-282.

[29] J.C. Traeger, R.G. McLoughlin, A.J.C. Nicholson, *Heat of formation for acetyl cation in the gas-phase*, J. Am. Chem. Soc., 104 (1982) 5318-5322.

[30] E.T.M. Selim, A.I. Helal, *Heat of formation of $CH_2{=}O^+H$ fragment ion*, Ind. J. Pure & Appl. Phys., 19 (1981) 977-980.

[31] M.A. Haney, J.L. Franklin, *Excess energies in mass spectra of some oxygen-containing organic compounds*, T. Faraday Soc., 65 (1969) 1794-1804.

[32] J.J. Butler, D.M.P. Holland, A.C. Parr, R. Stockbauer, *A threshold photoelectron photoion coincidence spectrometric study of dimethyl ether (CH_3OCH_3)*, Int. J. Mass Spectrom. Ion Process., 58 (1984) 1-14.

[33] P. Warneck, *Photoionisation von Methanol und Formaldehyd*, Zeitschrift Fur Naturforschung, 26 (1971) 2047-2057.

[34] T. Nishimura, Q.M. Zha, G.G. Meisels, *Unimolecular dissociation of energy-selected methyl formate ion*, J. Chem. Phys., 87 (1987) 4589-4597.

[35] A.B. King, F.A. Long, *Mass spectra of some simple esters and their interpretation by quasi-equilibrium theory*, J. Chem. Phys., 29 (1958) 374-382.

[36] S.G. Lias, J.E. Bartmess, J.F. Liebman, J.L. Holmes, R.D. Levin, G.M. Mallard, *Gas-Phase Ion and Neutral Thermochemistry*, American Chemical Society, American Institute of Physics, National Bureau of Standards, New York, NY, 1988.

[37] C.G. Freeman, P.W. Harland, M.J. McEwan, *Thermal-energy charge-transfer reactions of acetone and biacetyl*, Chem. Phys. Lett., 64 (1979) 596-600.

[38] D. Smith, N.G. Adams, T.M. Miller, *Laboratory study of reactions of N^+, N_2^+, N_3^+, N_4^+, O^+, O_2^+, and NO^+ ions with several molecules at 300 K*, J. Chem. Phys., 69 (1978) 308-318.

[39] R.G. Cooks, J.H. Beynon, R.M. Caprioli, G.R. Lester, *Metastable Ions*, Elsevier Scientific Publishing Company, Amsterdam, The Netherlands, 1973.

[40] N.S. Shuman, W.R. Stevens, T. Baer, *Dissociation dynamics of energy-selected acetic acid ions: The gas phase heat of formation of the acetyl ion*, Int. J. Mass Spectrom., 294 (2010) 88-92.

[41] T. Nishimura, Q.M. Zha, P.R. Das, Y. Niwa, G.G. Meisels, *On the dissociation dynamics of energy-selected dimethyl ether ions*, Int. J. Mass Spectrom. Ion Process., 113 (1992) 177-189.

[42] W.J. Bouma, R.H. Nobes, L. Radom, *On the nature of the methoxy cation*, Org. Mass Spectrom., 17 (1982) 315-317.

[43] J.H. Beynon, R.A. Saunders, A.E. Williams, *High resolution mass spectra of aliphatic esters*, Anal. Chem., 33 (1961) 221-225.

[44] D. VanRaalte, A.G. Harrison, *Ionization and dissociation of formate esters by electron impact*, Can. J. Chem.-Rev. Can. Chim., 41 (1963) 2054-2059.

4 Reactivity and Thermochemistry of Dicyanamide: $N(CN)_2^-$

4.1 Introduction

Although they have been known for more than 100 years,[1] ionic liquids, or salts with a melting point ≤ 100 °C, have recently received renewed interest in the chemical literature. Ionic liquids exist with a wide variety of cation and anion components; in fact, their properties can be customized by switching or modifying the cations or anions. As a liquid salt, they have many applications. Some synthetic chemists employ ionic liquids as reusable solvents because of their low vapor pressure,[2] and ionic liquids have even been shown to participate in synthesis reactions.[3] Because of their inherent stability, they are being used as the electrolytic medium in batteries, capacitors, and solar cells.[4, 5] In addition, a number of materials chemists are investigating ionic liquids as next-generation bipropellant hypergolic fuels in efforts to replace hydrazine based fuels; storage of hydrazine based fuels is challenging because of their toxic, corrosive, and volatile nature. Several ionic liquids exhibit hypergolic behavior,[6-12] providing a possible replacement.

Dicyanamide, $N(CN)_2^-$, is a common anion of ionic liquids; as an anion, it exhibits hypergolic behavior when paired with certain cations. Furthermore, dicyanamide generates ionic liquids with relatively low viscosities, allowing for more efficient delivery in propulsion applications. When paired with 1-propargyl-3-methylimidazolium, the resulting ionic liquid melts at 17 °C and is stable up to 144 °C. Upon mixing with white-fuming nitric acid, 1-propargyl-2-methylimidazolium dicyanamide will undergo hypergolic ignition with a 15 ms delay time.[6] An ignition delay time of ≤ 5 ms is preferred for real-world applications; this can be achieved by altering the cation or creating ionic liquid mixtures.[7]

The hypergolic interaction between dicyanamide and nitric acid has been a hot topic of study in the last seven years.[6, 9, 13, 14] In 2008, Chambreau and coworkers proposed that 1,5-dinitrobiuret is formed during the hypergolic reaction between dicyanamide containing ionic liquids and nitric acid.[9] Since this

report, several studies have theoretically investigated the decomposition dynamics of 1,5-dinitrobiuret.[15-17] While dissociation dynamics is a popular topic, fewer studies have focused on the formation pathway of 1,5-dinitrobiuret. This study will computationally investigate energetics of the previously proposed formation pathway[9] of 1,5-dinitrobiuret through stationary points, including transitions states, along a multidimensional reaction coordinate.

In addition to its unique properties in the liquid phase, dicyanamide is one of the very few anions that has been found not to exhibit reactivity with H atom,[18] the most abundant element in the universe. Dicyanamide is believed to be present in the atmosphere of Saturn's moon Titan.[19] It is also likely a component of the dense interstellar clouds where CN^-, C_3N^-, and C_5N^- have been observed.[20-22] Because of its large electron binding energy, 4.135 eV,[23] dicyanamide may survive in regions of the interstellar medium where most anions would undergo photodetachment. This study investigates the reactivity of dicyanamide with many astronomically abundant species, including N and O atoms.

4.2 Experimental

The experiments were carried out at 298 K with a Selected Ion Flow Tube (SIFT) using the home-built electrospray-ionization (ESI) source. To generate the dicyanamide signal, a 6×10^{-5} M solution of sodium dicyanamide (≥96%, Fluka) in acetonitrile (99.8%, Sigma-Aldrich) is used with the ESI source. Typical syringe pump flow rates are 0.2-50 μL/min.

The reactivity of dicyanamide with H_2, O_2, H_2O_2, DBr, HCl, NH_3, N_2O, SO_2, COS, CO_2, CH_3OH, H_2O, CH_4, N_2, CF_4, and SF_6 was also investigated, but the reaction rate constants are below the detection limit. The lack of reactivity for these neutral gases was confirmed by introducing a high flow of the neutral gas into the flow tube at the longest reaction distance. Neither dicyanamide depletion nor new ionic products were observed.

We have also investigated the reactivity of dicyanamide with ground state N and O atoms, which were introduced into the reaction flow tube by use of a microwave discharge. Microwave generation of N and O atoms is a well-established technique and has been described in Chapter 2. The N atoms are generated by flowing (~0.6 STP cm^3/s) N_2 gas (99.999%, Airgas) through an Evenson cavity supplied with 50 W of microwave radiation. The overall efficiency of generating N atoms from this technique is approximately 1–3%. The O atoms are then formed by titrating the N atoms with NO (4% in He, Airgas), which forms ground state O atom by the reaction $N + NO \rightarrow N_2 + O$. The titration endpoint for this process is found by plotting the natural log of the ion signal as a function of NO flow. The titration endpoint reveals the concentration of O atoms introduced in the flow tube and subsequently determines the initial concentration of N atoms in the absence of NO. The microwave discharge is also used to obtain excited state O_2 molecules, O_2 ($^1\Delta$). This experiment is performed by flowing O_2 through the microwave discharge. Although no reactivity of dicyanamide anion with N(^{4}S), O(^{3}P), and O_2($^1\Delta$) was observed, the presence of these neutral reactants was confirmed by studies with other ions that are known to be reactive.

To investigate the reactivity of dicyanamide with sulfuric acid, we coupled a low-volatility neutral reagent inlet to our reaction flow tube by adapting the methods used by Viggiano et al.[24] A Pyrex bulb was filled with glass wool, and then fitted on both ends with 6 mm Pyrex tubing. Approximately 1 mL of sulfuric acid was added to the glass wool. A flow of N_2 (~0.2 STP cm^3/s, UHP, Airgas) enters the glass bulb through a metering valve and flowmeter, and carries sulfuric acid into the flow tube. The glass bulb and reagent inlet were heated to approximately 100 °C. Although no reaction was observed between sulfuric acid and dicyanamide, the presence of sulfuric acid was verified by investigating its proton transfer reaction with NO_3^-, which occurs at the collision rate ($k \sim 2.6 \times 10^{-9}$ cm^3/s).[25] Proton transfer was confirmed by observing the loss of NO_3^- and generation of HSO_4^-.

4.3 Calculations

Intermediates and transition states along the potential energy surface for the interaction of dicyanamide with two nitric acid molecules were computed at the B3LYP/Aug-cc-pVDZ level of theory. The acidities of dicyanamide, and the optimized geometries of dicyanamide clusters with nitric acid are reported using the MP2/6-311++G(d,p) level of theory; MP2/6-311++G(d,p) provides good agreement with experimental results in our previous studies.[26-28] All theoretical thermochemical values are reported in terms of enthalpy. The values have been corrected for zero-point energy using the rigid-rotor–harmonic-oscillator approximation at 298 K. Transition states were verified by the existence of one imaginary vibrational frequency and confirmed with IRC calculations. Optimized intermediates contain no imaginary frequencies. Cartesian coordinates for the optimized geometries are reported in Appendix B.

4.4 Results and Discussion

The dicyanamide anion is a very stable species with an experimental electron-binding energy of 4.135 ± 0.010 eV.[23] Our work explored its reactivity with several neutrals. In efforts to characterize the reactivity of dicyanamide in the gas-phase, we explored its reactivity with HNO_3, H_2SO_4, H, N, O, O_2, H_2O_2, DBr, HCl, NH_3, N_2O, SO_2, COS, CO_2, CH_3OH, H_2O, CH_4, N_2, CF_4, and SF_6.

However, only one neutral reagent, nitric acid, reacted rapidly enough with dicyanamide for product detection by the SIFT technique. The reaction of dicyanamide with nitric acid occurs with a pseudo-first order reaction rate constant of 2.7×10^{-10} cm^3/s. Only one direct product, the cluster of nitric acid with dicyanamide, was observed. However, subsequent addition of another nitric acid was observed as a secondary product.

For the unreactive neutral reagents, we can place an upper limit on their reaction rate constants. These values are estimated based on discernible ion-signal depletion and the number density of the neutral reagent that can be introduced into the reaction flow tube. For the neutral reagents generated from

microwave discharge plasmas, i.e., N, O, and $O_2(^1\Delta)$, as well as for sulfuric acid which has low volatility, we designate an upper limit to the reaction rate constant of 5×10^{-12} cm^3/s. For the neutral reagents with high vapor pressures, i.e. O_2, H_2O_2, DBr, HCl, NH_3, N_2O, SO_2, COS, CO_2, CH_3OH, H_2O, CH_4, N_2, CF_4, and SF_6, we assign an upper limit to their reaction rate constant of 1×10^{-12} cm^3/s. The lack of reactivity with $O(^3P)$ and $O_2(^1\Delta)$ is surprising, as these reagents are highly reactive with a wide variety of reagents. The absence of reactivity with H_2SO_4 allows us to put an upper limit on the acidity of the parent molecule, HNCNCN, of $\Delta H_{acid} < 309.6 \pm 5.4$ kcal/mol.

The lack of reactivity of dicyanamide has some important interstellar implications, i.e., dicyanamide could survive the harsh chemical conditions of the interstellar medium as it will not react with the abundant atomic species, H, $O(^3P)$, and $N(^4S)$. Furthermore, the neutral molecules NH_3, H_2O, CH_3OH, H_2, COS, SO_2, CH_4, N_2O, N_2, and O_2 have been detected in the ISM,[29-38] but our experimental results show no detectable reactivity with dicyanamide. Additionally, a recent rendezvous of Saturn's moon Titan by the Cassini spacecraft provided a negative-ion mass spectrum of Titan's nitrogen- and methane-rich atmosphere. Dicyanamide is inferred to be present, as there is a strong presence of m/z 66 and several other peaks corresponding to adducts of m/z 66 with neutral species, including HCN, HCCH, and H_2.[19] The presence of dicyanamide is not surprising, since the components of dicyanamide, i.e., N and C atoms, are abundant in Titan's atmosphere. The intense ionization environment intrinsic to planetary atmospheres could provide a synthesis route for dicyanamide, and upon its formation dicyanamide will be long lived due to its chemical stability. A laboratory study of the microwave spectrum of dicyanamide—which is a bent molecule with a calculated dipole of approximately 1 Debye—would allow observational astronomers to search for its presence in the interstellar medium.

4.4.1 Formation of 1,5-dinitrobiuret

The mixing of nitric acid with ionic liquids containing the dicyanamide anion results in hypergolic behavior.[6] For this reason, the fundamental interaction between nitric acid and dicyanamide is of great

interest. An insightful study by Chambreau and coworkers acquired infrared spectra of the evolved vapor of 1-butyl-3-methylimidizole dicyanamide with nitric acid.[9] Their work suggests a mechanism where dicyanamide interacts with two nitric acid molecules to form deprotonated 1,5-dinitrobiuret; their studies computationally defined the thermochemical energetics of several reactions. However, they did not characterize the entire mechanism; therefore, we have calculated stationary points along a multidimensional surface for the gas-phase interaction of dicyamide with one and two nitric acid molecules to form dicyanamide (Figure 4.1).

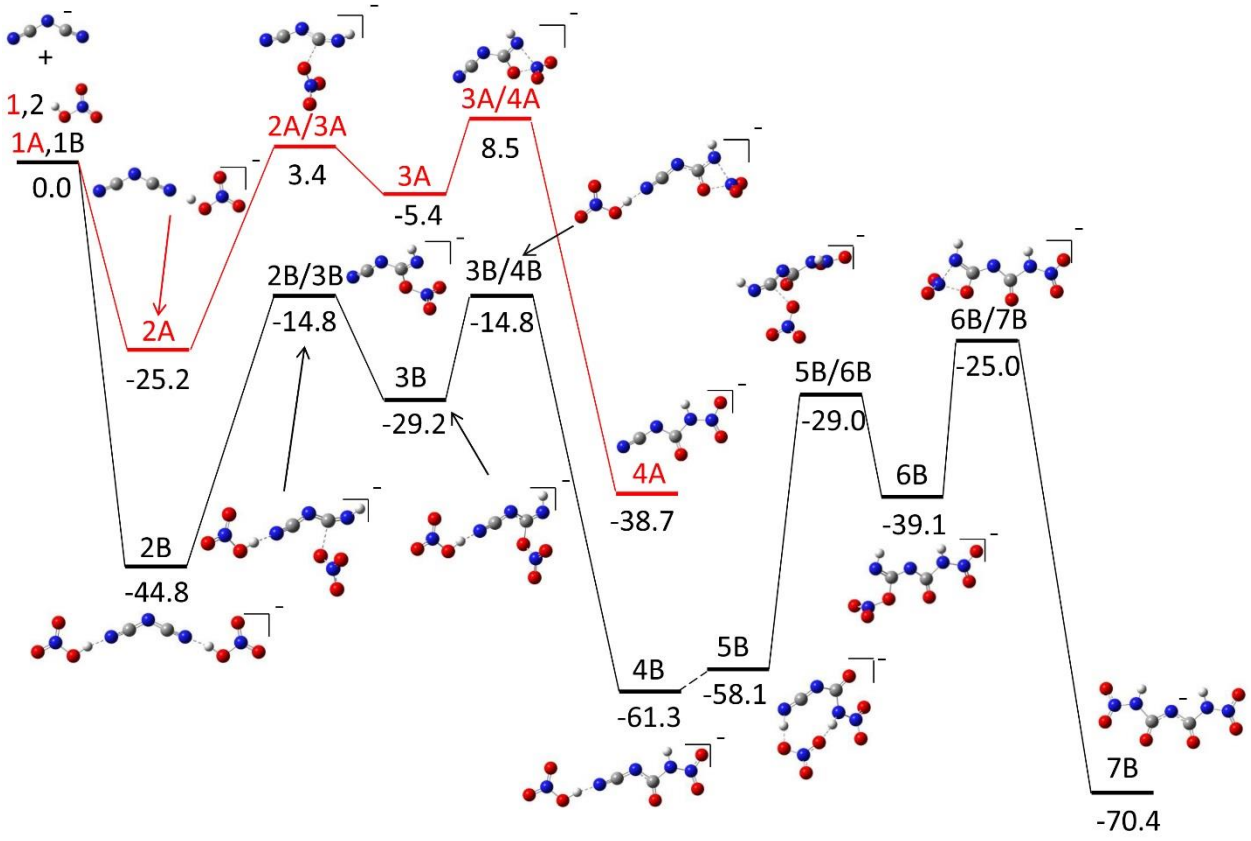

Figure 4.1. Stationary points for the reaction of dicyanamide with two nitric acid molecules
The multi-dimensional potential energy surface provided above shows the interaction of dicyanamide with two nitric acid molecules to form deprotonated 1,5-dinitrobiuret [7B]. The energies listed are calculated with the B3LYP/Aug-cc-pVDZ method, and presented in units of kcal/mol. Geometries are posted in Appendix B.

The multidimensional potential energy diagram of dicyanamide with nitric acid to form 1,5-dinitrobiuret illuminates several interesting points. First, the formation of dicyanamide-nitric acid clusters are highly exothermic by 25 kcal/mol [2A] and 45 kcal/mol [2B] for the addition of one or two nitric acid molecules, respectively. Second, for our experiment, the interaction of dicyanamide with one nitric acid is limited to forming the hydrogen-bonded cluster [2A] because transferring the nitrate to the nitrile carbon [3A] must overcome an endothermic barrier of 3 kcal/mol [2A/3A]. Conversely, the addition of a second nitric acid lowers the transition states below the energy of the reactants, therefore supporting Chambreau's proposed formation of 1,5-dinitrobiuret.[9] Although it is possible that we are generating 1,5-dinitrobiuret as a secondary product in our flow tube, we cannot confirm the structure; in our experiment, products such as [2B], [3B], [4B], etc. cannot be differentiated because they possess the same mass-to-charge ratio. Finally, the terminal product on the potential energy surface, deprotonated 1,5-dinitrobiuret [7B], is 70 kcal/mol lower in energy than dicyanamide with two nitric acid molecules, suggesting a strong thermodynamic driving force for the formation of 1,5-dinitrobiuret.

4.4.2 Dicyanamide Proton Affinity and Solvent Molecule Affinity

An important mechanistic step in the formation of 1,5-dinitrobiuret is proton transfer between nitric acid and dicyanamide. Chambreau's method of forming 1,5-dinitrobiuret requires proton transfer from nitric acid to dicyanamide, followed by subsequent nucleophilic attack on the carbon atom of protonated dicyanamide by nitrate. While our experimental findings provide us with an upper limit for the proton affinity of dicyanamide ($< 310 \pm 5$ kcal/mol), we have further investigated the acidity of dicyanamide computationally with a higher level of theory than was previously reported in the literature, and the lowest energy structures for the two protonated forms of dicyanamide are shown in Figure 4.2.

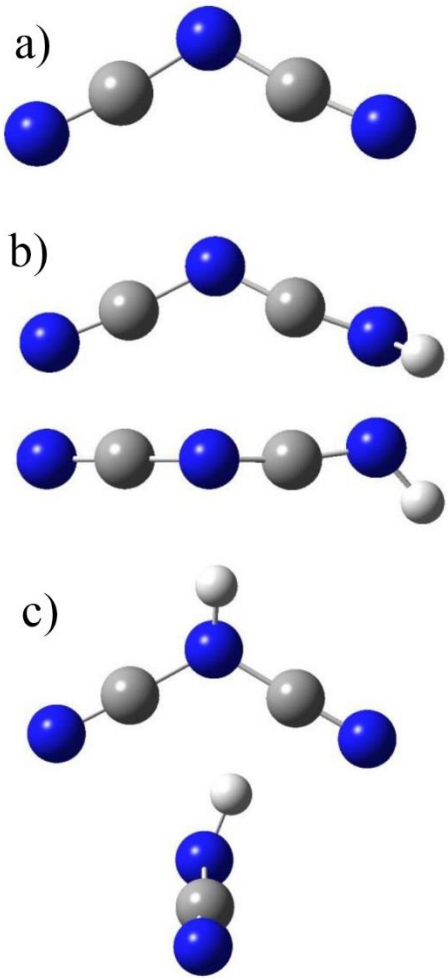

Figure 4.2 Lowest energy structures for dicyanamide and protonated dicyanamide
(a) dicyanamide, (b) terminally protonated dicyanamide, and (c) centrally protonated dicyanamide, optimized at the MP2/6-311++G(d,p) level of theory. Geometries posted in Appendix B.

As illustrated, dicyanamide has two protonation sites: the terminal nitrile and central nitrogen. Our computational studies, as well as computational and experimental reports from the literature, conclude that it is more favorable to protonate dicyanamide on the terminal nitrile nitrogen than on the central nitrogen.[9, 39] The B3LYP/6-31+G(d,p) calculations reported by Chambreau et al. and the MP2/6-311++G(d,p) calculations from this work indicate that protonation on the terminal nitrile nitrogen is more favorable than on the central nitrogen by 7.6 and 1.2 kcal/mol, respectively.[9] This discrepancy might arise from differences in the optimized geometry of the centrally protonated tautomer. The optimization of

centrally protonated dicyanamide (Figure 4.2c) at the MP2/6-311++G(d,p) level of theory positions the hydrogen atom out of the molecular plane. This is distinctive between the two levels of theory used, for the same tautomer optimized at the B3LYP level, positioned the hydrogen atom within the molecular-plane, thereby preserving the intrinsic C_{2V} symmetry of dicyanamide. In moving from B3LYP/6-31+G(d,p) to MP2/6-311++G(d,p), the acidity of the terminally and centrally protonated tautomers changed by -1.9 and 4.5 kcal/mol, respectively, further suggesting that the shift in acidity value for the centrally protonated tautomer occurred in large part due to the differences in the optimized geometry. Nevertheless, even when structures are nearly identical, different theoretical methods can provide different energetic values. Further experimental and computational investigation would be valuable to provide a better understanding of the proton affinity of dicyanamide.

The question remains: is it possible for dicyanamide to accept a proton from nitric acid? From thermodynamic considerations, when dicyanamide encounters a single nitric acid molecule at room temperature, proton transfer is not observed. Theoretical results support this observation; despite the level of theory, proton transfer from nitric acid to dicyanamide is endothermic by at least 15 kcal/mol.

We therefore have conducted calculations to examine higher order clusters of dicyanamide with nitric acid to explore how proton transfer energetics change as a function of the number of nitric acid molecules in the cluster. Figure 4.3 shows the optimized geometry of dicyanamide with one, two, and three nitric acid molecules.

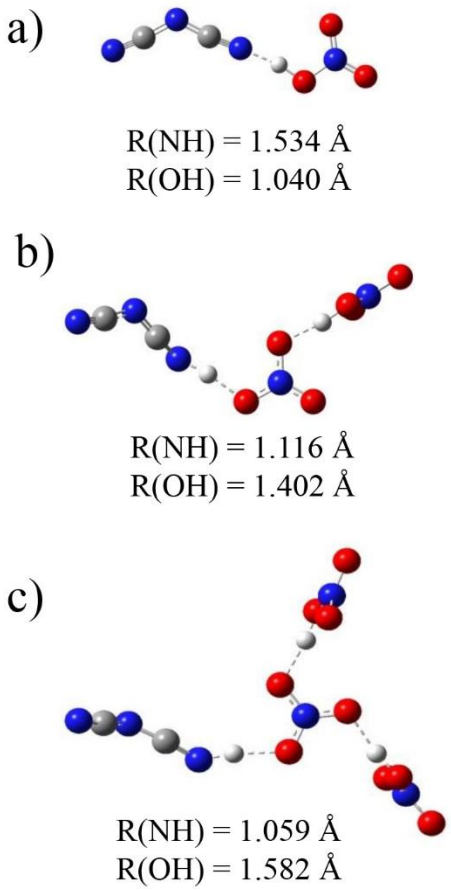

Figure 4.3 Lowest energy structures of dicyanamide clustered with nitric acid
Dicyanamide clustered with one (a), two (b), and three (c) nitric acid molecules optimized at the MP2/g-311++G(d,p) level of theory. Geometries posted in Appendix B.

When a bimolecular cluster between dicyanamide and one nitric acid forms, the hydrogen-bonded proton resides predominantly on the oxygen atom of nitrate (Figure 4.3a). However, when an additional nitric acid is added to the cluster, the lowest-energy structure locates the shared proton predominantly on dicyanamide (Figure 4.3b). Furthermore, adding a third nitric acid molecule onto the final-unoccupied nitrate oxygen (Figure 4.3c) results in a structure where the dicyanamide hydrogen bond length is ~0.5 Å shorter than the oxygen-hydrogen bond length.

To further investigate the effects of clustering, the thermochemistry of proton transfer between dicyanamide and nitric acid was investigated for the following reaction.

$NCNCN^-(HNO_3)_n + HNO_3 \rightarrow NCNCNH + NO_3^-(HNO_3)_n$

The thermodynamic values below are reported for proton transfer to the terminal nitrile nitrogen. For this reaction, when n = 0, the zero-point-thermally-corrected enthalpy for reaction at the MP2/6-311++G(d,p) level of theory is 16.6 kcal/mol endothermic. Therefore, in the bimolecular interaction of dicyanamide with nitric acid, proton transfer would not occur. Increasing the solvation of dicyanamide with nitric acid such that n = 1 decreases the endothermicity from 16.6 to 9.8 kcal/mol. Subsequently increasing the solvation to n = 2 and n = 3 further reduces the endothermicity of proton transfer to 4.7 and 3.0 kcal/mol, respectively. This trend and the results from Figure 4.3 suggest that proton transfer can occur when dicyanamide encounters a cluster of nitric acid molecules such as is possible on the surface of a nitric acid droplet.

The interaction of dicyanamide-containing ionic liquids with nitric acid has been of increasing interest because these liquids hold promise as a next-generation hypergolic fuel. The results of this study suggest that interactions at the gas-liquid or liquid-liquid interface are very important for hypergolic ignition. Indeed, hypergolic reactivity occurs when a macroscopic droplet of ionic liquid is added to a cuvette containing a macroscopic quantity of nitric acid.[6] For our gas-phase studies, we have determined that solvation of dicyanamide by nitric acid is highly exothermic, and this excess energy can be used to promote energetic chemistry such as, but not limited to, proton transfer; even though the self-sustaining hypergolic reactions are only observed when dicyanamide is paired with certain cations such as 1-propargyl-3-methylimidazolium, 'reactivity' is observed even when dicyanamide is paired with inert cations such as Na^+ or 1-butyl-3-methylimidazolium.[9, 13]

4.5 Conclusion

The dicyanamide anion is extremely stable, and exhibits no reactivity with a variety of neutral reagents, including H_2SO_4, H, N, O, and $O_2(^1\Delta)$. However, dicyanamide readily clusters with nitric acid, and the ionic adducts are detected in our studies. Our computational results indicate that the association

of dicyanamide and nitric acid is exothermic by about 25 kcal/mol. This energy may be responsible for initiating the hypergolic phenomenon that is observed when the two liquids are mixed.

The intrinsic stability of dicyanamide suggests that it may exist in many astrochemical environments; measurement of the microwave spectrum of this anion would allow observational astronomers to search for this species in the interstellar medium.

4.6 References

[1] C.A. Angell, Y. Ansari, Z.F. Zhao, *Ionic Liquids: Past, present and future*, Faraday Discuss., 154 (2011) 9-27.

[2] J.J. Jodry, K. Mikami, *Ionic Liquids*, in: K. Mikami (Ed.) Green reaction media in organic synthesis, Blackwell Publishing Ltd, Kundli, 2005, pp. 9-54.

[3] C. Chiappe, D. Pieraccini, *Ionic liquids: solvent properties and organic reactivity*, J. Phys. Org. Chem., 18 (2005) 275-297.

[4] J.F. Wishart, *Energy applications of ionic liquids*, Energy Environ. Sci., 2 (2009) 956-961.

[5] M. Armand, F. Endres, D.R. MacFarlane, H. Ohno, B. Scrosati, *Ionic-liquid materials for the electrochemical challenges of the future*, Nat. Mater., 8 (2009) 621-629.

[6] S. Schneider, T. Hawkins, M. Rosander, G. Vaghjiani, S. Chambreau, G. Drake, *Ionic liquids as hypergolic fuels*, Energy Fuels, 22 (2008) 2871-2872.

[7] S.Q. Li, H.X. Gao, J.M. Shreeve, *Borohydride Ionic Liquids and Borane/Ionic-Liquid Solutions as Hypergolic Fuels with Superior Low Ignition-Delay Times*, Angew. Chem.-Int. Edit., 53 (2014) 2969-2972.

[8] S. Schneider, T. Hawkins, Y. Ahmed, M. Rosander, L. Hudgens, J. Mills, *Green Bipropellants: Hydrogen-Rich Ionic Liquids that Are Hypergolic with Hydrogen Peroxide*, Angew. Chem.-Int. Edit., 50 (2011) 5886-5888.

[9] S.D. Chambreau, S. Schneider, M. Rosander, T. Hawkins, C.J. Gallegos, M.F. Pastewait, G.L. Vaghjiani, *Fourier transform infrared studies in hypergolic ignition of ionic liquids*, Journal of Physical Chemistry A, 112 (2008) 7816-7824.

[10] P.D. McCrary, G. Chatel, S.A. Alaniz, O.A. Cojocaru, P.A. Beasley, L.A. Flores, S.P. Kelley, P.S. Barber, R.D. Rogers, *Evaluating ionic liquids as hypergolic fuels: Exploring reactivity from molecular structure*, Energy Fuels, 28 (2014) 3460-3473.

[11] Q.H. Zhang, P. Yin, J.H. Zhang, J.M. Shreeve, *Cyanoborohydride-Based Ionic Liquids as Green Aerospace Bipropellant Fuels*, Chem.-Eur. J., 20 (2014) 6909-6914.

[12] Y.Q. Zhang, J.M. Shreeve, *Dicyanoborate-Based Ionic Liquids as Hypergolic Fluids*, Angew. Chem.-Int. Edit., 50 (2010) 935-937.

[13] T. Litzinger, S. Iyer, *Hypergolic Reaction of Dicyanamide-Based Fuels with Nitric Acid*, Energy Fuels, 25 (2010) 72-76.

[14] L. Catoire, S.D. Chambreau, G.L. Vaghjiani, *Chemical kinetics interpretation of hypergolicity of dicyanamide ionic liquid-based systems*, Combust. Flame, 159 (2011) 1759-1768.

[15] R. Sun, M.R. Siebert, L. Xu, S.D. Chambreau, G.L. Vaghjiani, H. Lischka, J. Liu, W.L. Hase, *Direct dynamics simulation of the activation and dissociation of 1,5-dinitrobiuret (HDNB)*, Journal of Physical Chemistry A, 118 (2014) 2228-2236.

[16] M.F. Russo, D. Bedrov, S. Singhai, A.C.T. van Duin, *Combustion of 1,5-dinitrobiuret (DNB) in the presence of nitric acid using ReaxFF molecular dynamics simulations*, Journal of Physical Chemistry A, 117 (2013) 9216-9223.

[17] J.B. Liu, S.D. Chambreau, G.L. Vaghjiani, *Thermal decomposition of 1,5-dinitrobiuret (DNB): direct dynamics trajectory simulations and statistical modeling*, Journal of Physical Chemistry A, 115 (2011) 8064-8072.

[18] Z. Yang, C.A. Cole, O. Martinez, M.Y. Carpenter, T.P. Snow, V.M. Bierbaum, *Experimental and theoretical studies of reactions between H atoms and nitrogen-containing carbanions*, Astrophys. J., 739 (2011) 10.

[19] A. Somogyi, M.A. Smith, V. Vuitton, R. Thissen, I. Komaromi, *Chemical ionization in the atmosphere? A model study on negatively charged "exotic" ions generated from Titan's tholins by ultrahigh resolution MS and MS/MS*, Int. J. Mass Spectrom., 316 (2012) 157-163.

[20] P. Thaddeus, C.A. Gottlieb, H. Gupta, S. Brunken, M.C. McCarthy, M. Agundez, M. Guelin, J. Cernicharo, *Laboratory and astronomical detection of the negative molecular ion C_3N^-*, Astrophys. J., 677 (2008) 1132-1139.

[21] J. Cernicharo, M. Guelin, M. Agundez, M.C. McCarthy, P. Thaddeus, *Detection of C_5N^- and vibrationally excited C_6H in IRC+10216*, Astrophys. J. Lett., 688 (2008) L83-L86.

[22] M. Agundez, J. Cernicharo, M. Guelin, C. Kahane, E. Roueff, J. Klos, F.J. Aoiz, F. Lique, N. Marcelino, J.R. Goicoechea, M.G. Garcia, C.A. Gottlieb, M.C. McCarthy, P. Thaddeus, *Astronomical identification of CN^-, the smallest observed molecular anion*, Astron. Astrophys., 517 (2010) 5.

[23] B. Jagoda-Cwiklik, X.B. Wang, H.K. Woo, J. Yang, G.J. Wang, M.F. Zhou, P. Jungwirth, L.S. Wang, *Microsolvation of the dicyanamide anion: $[N(CN)_2^-](H_2O)_n$ (n=0-12)*, Journal of Physical Chemistry A, 111 (2007) 7719-7725.

[24] A.A. Viggiano, J.V. Seeley, P.L. Mundis, J.S. Williamson, R.A. Morris, *Rate constants for the reactions of $XO_3^-(H_2O)_n$ (X = C, HC, and N) and $NO_3^-(HNO_3)_n$ with H_2SO_4: Implications for atmospheric detection of H_2SO_4*, Journal of Physical Chemistry A, 101 (1997) 8275-8278.

[25] A.A. Viggiano, R.A. Perry, D.L. Albritton, E.E. Ferguson, F.C. Fehsenfeld, *Stratospheric negative-ion reaction-rates with H_2SO_4*, Journal of Geophysical Research-Oceans and Atmospheres, 87 (1982) 7340-7342.

[26] D.L. Thomsen, J.N. Reece, C.M. Nichols, S. Hammerum, V.M. Bierbaum, *Investigating the alpha-effect in gas-phase S_N2 reactions of microsolvated anions*, J. Am. Chem. Soc., 135 (2013) 15508-15514.

[27] D.L. Thomsen, C.M. Nichols, J.N. Reece, S. Hammerum, V.M. Bierbaum, *The alpha-effect and competing mechanisms: The gas-phase reactions of microsolvated anions with methyl formate*, J. Am. Soc. Mass Spectrom., 25 (2014) 159-168.

[28] D.L. Thomsen, J.N. Reece, C.M. Nichols, S. Hammerum, V.M. Bierbaum, *The alpha-effect in gas-phase S_N2 reactions of microsolvated anions: Methanol as a solvent*, Journal of Physical Chemistry A, 118 (2014) 8060-8066.

[29] A.C. Cheung, D.M. Rank, C.H. Townes, D.D. Thornton, W.J. Welch, *Detection of NH_3 molecules in the interstellar medium by their microwave emission*, Physical Review Letters, 21 (1968) 1701-1705.

[30] A.C. Cheung, D.M. Rank, C.H. Townes, D.D. Thornton, W.J. Welch, *Detection of water in interstellar regions by its microwave radiation*, Nature, 221 (1969) 626-628.

[31] J.A. Ball, C.A. Gottlieb, A.E. Lilley, H.E. Radford, *Detection of methyl alcohol in Sagittarius*, Astrophys. J., 162 (1970) L203-L210.

[32] G.R. Carruthe, *Rocket observation of interstellar molecular hydrogen*, Astrophys. J., 161 (1970) L81-L85.

[33] K.B. Jefferts, A.A. Penzias, R.W. Wilson, P.M. Solomon, *Detection of interstellar carbonyl sulfide*, Astrophys. J., 168 (1971) L111-L113.

[34] L.E. Snyder, J.M. Hollis, B.L. Ulich, F.J. Lovas, D.R. Johnson, D. Buhl, *Radio detection of interstellar sulfur-dioxide*, Astrophys. J., 198 (1975) L81-L84.

[35] J.H. Lacy, J.S. Carr, N.J. Evans, F. Baas, J.M. Achtermann, J.F. Arens, *Discovery of interstellar methane - observations of gaseous and solid CH_4 absorption toward young stars in molecular clouds*, Astrophys. J., 376 (1991) 556-560.

[36] L.M. Ziurys, A.J. Apponi, J.M. Hollis, L.E. Snyder, *Detection of interstellar N_2O - A new molecule containing an N-O bond*, Astrophys. J., 436 (1994) L181-L184.

[37] D.C. Knauth, B.G. Andersson, S.R. McCandliss, H.W. Moos, *The interstellar N_2 abundance towards HD 124314 from far-ultraviolet observations*, Nature, 429 (2004) 636-638.

[38] P.F. Goldsmith, R. Liseau, T.A. Bell, J.H. Black, J.H. Chen, D. Hollenbach, M.J. Kaufman, D. Li, D.C. Lis, G. Melnick, D. Neufeld, L. Pagani, R. Snell, A.O. Benz, E. Bergin, S. Bruderer, P. Caselli, E. Caux, P. Encrenaz, E. Falgarone, M. Gerin, J.R. Goicoechea, A. Hjalmarson, B. Larsson, J. Le Bourlot, F. Le Petit, M. De Luca, Z. Nagy, E. Roueff, A. Sandqvist, F. van der Tak, E.F. van Dishoeck, C. Vastel, S. Viti, U. Yildiz, *Herschel measurements of molecular oxygen in Orion*, Astrophys. J., 737 (2011) 17.

[39] B.V. Lotsch, J. Senker, W. Schnick, *Characterization of the thermally induced topochemical solid-state transformation of $NH_4[N(CN)_2]$ into $NCN=C(NH_2)_2$ by the means of X-ray and neutron diffraction as well as Raman and solid-state NMR spectroscopy*, Inorg. Chem., 43 (2004) 895-904.

5 Gas-Phase Acidities of the Nitrated Azoles

5.1 Introduction

Azoles, five-membered aromatic rings in which one or more CH is replaced by N, are important organic compounds relevant to biological and material sciences. Pyrrole and imidazole, two of the simplest azoles, are found naturally as components of the amino acids tryptophan and histidine, the nucleobases adenine and guanine, and heme B. Because of the strong electron donor interaction of the nitrogen atoms, pyrazole and imidazole are known to coordinate with metal ions as stable ligands.[1] Furthermore, azole compounds are ubiquitous components of ionic liquids. Although ionic liquids have been known for over 100 years,[2] there has been a resurgence of interest in their application and characterization. These compounds are unusual because their melting point is ≤ 100 °C. This property has led to the use of ionic liquids as reusable green solvents because of their low vapor pressure.[3] Because of their stability, these compounds are finding use as novel electrolytic compounds in batteries, capacitors, and solar cells.[4, 5] Additionally, ionic liquids are under study for use as a next-generation hypergolic fuel[6] and as the ionic medium in ion thrusters.[7] In some cases, modified azole compounds have found use as both the cationic and anionic species in ionic liquids.[8, 9] For example, 4-nitroimidazolate, an anion studied herein, has been combined with 1-butyl-3-methylimidazolium to produce a compound that melts at –63 °C and is thermally stable to 185 °C.[9] In this work, we examine the gas-phase acidity of several nitrated azoles in an effort to characterize the stability of their conjugate bases, i.e., their corresponding anions. The nitrated molecules of this study, illustrated in Figure 5.1 below the parent azoles, vary by the placement of the ring-nitrogen atom, as well as the placement of the nitro group.

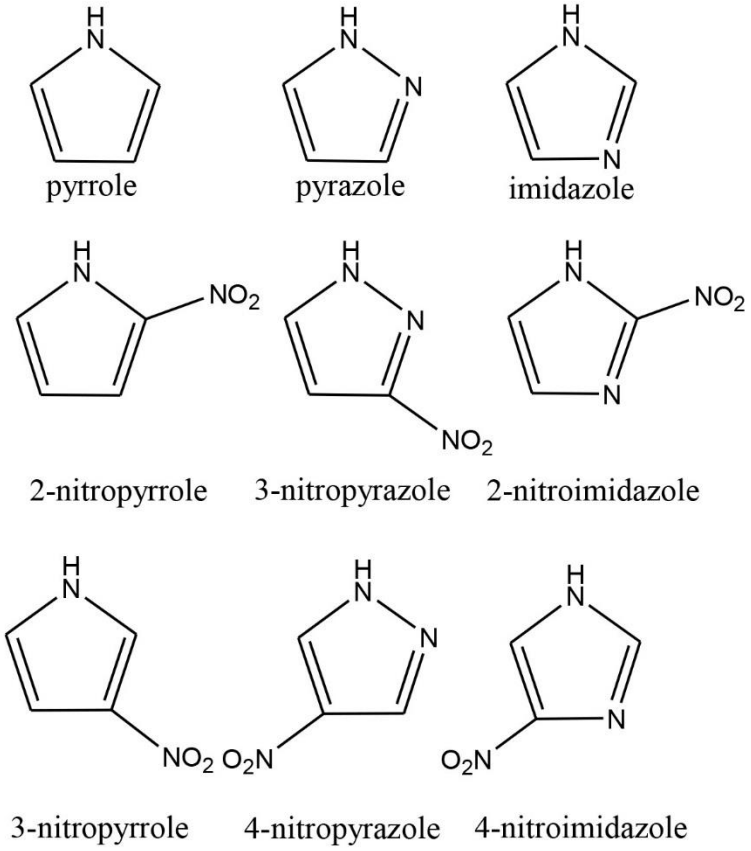

Figure 5.1 Selected azoles and their nitrated derivatives.
The acidic hydrogen is indicated on the pertinent nitrogen atom.

The gas-phase acidity of molecules is of fundamental interest to many chemists. This property reflects the intrinsic stabilities of molecules and their deprotonated anions. It is common practice to determine the acidity of molecules by relative methods that compare a molecule of unknown acidity to one for which the acidity has been previously determined. Several mass-spectrometry approaches are used to study the relative gas-phase acidities of molecules including proton-transfer equilibrium,[10-16] bracketing,[17, 18] and the kinetic method.[19-28] Historically, our lab has used the Flowing Afterglow-Selected Ion Flow Tube (FA-SIFT) to determine the gas-phase acidity of molecules.[14-17] However, we were not able to use the FA-SIFT for this study because both the nitroazoles and the reference organic acids are not sufficiently

volatile. Instead, we employed Cook's kinetic method[20] and a triple quadrupole instrument to determine the gas-phase acidities of the nitrated azoles.

The kinetic method is a competitive dissociation technique that examines the relative proton affinity of two anions (gas-phase acidity) or two neutrals (proton affinity). The technique monitors the collision induced fragmentation of anionic–proton-bound–hetero dimers. (Scheme 5.1)

$$[A_0\text{—}H\text{—}A_i]^- + N_2 \xrightarrow{k_i} HA_0 + A_i^- + N_2$$
$$\xrightarrow{k_0} A_0^- + HA_i + N_2$$

Scheme 5.1 Competitive dissociation of anionic proton-bound heterodimers

In Scheme 5.1, HA_i represents a series of reference acids with known gas-phase acidities, and HA_0 represents a compound of unknown acidity. The ratio of the intensities of the two product ions (A_i^- and A_0^-) is directly related to the ratio of the two rate constants (k_i and k_0). N_2 is the collision gas used for this experiment.

The kinetic method has been used extensively over the last 20 years. The extended kinetic method, an improvement over Cook's standard method,[20] was introduced by Fensleau and coworkers.[23] This approach requires that the reference acids are functionally similar among themselves, but different from the unknown acid under investigation. This allows the assumption that the entropic contributions for proton transfer between the unknown and reference acid anions are constant [$\Delta\Delta S°(HA_0,HA_i) = \Delta S°_{acid}(HA_i) - \Delta S°_{acid}(HA_0) \approx$ constant]. This assumption becomes a good approximation when the reference acids are thoughtfully chosen to be similar in structure as well as functionality. The extended kinetic method also requires that the tandem mass spectrometry experiments are performed over multiple collision activation conditions. To perform the analysis, the logarithms of the ratio of the two rate

constants ($\ln[k_i/k_0]$) from Scheme 5.1 are plotted against proton affinities of the reference anions, $\Delta H°_{acid}(HA_i)$. This provides the relationship:

$$ln\frac{[A_i^-]}{[A_0^-]} \approx ln\frac{k_i}{k_0} \approx -\frac{\Delta H^\circ_{acid}(HA_i)}{RT_{eff}} + \frac{GA^{app}(HA_0)}{RT_{eff}} \qquad \textbf{5.1}$$

In equation 5.1, the apparent gas-phase acidity term, GA^{app}, is the analog of the apparent gas-phase basicity introduced by Wesdemiotis and coworkers.[24] At the x-intercept (where the ratio of k_i/k_0 equals 1), $GA^{app}(HA_0) = \Delta H°_{acid}(HA_i)$. The effective temperature (T_{eff}) represents the internal energy of the collisionally activated heterodimer. It is not a true thermodynamic temperature, but rather a measure of the distribution of the energy available to the dimer.[22, 29, 30] When $\ln[A_i^-/A_0^-]$ is plotted against $\Delta H°_{acid}(HA_i)$, a linear regression is obtained with slope equal to $-1/RT_{eff.}$ Each unique collision activation condition provides a characteristic T_{eff} and $GA^{app}(HA_0)$. Because the extended kinetic method requires the use of multiple activation conditions, multiple T_{eff} and $GA^{app}(HA_0)$ values are obtained. The $GA^{app}(HA_0)$ values are then plotted versus T_{eff} using the relationship:

$$GA^{app}(HA_0) = \Delta H°_{acid}(HA_0) - T_{eff}\Delta\Delta S^\circ(HA_0, HA_i) \qquad \textbf{5.2}$$

For equation 5.2, $\Delta\Delta S°(HA_0,HA_i)$ is provided by the slope of the line, while determination of the y-intercept gives $\Delta H°_{acid}(HA_0)$. This two plot technique for determining $\Delta H°_{acid}(HA_0)$ was first introduced by Armentrout[25] as the "alternative method."

More recently, another method for analyzing extended kinetic method data, called the 'Orthogonal Distance Regression (ODR)' by Ervin and Armentrout[26] or the 'isoequilibrium (or isothermal) point' method by Bouchoux et al.[19] has been described. Instead of using two plots to find $\Delta H°_{acid}(HA_0)$, the isoequilibrium method determines the values of $\Delta H°_{acid}(HA_0)$ and $\Delta\Delta S°(HA_0,HA_i)$ from a single plot in which the linear regressions of $\ln(k_i/k_0)$ vs. $\Delta H°_{acid}(HA_i)$ have converged to a single point, called the isoequilibrium point.[19, 27] Problematically, several experiments have shown the existence of multiple

isoequilibrium points.[21] Therefore, a treatment has been developed which forces the convergence of an isoequilibrium point.[26, 28] However, it has been found that results for data analyzed using the isoequilibrium and alternative methods deviate by less than 0.5 kcal/mol when compared over the same collision energy range.[21]

5.2 Experimental

The MS/MS experiments were performed on a QTrap 4000 (AB SCIEX, Toronto, Canada),[31] triple quadrupole mass spectrometer; the QTrap is described in detail in Chapter 2. Using ESI allowed facile introduction of the proton-bound hetero dimers into the gas-phase. The QTrap is used to perform collision induced dissociation (CID) on the mass-selected proton-bound heterodimers, Scheme 5.1. Collision energies from 5–22 eV (lab frame) are used. The collision energies are not corrected for perturbations of the true zero of energy, nor are they corrected for multiple collision events. The intensity of ion fragments and undissociated parent ions are monitored with Q_3, which is coupled to an electron multiplier. Typical, raw CID spectra from a kinetic method experiment are shown in Figure 5.2.

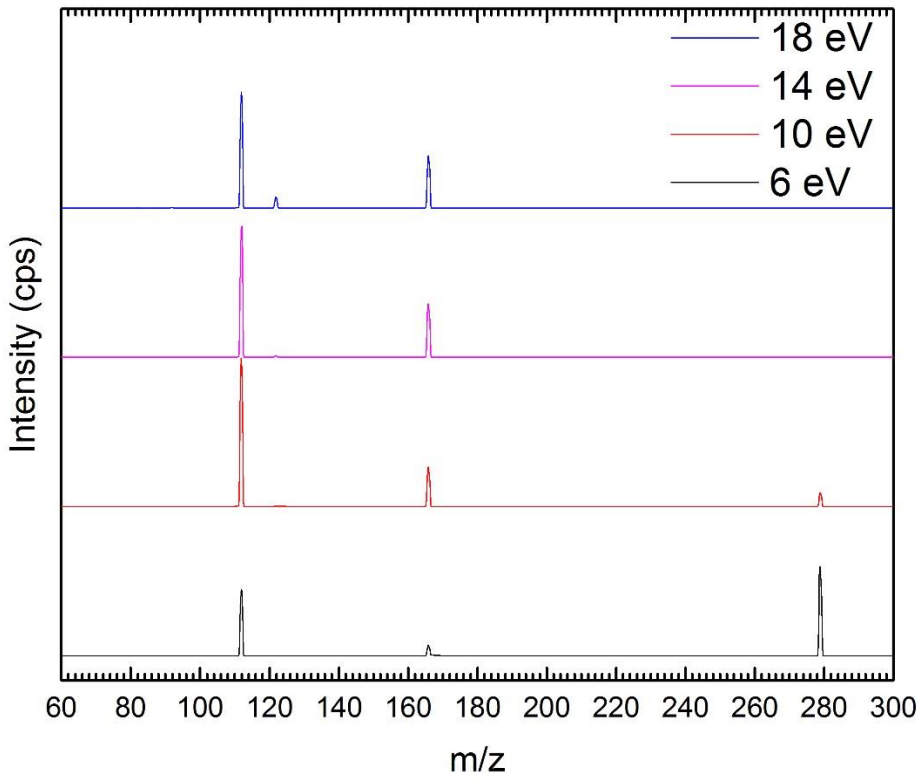

Figure 5.2 CID spectra for the proton-bound heterodimer of 2-nitroimidazole and 3-nitrobenzoic acid at four collision energies
m/z 279, 166, and 112 correspond to the proton-bound heterodimer, deprotonated 3-nitrobenzoic acid, and deprotonated 2-nitroimidazole, respectively. m/z 122 corresponds to the loss of CO_2 from deprotonated 3-nitrobenzoic acid. The four spectra illustrate how the relative intensities of the CID fragments will change as a function of collision energy. Note that these experiments are duplicated for *each* reference acid when performing an extended kinetic method experiment.

The kinetic method data were analyzed using the alternative method.[25] Statistical analysis of the data was performed using Igor Pro (WaveMetrics, Inc.; Lake Oswego, Oregon, USA), which implements the freely available software package, ODRPACK95.[32] The first plots of $\ln[A_i^-/A_0^-]$ vs. $\Delta H°_{acid}(HA_i)$ were weighted using ordinary least squares with respect to the standard deviations of $\ln[A_i^-/A_0^-]$ at the 95% confidence interval. The experimental errors for the acidities of the reference acids, $\Delta H°_{acid}(HA_i)$, were not included in the statistical analysis of the linear regressions of the first plots. For the second plots of

GA^{app} vs. T_{eff}, weighted ODR was implemented to determine $\Delta\Delta S°$ and $\Delta H°_{acid}(HA_0)$ using the curve-fitting function ODR=2 in Igor Pro, also at the 95% confidence interval. Although we use ODR to weight the linear regressions of the second plots, we are not using the isoequilibrium method described by Ervin and Bouchoux.[19, 26-28]

All of the chemicals used in this study were purchased from Sigma-Aldrich (St. Louis, Missouri, USA) except for 2-nitropyrrole, 3-nitropyrrole, and 3-nitropyrazole which were purchased from Oxchem Corporation (Irwindale, California, USA), Acella Pharmaceuticals (San Diego, California, USA), and Matrix Scientific (Columbia, South Carolina, USA), respectively.

5.3 Calculations

Theoretical calculations were carried out using the *Gaussian 09* suite of programs.[33] Hybrid functional calculations at the B3LYP/aug-cc-pVTZ level of theory were used to determine theoretical $\Delta G°_{acid}$, $\Delta H°_{acid}$, and $\Delta S°_{acid}$ values for the unknown nitroazoles investigated in this study. Thermal corrections to entropy and free energy were applied under the rigid-rotor harmonic-oscillator approximation.

In addition to reporting theoretical $\Delta G°_{acid}$ values, we also report $\Delta G°_{acid,experiment}$ values determined by a combination of theory and experiment where $\Delta G°_{acid,experiment} = \Delta H°_{acid,experiment} - T\Delta S°_{acid,theory}$.

5.4 Results

The reference acids used for this study are listed in Table 5.1. The $\Delta H°_{acid}$ and $\Delta G°_{acid}$ values were previously determined using ion-molecule reaction equilibrium methods.[10-13] $\Delta H°_{acid}$ for **7** (4-cyanobenzoic acid) was redetermined for use in this study with the extended kinetic method and the alternative method for data analysis.[25] The new value of $\Delta H°_{acid}(HA_i)$ = 329.4±2.2 kcal/mol was used for subsequent experiments in which **7** was employed as a reference; this value agrees with the previously determined value, 327.8±2.1 kcal/mol,[34] within experimental error. For its experimental determination, **7**

was referenced against the carboxylic acids **5**, **6**, **8**, **9**, **10**, and **11**. Because **7**, like the reference acids it was compared to, is a carboxylic acid, the second plot of GA^{app} vs. T_{eff} is characterized by a line with a small slope, where $\Delta\Delta S°=0.533\pm0.303$ cal/(mol·K). This result is expected for proton transfer between functionally and structurally similar anions.

Table 5.1 Reference acids

Reference Acid	Literature[a]		Theory[b]	
	$\Delta H°_{acid}$	$\Delta G°_{acid}$	$\Delta H°_{acid}$	$\Delta G°_{acid}$
1: phenylacetic acid	341.5(±2.1)	334.5(±2.0)	339.8	332.7
2: 3-toluic acid	340.6(±2.1)	333.6(±2.0)	340.8	332.9
3: benzoic acid	340.2(±2.2)	333.1(±2.0)	340.0	332.3
4: phenoxyacetic acid	338.0(±2.2)	331.0(±2.0)	335.8	328.4
5: chloroacetic acid	336.5(±2.2)	329.0(±2.0)	332.7	325.6
6: 4-(trifluoromethyl)benzoic acid	332.3(±2.1)	325.3(±2.0)	331.9	324.3
7: 4-cyanobenzoic acid[c]	329.4(±2.2)	321.7(±2.4)	329.0	321.3
8: 3-nitrobenzoic acid	329.1(±2.1)	322.1(±2.0)	328.8	321.1
9: 4-nitrobenzoic acid	328.1(±2.2)	321.1(±2.0)	327.5	319.7
10: salicylic acid	325.5(±2.2)	317.8(±2.0)	328.0	320.6
11: 3,5-bis(trifluoromethyl)benzoic acid	324.4(±2.1)	317.4(±2.0)	325.8	318.1

[a]Values from the NIST Chemistry WebBook (Ref. 34). [b]Theoretical calculations were carried out using Gaussian 09 at the B3LYP/aug-cc-pVTZ level of theory, and thermal corrections to entropy and free energy are included under the rigid rotor-harmonic oscillator approximation for T = 298 K. [c]The ΔH° and ΔG° values for **7** were redetermined before use in this experiment using the extended kinetic method with the alternative method for data analysis.

The nitrated azole species in this study were extensive enough in their $\Delta H°_{acid}(HA_0)$ values to warrant their pairing with three separate groups of reference acids. 2- and 3-nitropyrrole were referenced against **1**, **2**, **3**, **4**, **5**, and **6**. 3- and 4-nitropyrazole were referenced against **5**, **6**, **7**, **8**, and **9**. Lastly, 2- and 4-nitroimidazole were referenced against **6**, **7**, **8**, **9**, **10**, and **11**. As shown, there is some overlap between the groups of reference acids and unknown acid pairs.

We collected data for each of the azole acid systems at multiple lab-frame collision energies from ~5-22 eV. The limit on the collision energy range is determined for each experiment by analyzing how smoothly the effective temperature (T_{eff}) rises with respect to the collision energies set by the

instrument.[21] Although the data can also be analyzed in the center-of-mass frame, Armentrout and coworkers reported that converting to the center-of-mass frame does not change the character of the results.[21] For that reason, we have analyzed the data in the conventional laboratory frame.

The ratios of the product ions, A_i^-/A_0^-, were determined by examining the peak heights of pertinent ions as extracted from MS/MS data. Notably, several of the carboxylic reference acids exhibited a loss of m/z 44 (CO_2) upon using higher collision energies (≥14 eV). Additionally, some of the species containing a nitro group ($–NO_2$) exhibited a loss of m/z 30 (NO). Chloride ion was observed as a secondary product ion when reference acid **5** was used. The intensities of the secondary product ions were accounted for by adding their intensities to the respective primary ion intensities and no further corrections were made.

Figure 5.3 shows five plots of $\ln[k_i/k_0]$ vs. $\Delta H°_{acid}(HA_i)$ for 4-nitropyrazole and its reference acids at the collision energies 5, 7, 10, 14 and 18 eV. Most reports overlay all regressions onto a single plot, and in an ideal situation the linear regressions of the different collision energies will cross at a single point, known as the isoequilibrium point. However, most extended kinetic method data deviate from a single crossing point,[21] and the data for this study are no exception. The slope of the linear regression decreases as the collision energy increase from Figure 5.3a to Figure 5.3e. This decrease in slope corresponds to an increase in T_{eff}, because slope is proportional to $1/T_{eff}$. Simultaneously, the x-intercept, indicated by a blue arrow, increases from Figure 5.3a to Figure 5.3e, corresponding to an increase in the GA^{app} term. The two values, GA^{app} and T_{eff}, are plotted in a second graph, shown as Figure 5.4. Analysis of the y-intercept and slope of the second plot provides values for $\Delta H°_{acid}(HA_0)$ and $\Delta\Delta S°(HA_0,HA_i)$, as shown by the relationship in equation 5.2.

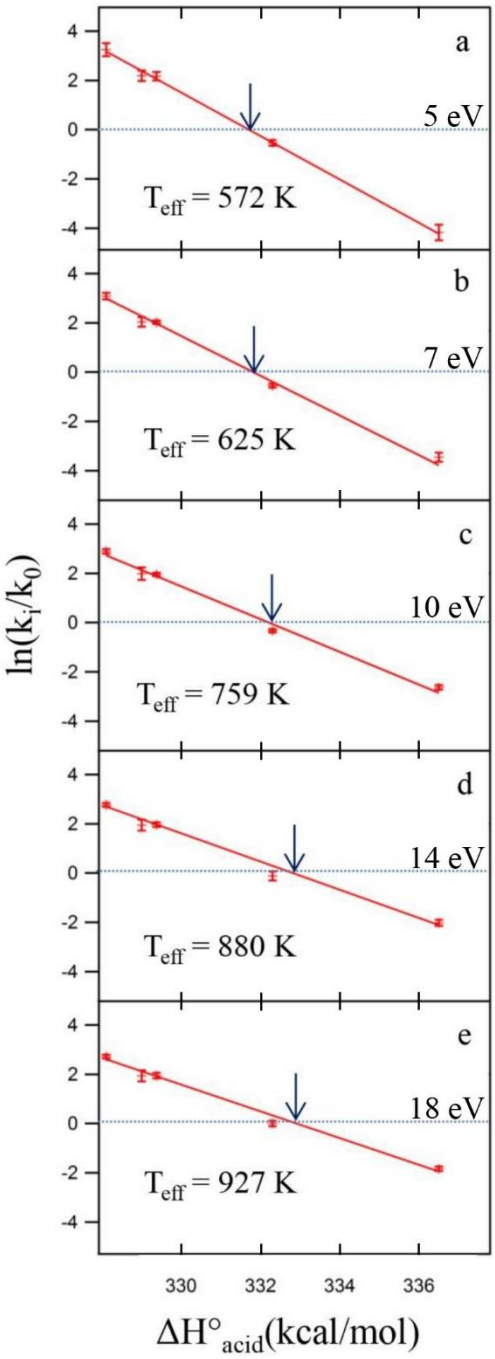

Figure 5.3 Plots of $\ln(k_i/k_0)$ vs. $\Delta H°_{acid}$ (kcal/mol) for 4-nitropyrazole.
Plots a, b, c, d, and e correspond to data taken at collision energies 5, 7, 10, 14, and 18 eV (lab frame), respectively. As the collision energy increases, the slope ($-1/RT_{eff}$) becomes less negative, and the x-intercept increases; at the x-intercept, $GA^{app} = \Delta H°_{acid}$. Note that the $\Delta H°_{acid}$ values plotted correspond to the reference acids **5**, **6**, **7**, **8**, and **9**, not 4-nitropyrazole.

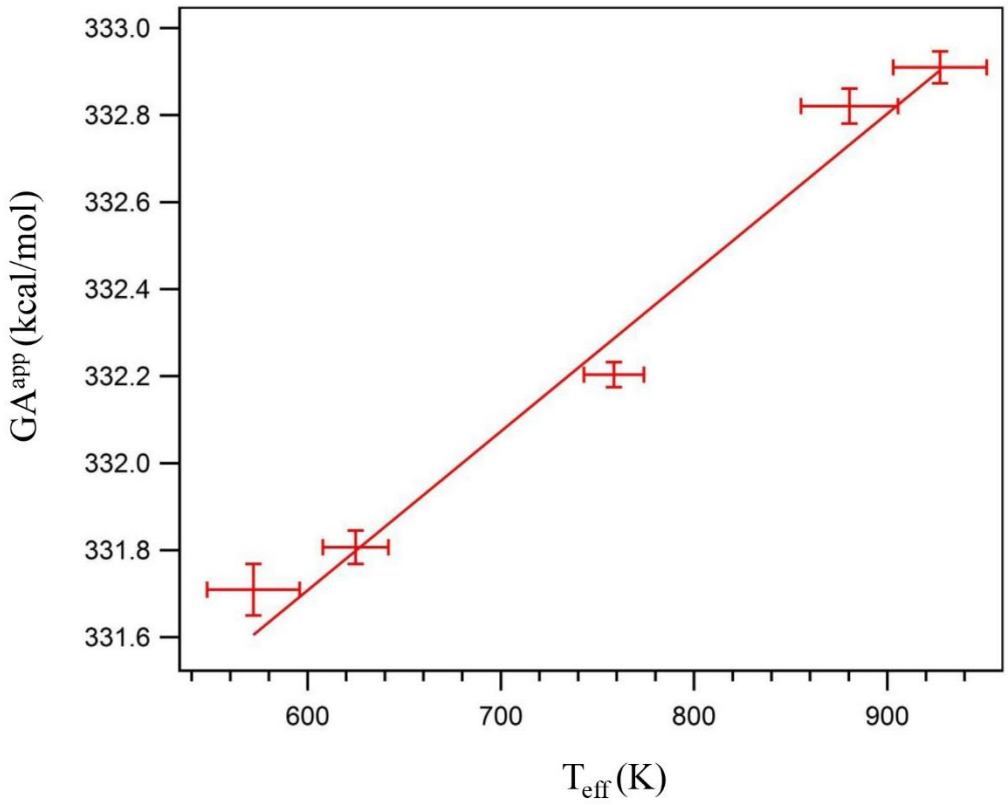

Figure 5.4 Plot of GA^{app} vs. T_{eff} values for 4-nitropyrazole.
The data in Figure 5.4 are provided by Figure 5.3. The points are weighted in both the dependent and independent variables at the 95% confidence interval using ODR; the error bars represent two standard deviations of the data. The slope and y-intercept of the weighted line gives values for $\Delta\Delta S°$ (3.7 cal/(mol·K)) and $\Delta H°_{acid}$ (329.5 kcal/mol), respectively.

Table 5.2 gives a complete summary of the results of our measurements. The experimental results $\Delta H°_{acid}(HA_0)$ were obtained by the alternative method of data analysis. Additionally, $\Delta H°_{acid}(HA_0)$ values were theoretically calculated for each nitrated azole. The calculated $\Delta H°_{acid}(HA_0)$ values agree with the experimental values within 1 kcal/mol, except for 3-nitropyrrole which deviates from the experimental value by 1.7 kcal/mol. We also report $\Delta G°_{acid}(HA_0)$ values for the unknowns; these values were determined by calculating $T\Delta S°_{acid}$ (T=298 K) and subtracting the result from the experimental $\Delta H°_{acid}$ values ($\Delta G°_{acid,experiment} = \Delta H°_{acid,experiment} - T\Delta S°_{acid,theory}$). This approach provides reasonably accurate $\Delta G°_{acid}$ values because the entropic contribution to the free energy of deprotonation can be calculated with

reasonable certainty. The absolute error reported for the $\Delta G°_{acid}$ values is ±2.4 kcal/mol because of the added uncertainty introduced by the calculation.

Table 5.2 Results of kinetic method and computational studies

Nitrated Azole	E_{coll}(eV)	T_{eff}(K)	Experiment			Theory[c]		
			$\Delta H°_{acid}$[a] (kcal/mol)	$\Delta\Delta S°$[a] [cal/(mol·K)]	$\Delta G°_{acid}$[b] (kcal/mol)	$\Delta H°_{acid}$ (kcal/mol)	$\Delta G°_{acid}$ (kcal/mol)	$T\Delta S°_{acid}$[d] (kcal/mol)
2-nitropyrrole	6–18	435–645	337.0(±2.2)	2.3(±0.2)	329.4 (±2.4)	336.0	328.4	7.6
3-nitropyrrole	6–18	560–880	335.8(±2.2)	3.2(±0.2)	328.4(±2.4)	334.1	326.6	7.4
3-nitropyrazole	6–18	690–1010	330.5(±2.2)	4.7(±0.3)	323.1(±2.4)	331.2	323.7	7.4
4-nitropyrazole	5–18	570–930	329.5(±2.2)	3.7(±0.3)	322.0(±2.4)	330.0	322.5	7.5
2-nitroimidazole	6–22	500–735	327.4(±2.2)	1.9(±0.3)	319.7(±2.4)	328.2	320.5	7.7
4-nitroimidazole	6–22	625–975	325.0(±2.2)	3.0(±0.3)	317.6(±2.4)	325.8	318.4	7.4

[a]The values $\Delta H°_{acid}$ and $\Delta\Delta S°$ were determined using the alternative method for extended kinetic method data analysis. ODR was used to weight the two values in the second plot. The errors for $\Delta H°_{acid}$ arise from the uncertainties of the reference acids. The experimental precision from the ODR statistical treatment of the data at the 95% confidence interval is much better (≤ ±0.4 kcal/mol) than the absolute error. [b]$\Delta G°_{acid,experiment}$ was determined by a combination of theory and experiment where ($\Delta G°_{acid,experiment} = \Delta H°_{acid,experiment} - T\Delta S°_{acid,theory}$). [c]Theoretical calculations were carried out using Gaussian 09 at the B3LYP/aug-cc-pVTZ level of theory, and thermal corrections to entropy and free energy are included under the rigid rotor-harmonic oscillator approximation. [d]T=298 K.

In addition to the experimental kinetic method measurements, we performed a theoretical investigation to determine the $\Delta H°_{acid}$(HA), $\Delta G°_{acid}$(HA), and electron affinity (EA) values for 24 azolate and nitrated-azolate species. These results supplement the experimental work by investigating higher order aza compounds, as well investigating azoles with two nitro groups. The results are presented in Table 5.3,[14-16, 34-38] which, in addition to theoretical values, compiles previously determined experimental values. The theoretical anion proton affinities agree with the experimental measurements within 3 kcal/mol.

Table 5.3 Experimental and theoretical thermochemical properties of nitrated azoles

Azole	Experiment			Theory[a]		
	$\Delta H°_{acid}$[b,c] (kcal/mol)	$\Delta G°_{acid}$[c,d] (kcal/mol)	EA[e] (eV)	$\Delta H°_{acid}$[b,c] (kcal/mol)	$\Delta G°_{acid}$[c,d] (kcal/mol)	EA[e] (eV)
pyrrole	359.54(±0.25)[14] 358.6(±2.2)[35]	350.9(±2.0)[14]	2.145(±0.010)[14]	360.1	352.6	2.104
2-nitropyrrole	337.0(±2.2)[f]			336.0	328.4	3.436
3-nitropyrrole	335.8(±2.2)[f]			334.1	326.6	3.416
2,3-dinitropyrrole				317.2	309.8	4.165
2,4-dinitropyrrole				315.0	307.4	4.487
2,5-dinitropyrrole				315.2	307.5	4.501
pyrazole	353.6(±2.4)[16]	346.4(±2.3)[16]	2.938(±0.005)[16]	355.7	348.1	2.908
3-nitropyrazole	330.5(±2.2)[f]			(N1)331.2 (N2)331.7	(N2)323.7 (N2)324.0	4.154
4-nitropyrazole	329.5(±2.2)[f]			330.0	322.5	4.220
3,4-dinitropyrazole				(N1)313.1 (N2)312.1	(N1)306.4 (N2)304.6	5.011
2,5-dinitropyrazole				311.3	303.7	5.125
imidazole	349.93(±0.72)[15] 350.1(±2.1)[36]	342.60(±0.40)[15] 342.8(±2.0)[36]	2.613(±0.006)[15]	350.8	343.3	2.562
2-nitroimidazole	327.4(±2.2)[f]			328.2	320.5	3.789
4-nitroimidazole	325.0(±2.2)[f]			(N1)325.8 (N3)326.6	(N1)318.4 (N3)319.0	3.865
2,4-dinitroimidazole				(N1)307.9 (N3)307.3	(N1)300.1 (N3)299.5	4.836
4,5-dinitroimidazole				309.6	302.5	4.851
1,2,3-triazole	(N2)346.4(±2.1)[37]	(N2)339.1(±2.0)[37]	3.447(±0.004)[38]	(N1)343.2 (N2)346.9	(N1)335.6 (N2)339.3	3.420
4-nitro-1,2,3-triazole				(N1)319.4 (N2)322.3 (N3)318.5	(N1)311.9 (N2)314.8 (N3)310.9	4.626
4,5-dinitro-1,2,3-triazole				(N1)301.5 (N2)304.9	(N1)294.1 (N2)297.9	5.377
1,2,4-triazole	(N1)344.2(±2.1)[34]	(N1)336.9(±2.0)[34]		(N1)345.2 (N4)339.4	(N1)337.7 (N4)331.9	3.367
3-nitro-1,2,4-triazole				(N1)321.8 (N2)322.6 (N4)317.2	(N1)314.6 (N2)314.8 (N4)309.5	4.503
3,5-dinitro-1,2,4-triazole				(N1)303.1 (N4)298.1	(N1)295.4 (N4)290.0	5.428

tetrazole	(N1)333.7(±2.1)[34]	(N1)326.4(±2.0)[34]	(N1)331.1 (N2)333.0	(N1)323.5 (N2)325.4	4.070
nitrotetrazole			(N1)308.4 (N2)310.2	(N1)300.6 (N2)302.9	5.172

[a]Theoretical values calculated using B3LYP/aug-cc-pVTZ methods. $\Delta H°_{acid}$ and $\Delta G°_{acid}$ are reported at 298 K using the rigid-rotor harmonic-oscillator approximation. EA are reported at 0 K including zero point energies. [b]Proton affinity of the anion. [c]The nitrogen-atom acid site is indicated in parentheses for both experimental and theoretical anion proton affinities and gas-phase acidities. [d]Gas-phase acidity. [e]Electron binding energy of the anion (electron affinity of the corresponding neutral radical). [f]Experimental values determined from this work.

5.5 Discussion

Recently, Armentrout and coworkers investigated the gas-phase acidities of rigid-planar-monohalogenated phenols using the B3LYP/aug-cc-pVTZ level of theory. (It is noteworthy to mention that they optimized the molecular geometries using a slightly smaller basis set, aug-cc-pVDZ.) Their experimental and theoretical 298 K acidity values present a fairly good correlation, with mean absolute deviations of 2±1 kcal/mol.[21] To further investigate the correlation between theory and experiment, we calculated the 298 K acidity values for the reference acids used in these studies, and found mean absolute deviations of 1±3 kcal/mol. However, when species containing halogens are removed, as well as phenoxyacetic acid, which likely has anharmonic vibrations due to the floppy nature of the etheral, carboxylic arm, the correlation is improved to 0±3 kcal/mol. Therefore, computations at the B3LYP/aug-cc-pVTZ level of theory should appropriately predict the gas-phase acidities of the rigid-planar-organic molecules investigated in Table 5.3 with a reasonable certainty**.**

The aza substituent effect was investigated previously by Taft et al.[36] Upon finding that imidazole is a stronger acid than pyrazole, they argued that the lone pair repulsion from the ring-nitrogen atoms on the pyrazole anion destabilizes it, making pyrazole a weaker acid than imidazole. Additionally, they report the conjugate bases of pyrazole and imidazole to be more stable than pyrrole by 4.8 and 8.4 kcal/mol, respectively. The work of Taft et al. exploits $\Delta G°_{acid}$(HA), while our work examines $\Delta H°_{acid}$(HA). However, relative differences between these two thermodynamic properties are comparable because the entropic contribution is roughly constant with TΔS usually changing by less than 1 kcal/mol for any given

pair of acids. Our work expands these observations and explores trends in nitration effects. Based on the difference in acidity between 2-nitropyrrole, 3-nitropyrrole and pyrrole; 3-nitropyrazole, 4-nitropyrazole and pyrazole; and 2-nitroimidazole, 4-nitroimidazole and imidazole, we report that when a nitro group is substituted onto an azole, it increases the acidity by 23.5±1.9 kcal/mol at the 95% confidence interval.[14-16] This is in perfect agreement with the experimentally determined differences in acidity between benzene and nitrobenzene, 24.2 kcal/mol.[18, 39]

As stated in the results, the anions under investigation for this study were sufficiently different in $\Delta H°_{acid}(HA_0)$ values to require their evaluation with three separate groups of reference acids. Although we report the absolute error for each measured $\Delta H°_{acid}(HA_0)$ as ±2.2 kcal/mol, the relative difference in acidity between each pair is 1.2±0.3 kcal/mol for 2-nitropyrrole and 3-nitropyrrole, 1.0±0.7 kcal/mol for 3-nitropyrazole and 4-nitropyrazole, and 2.4±0.6 kcal/mol for 2-nitroimidazole and 4-nitroimidazole. Relative uncertainties are reported at the 95% confidence interval (2σ). This ordering is reinforced because the acidities of each pair were determined using the same reference acids. Furthermore, the experiments are much more precise (±0.4 kcal/mol) than the absolute uncertainty (±2.2 kcal/mol). This allows us to arrange with confidence the proposed azoles in order of increasing acidity as 2-nitropyrrole, 3-nitropyrrole, 3-nitropyrazole, 4-nitropyrazole, 2-nitroimidazole, and 4-nitroimidazole, which have $\Delta H°_{acid}$ (kcal/mol) values of 337.0, 335.8, 330.5, 329.5, 327.4, and 325.0, respectively. To provide some context, other common anions of ionic liquids including Cl^-, Br^-, $CF_3SO_3^-$, and NTf_2^- have $\Delta H°_{acid}$ (kcal/mol) values of 333.40, 323.54, 305.4, and 293.3, respectively.

The differences in acidity among the nitrated azoles can be attributed to nitrogen atom and nitro group placement. Imidazole is more acidic than pyrazole because pyrazole is destabilized by the adjacent placement of the two nitrogen atoms. A similar destabilization occurs when a nitro group is located adjacent to a ring-nitrogen atom. The optimized equilibrium geometries for each of the six nitrated azoles experimentally investigated in this study yield planar molecules. Therefore, the oxygen atoms of the nitro groups are in close proximity to the neighboring ring atoms. This orientation introduces a region of high

electron density in proximity to ring atoms that are adjacent to the nitro group. Understanding the geometries helps us explain the relative ordering between the sub groups. 2-nitropyrrole is a weaker acid than 3-nitropyrrole because the electron dense region of the oxygen atom is repulsive towards the electron dense region of the ring-nitrogen atom. This same argument holds for the difference in acidity between 3- and 4-nitropyrazole; 4-nitropyrazole is more acidic than 3-nitropyrazole because 3-nitropyrazole faces a higher degree of electron repulsion when the electron dense oxygen atom is in close proximity to the electron dense ring-nitrogen atom. Lastly, the difference in acidity between 2- and 4-nitroimidazole is more pronounced because the nitro group of 2-nitroimidazole is placed between two ring-nitrogen atoms, resulting in greater electron density overlap. In summary, when a nitro group is placed on an azole ring adjacent to a ring nitrogen atom, it will destabilize the anion by about 1.1±0.3 kcal/mol as compared to the isomer with the nitro group located away from the ring-nitrogen atom.

A few more trends are evident from the additional theoretical investigation, which are consistent with our chemical intuition. First, for higher order aza substitution, molecules of higher acidity are produced. Second, as the number of nitro groups on the molecule increases, stronger acids are generated. The electron withdrawing properties of the ring-nitrogen atoms and the nitro groups stabilize the additional electronic charge of the anion, allowing the parent molecule to more easily lose a proton. Again, we found within the dinitro compounds that the nitro group placement can affect the stability of the anion. Placing the nitro groups adjacent to each other will decrease the anion's stability by about 2 kcal/mol. (See the difference between 2,3- and 2,4-dinitropyrrole, and 2,4- and 4,5-dinitroimidazole.) While this result is consistent with an increase in electrostatic repulsion, spatial constraint issues are also contributing, i.e. 2,4-dinitropyrrole and 2,4-dinitroimidazole are planar while our calculations show that the nitro-group–oxygen atoms of 2,3-dinitropyrrole and 4,5-dinitroimidazole are outside of the molecular plane. Finally, as the acidity of the molecule increases, the electron binding energy of the conjugate base, or anion, also increases. Both of these trends indicate an increase in the stability of the anion.

5.6 Conclusion

We have employed the extended kinetic method with the alternative method of data analysis to determine $\Delta H°_{acid}$ for six nitrated-azole compounds. The success of this work is attributed to employing reliable reference acids of similar function and structure. The reference acids used were similar in acidity (± 6 kcal/mol) to the acidity of the nitrated azoles, and the reference acids' acidity range encompassed the acidity of the nitrated azoles. The results of this experiment elucidate trends in the mono-nitration of pyrrole, pyrazole, and imidazole. We conclude that the pertinent anions of this study are very stable, and they should be capable of generating robust ionic liquids. In addition, previous studies have shown that the basicity of an ionic liquid is dominated by the gas-phase basicity of the anion.[8, 40] Therefore, these experimental measurements provide insight into the Lewis-base properties of ionic liquids in which the anions of this study are employed.

Furthermore, 4-nitroimidazole, the strongest acid of this study, has already found use as the anionic component of ionic liquids in a recent study of azole based ionic liquids conducted by Rogers and coworkers.[9] For future work, it would be interesting to investigate the gas-phase acidity of the remaining molecules of Rogers' report including the nitrated triazoles, tetrazoles, benzoimidazoles, and benzotriazoles. In addition to our experimental work, we have computationally determined the gas-phase acidity of five other azolate anions found in Rogers' study including 2,4-dinitroimidazole; 4,5-dinitroimidazole; 4-nitro-1,2,3-triazole; 3,5-dinitro-1,2,4-triazole; and tetrazole ($\Delta H°$acid = 307, 310, 319, 298, and, 331 kcal/mol, respectively, for the most acidic sites). These results suggest that most of the azolate based ionic liquids should have a reasonably low melting point while maintaining thermal stability up to around 200 °C. From our investigation, no clear trend between acidity and ionic liquid melting point is revealed. Conversely, the thermal stability of the ionic liquid pair increases with the gas-phase stability of the anion.[9]

Finally, these studies indicate that the addition of a nitro group to an aromatic ring will increase the compound's acidity/anionic-stability by about 23.5±1.9 kcal/mol. Moreover, these molecules are marginally destabilized by about 1.1±0.3 kcal/mol when the nitro group is placed adjacent to a ring-nitrogen atom. By understanding these trends, researchers will have greater control over the thermodynamic properties of novel ionic liquids.

5.7 References

[1] J. Reedijk, *Pyrazoles and imidazoles as ligands. Part I. Some simple metal(II) perchlorates and tetrafluoroborates solvated by neutral pyrazole and imidazole*, Recueil Des Travaux Chimiques Des Pays-Bas, 88 (1969) 1451-1470.

[2] C.A. Angell, Y. Ansari, Z.F. Zhao, *Ionic Liquids: Past, present and future*, Faraday Discuss., 154 (2011) 9-27.

[3] J.J. Jodry, K. Mikami, *Ionic Liquids*, in: K. Mikami (Ed.) Green reaction media in organic synthesis, Blackwell Publishing Ltd, Kundli, 2005, pp. 9-54.

[4] J.F. Wishart, *Energy applications of ionic liquids*, Energy Environ. Sci., 2 (2009) 956-961.

[5] M. Armand, F. Endres, D.R. MacFarlane, H. Ohno, B. Scrosati, *Ionic-liquid materials for the electrochemical challenges of the future*, Nat. Mater., 8 (2009) 621-629.

[6] S. Schneider, T. Hawkins, M. Rosander, G. Vaghjiani, S. Chambreau, G. Drake, *Ionic liquids as hypergolic fuels*, Energy Fuels, 22 (2008) 2871-2872.

[7] Y.H. Chin, R.A. Dressler, *Ionic Liquids for Space Propulsion*, in: J.F. Brennecke, R.D. Rogers, K.R. Seddon (Eds.) Ionic Liquids IV: Not Just Solvents Anymore, Amer Chemical Soc, Washington, 2007, pp. 138-160.

[8] A.R. Katritzky, S. Singh, K. Kirichenko, J.D. Holbrey, M. Smiglak, W.M. Reichert, R.D. Rogers, *1-butyl-3-methylimidazolium 3,5-dinitro-1,2,4-triazolate: a novel ionic liquid containing a rigid, planar energetic anion*, Chem. Commun., (2005) 868-870.

[9] M. Smiglak, C.C. Hines, T.B. Wilson, S. Singh, A.S. Vincek, K. Kirichenko, A.R. Katritzky, R.D. Rogers, *Ionic Liquids Based on Azolate Anions*, Chem.-Eur. J., 16 (2010) 1572-1584.

[10] J.F. Cai, R.D. Topsom, A.D. Headley, I. Koppel, M. Mishima, R.W. Taft, S. Veji, *Acidities of substituted acetic acids*, Theochem-J. Mol. Struct., 45 (1988) 141-146.

[11] R.W. Taft, R.D. Topsom, *The Nature and Analysis of Substituent Effects*, Progress in Physical Organic Chemistry, 16 (1987) 1-83.

[12] T.B. McMahon, P. Kebarle, *Intrinsic acidities of substituted phenols and benzoic-acids determined by gas-phase proton-transfer equilibria*, J. Am. Chem. Soc., 99 (1977) 2222-2230.

[13] G. Caldwell, R. Renneboog, P. Kebarle, *Gas-phase acidities of aliphatic carboxylic-acids based on measurements of proton-transfer equilibria*, Can. J. Chem.-Rev. Can. Chim., 67 (1989) 611-618.

[14] A.J. Gianola, T. Ichino, R.L. Hoenigman, S. Kato, V.M. Bierbaum, W.C. Lineberger, *Thermochemistry and electronic structure of the pyrrolyl radical*, J. Phys. Chem. A, 108 (2004) 10326-10335.

[15] A.J. Gianola, T. Ichino, R.L. Hoenigman, S. Kato, V.M. Bierbaum, W.C. Lineberger, *Photoelectron spectra and ion chemistry of imidazolide*, J. Phys. Chem. A, 109 (2005) 11504-11514.

[16] A.J. Gianola, T. Ichino, S. Kato, V.M. Bierbaum, W.C. Lineberger, *Thermochemical studies of pyrazolide*, J. Phys. Chem. A, 110 (2006) 8457-8466.

[17] N. Eyet, V.M. Bierbaum, *Gas-phase acidities of thiocarboxylic acids*, Int. J. Mass Spectrom., 265 (2007) 267-270.

[18] X. Cheng, J.J. Grabowski, *Gas-phase acidity of nitrobenzene from flowing afterglow bracketing studies*, Rapid Commun. Mass Spectrom., 3 (1989) 34-36.

[19] G. Bouchoux, M. Sablier, F. Berruyer-Penaud, *Obtaining thermochemical data by the extended kinetic method*, J. Mass Spectrom., 39 (2004) 986-997.

[20] R.G. Cooks, J.T. Koskinen, P.D. Thomas, *Special feature: Commentary - The kinetic method of making thermochemical determinations*, J. Mass Spectrom., 34 (1999) 85-92.

[21] S. Bourgoin-Voillard, C. Afonso, D. Lesage, E.L. Zins, J.C. Tabet, P.B. Armentrout, *Critical evaluation of kinetic method measurements: Possible origins of nonlinear effects*, J. Am. Soc. Mass Spectrom., 24 (2013) 365-380.

[22] P.G. Wenthold, *Determination of the proton affinities of bromo- and iodoacetonitrile using the kinetic method with full entropy analysis*, J. Am. Soc. Mass Spectrom., 11 (2000) 601-605.

[23] X.H. Cheng, Z.C. Wu, C. Fenselau, *Collision energy-dependence of proton-bound dimer dissociation - entropy effects, proton affinities, and intramolecular hydrogen-bonding in protonated peptides*, J. Am. Chem. Soc., 115 (1993) 4844-4848.

[24] M.J. Nold, B.A. Cerda, C. Wesdemiotis, *Proton affinities of the N- and C-terminal segments arising upon the dissociation of the amide bond in protonated peptides*, J. Am. Soc. Mass Spectrom., 10 (1999) 1-8.

[25] P.B. Armentrout, *Entropy measurements and the kinetic method: A statistically meaningful approach*, J. Am. Soc. Mass Spectrom., 11 (2000) 371-379.

[26] K.M. Ervin, P.B. Armentrout, *Systematic and random errors in ion affinities and activation entropies from the extended kinetic method*, J. Mass Spectrom., 39 (2004) 1004-1015.

[27] G. Bouchoux, F. Djazi, F. Gaillard, D. Vierezet, *Application of the kinetic method to bifunctional bases MIKE and CID-MIKE test cases*, Int. J. Mass Spectrom., 227 (2003) 479-496.

[28] G. Bouchoux, *Evaluation of the protonation thermochemistry obtained by the extended kinetic method*, J. Mass Spectrom., 41 (2006) 1006-1013.

[29] K. Vekey, *Internal energy effects in mass spectrometry*, J. Mass Spectrom., 31 (1996) 445-463.

[30] L. Drahos, K. Vekey, *Special feature: Commentary - How closely related are the effective and the real temperature*, J. Mass Spectrom., 34 (1999) 79-84.

[31] J.W. Hager, *A new linear ion trap mass spectrometer*, Rapid Commun. Mass Spectrom., 16 (2002) 512-526.

[32] P.T. Boggs, J.R. Donaldson, R.H. Byrd, R.B. Schnabel, *ODRPACK95 - software for weighted orthogonal distance regression*, ACM Trans. Math. Softw., 15 (1992) 348-364.

[33] M.J. Frisch, G.W. Trucks, H.B. Schlegel, G.E. Scuseria, M.A. Robb, J.R. Cheeseman, G. Scalmani, V. Barone, B. Mennucci, G.A. Peterson, H. Nakatsuji, M. Caricato, X. Li, H.P. Hratchian, A.F. Izmaylov, J. Bloino, G. Zheng, J.L. Sonnenberg, M. Hada, M. Ehara, K. Toyota, R. Fukuda, J. Hasegawa, T. Nakajima, Y. Honda, O. Kitao, H. Nakai, T. Vreven, J.A. Montgomery Jr., J.E. Peralta, F. Ogliaro, M. Bearpark, J.J. Heyd, E. Brothers, K.N. Kudin, V.N. Staroverov, R. Kobayashi, J. Normand, K. Raghavachari, A. Rendell, J.C. Burant, S.S. Iyengar, J. Tomasi, M. Cossi, N. Rega, J.M. Millam, M. Klene, J.E. Knox, J.B. Cross, V. Bakken, C. Adamo, J. Jaramillo, R. Gomperts, R.E. Stratmann, O. Yazyev, A.J. Austin, R. Cammi, C. Pomelli, J.W. Ochterski, R.L. Martin, K. Morokuma, V.G. Zakrzewski, G.A. Voth, P. Salvador, J.J. Dannenberg, S. Dapprich, A.D. Daniels, Ö. Farkas, J.B. Foresman, J.V. Ortiz, J. Cioslowski, D.J. Fox, *Gaussian 09*, Gaussian, Inc., Wallingford CT, 2009.

[34] S.G. Lias, J.E. Bartmess, J.F. Liebman, J.L. Holmes, W.G. Mallard, *NIST Chemistry WebBook*, in: P.J. Lindstrom, W.G. Mallard (Eds.) Ion Energetics Data, National Institute of Standards and Technology, Gaithersburg, MD, 2014.

[35] J.E. Bartmess, J.A. Scott, R.T. McIver, *Scale of Acidities in the Gas-Phase from Methanol to Phenol*, J. Am. Chem. Soc., 101 (1979) 6046-6056.

[36] R.W. Taft, F. Anvia, M. Taagepera, J. Catalan, J. Elguero, *Electrostatic proximity effects in the relative basicities and acidities of pyrazole, imidazole, pyridazine, and pyrimidine*, J. Am. Chem. Soc., 108 (1986) 3237-3239.

[37] J. Catalan, R.M. Claramunt, J. Elguero, J. Laynez, M. Menendez, F. Anvia, J.H. Quian, M. Taagepera, R.W. Taft, *Basicity and Acidity of Azoles - the Annelation Effect in Azoles*, J. Am. Chem. Soc., 110 (1988) 4105-4111.

[38] T. Ichino, D.H. Andrews, G.J. Rathbone, F. Misaizu, R.M.D. Calvi, S.W. Wren, S. Kato, V.M. Bierbaum, W.C. Lineberger, *Ion chemistry of 1H-1,2,3-Triazole*, J. Phys. Chem. B, 112 (2008) 545-557.

[39] R.F. Gunion, M.K. Gilles, M.L. Polak, W.C. Lineberger, *Ultraviolet photoelectron-spectroscopy of the phenide, benzyl and phenoxide anions, with ab initio calculations*, Int. J. Mass Spectrom. Ion Process., 117 (1992) 601-620.

[40] L. Crowhurst, P.R. Mawdsley, J.M. Perez-Arlandis, P.A. Salter, T. Welton, *Solvent-solute interactions in ionic liquids*, Phys. Chem. Chem. Phys., 5 (2003) 2790-2794.

6 Gas-Phase Investigations of the α-Effect

6.1 Introduction

About 50 years ago, Pearson and Edwards initiated comprehensive studies of the rates of nucleophilic chemical reactions in solution. They discovered that some nucleophiles react more rapidly than expected based purely on the basicity of the nucleophile.[1] These highly-reactive super-nucleophiles were named α-nucleophiles, as they were observed to possess a lone pair of electrons on the atom adjacent to the attacking center, Figure 6.1. Their enhanced reactivity was named the α-effect.

Figure 6.1 α-nucleophiles
α-nucleophiles possess one or more lone pair of electrons (red) on the atom adjacent to the nucleophilic atom. The α-nucleophile may be anionic (i.e., peroxide, hypochlorite) or neutral (i.e., hydrazine, hydroxylamine).

Since Pearson and Edward's discovery, the origin of the α-effect has been discussed in great detail. Some suggested reasons for enhanced nucleophilicity of α-nucleophiles include ground-state destabilization, transition-state stabilization, and solvent effects. The first two reasons imply that the enhanced reactivity arises from intrinsic properties of the α-nucleophiles, while the latter arises from differential solvation of the α-nucleophiles compared with the normal-nucleophiles.

The notion of ground-state destabilization assumes that the lone pairs of electrons on the α-atom experience electrostatic repulsion with the lone pairs at the reaction center. The ground-state destabilization effect would increase the energy of the ground-state of the α-nucleophiles,[2-4] resulting in a lower relative transition-state barrier therefore increasing the rate of reaction. Nonetheless, this argument is problematic because ground-state destabilization would not only affect the rate of the reaction, but also

affect the basicity of the nucleophile under investigation.[5-7] Therefore, no deviation from the rate-energy relationship portrayed by Brønsted correlations (vide infra) would be observed.

Transition-state stabilization has also been proposed as a reason for the increased reactivity of α-nucleophiles vs. normal-nucleophiles. An increase in the stability of the transition state would result in a reduction of the transition-state barrier height thereby increasing the rate of reaction. The best chemical argument for transition-state stabilization follows the assumption that nucleophilic reactions occur through a single-electron transfer process.[8, 9] Because nucleophilic reactions occur through incipient bond formation, rationalizing the mechanism through single-electron transfer is certainly reasonable. If single-electron transfer is occurring, the nucleophile will resemble a radical in the transition state, and it is well known that radicals are stabilized by neighboring lone pairs.[10]

Since its discovery, the α-effect has been observed in diverse solvents,[5, 11-16] although the magnitude of the α-effect ($Eff_{\alpha\text{-}Nu}/Eff_{normal\text{-}Nu}$) is highly solvent dependent.[5, 17] The results suggest that α-nucleophiles are more easily desolvated than normal nucleophiles in some environments. It is possible that the diffuse charge of the α-nucleophiles assists desolvation at the reaction center when compared to normal-nucleophiles. However, these results alone cannot dismiss the possibility of an intrinsic contribution to the α-effect.

This chapter will summarize several gas-phase α-effect experiments executed using the selected ion flow tube (SIFT). Thanks to context provided by decades of discussion and experimentation, the α-effect has been observed in the gas-phase.[18-24] The first section on Marcus theory will discuss experiments for observing the α-effect in the gas-phase; in particular, the reaction must not be too exothermic or else small changes in the intrinsic transition-state barrier between nucleophiles will be masked.[20] The following section examines the α-effect through S_N2 and E2 reactions, and reports a minor intrinsic contribution to the α-effect.[21] Micro-solvation is the topic of the next section, and the micro-solvation studies reveal that, even in the presence of a single solvent molecule, the magnitude of the α-effect is

dramatically increased.[23, 24] The final section reports α-effect studies through competing reaction mechanisms with methyl formate. Again, a minor intrinsic component of the α-effect is revealed,[21] and investigations of the micro-solvated nucleophiles show a large enhancement of the α-effect.[22]

6.2 Marcus Theory and the α-Effect in Gas-Phase S_N2 Reactions

Marcus theory was developed to describe barriers associated with single electron transfer dynamics. Moreover, the theory is generally relevant for describing gas-phase double-well potentials, such as those observed in S_N2 reactions.[25] Gas-phase identity S_N2 reactions (where the attacking and leaving groups are identical) are inherently thermoneutral, but may have an intrinsic barrier, $\Delta H^{\ddagger}_{intrinsic}$. Conversely, the activation barriers for non-identity S_N2 reactions is influenced by the reaction thermodynamics. When the reaction is exothermic, the overall activation barrier, $\Delta H^{\ddagger}_{activation}$, is reduced by thermodynamic driving forces. Figure 6.2 provides a diagram for this relationship.

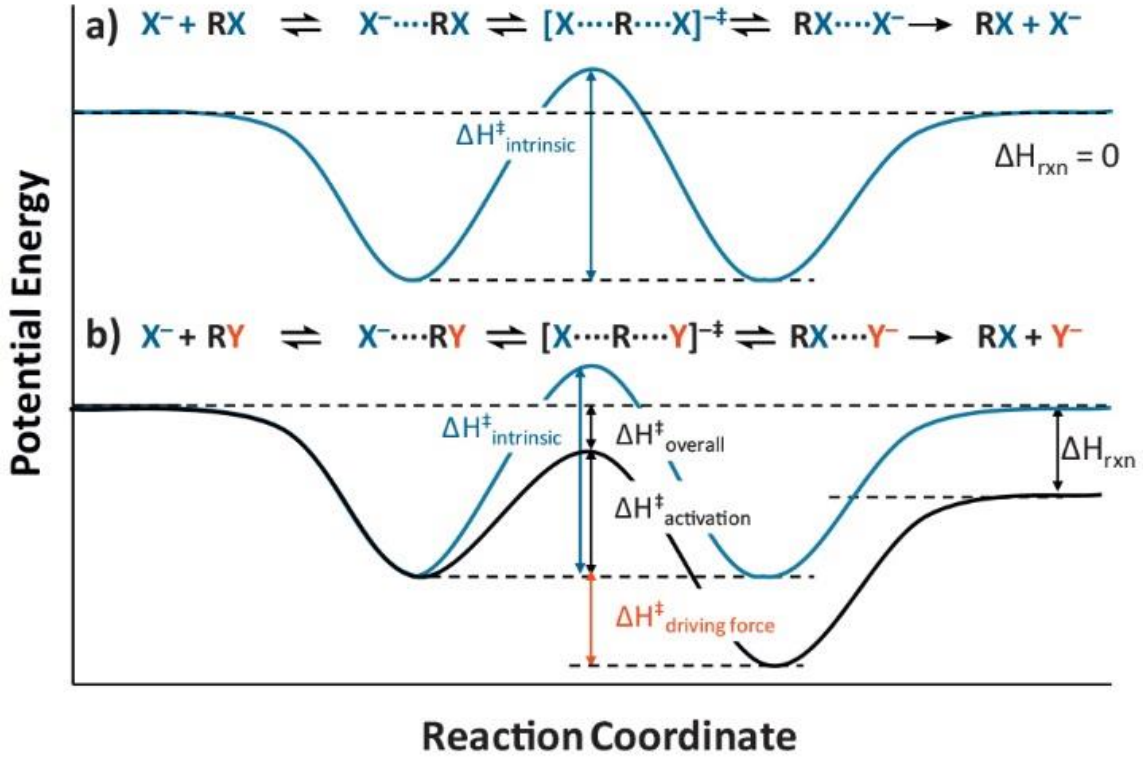

Figure 6.2 Marcus Theory for a S_N2 potential energy surface
The S_N2 potential energy surface for an identity reaction (a) and a non-identity reaction (b). The quantity $\Delta H^{\ddagger}_{intrinsic}$ represents the central barrier of an identity reaction. The central barrier for a non-identity reaction ($\Delta H^{\ddagger}_{activation}$) is modified by the thermodynamic driving force, $\Delta H^{\ddagger}_{driving\ force}$. The central barrier is often described relative to the reactant energy, $\Delta H^{\ddagger}_{overall}$.

Marcus Theory models the magnitude of the reduction in $\Delta H^{\ddagger}_{activation}$ for non-identity reactions; the results match well with experimental findings.[26] Marcus's formulation follows equation 6.1.

$$\Delta H^{\ddagger}_{activation} = \Delta H^{\ddagger}_{intrinsic} + \Delta H^{\ddagger}_{driving\ force} \qquad \textbf{6.1}$$

$\Delta H^{\ddagger}_{driving\ force}$ is calculated using equation 6.2,

$$\Delta H^{\ddagger}_{driving\ force} = \Delta H_{rxn}/2 + (\Delta H_{rxn})^2/(16 \times (\Delta H^{\ddagger}_{intrinsic} - \Delta H_{well})) \qquad \textbf{6.2}$$

where ΔH_{well} is the complexation energy of the reactant ion-dipole complex. When discussing a non-identity reaction, $\Delta H^{\ddagger}_{intrinsic}$ is determined by considering the intrinsic barrier for the identity reaction of the anion ($\Delta H^{\ddagger}_{(X,X)}$) and the substrate ($\Delta H^{\ddagger}_{(Y,Y)}$), equation 6.3.

$$\Delta H^{\ddagger}_{intrinsic} = \Delta H^{\ddagger}_{(X,Y)} = [\Delta H^{\ddagger}_{(X,X)} + \Delta H^{\ddagger}_{(Y,Y)}]/2 \qquad \textbf{6.3}$$

Figure 6.3 provides a graphical representation of equations 6.1 and 6.2 as a function of reaction exothermicity, ΔH_{rxn}. $\Delta H^{\ddagger}_{activation}$ correlates with ΔH_{rxn} at lower exothermicities, maintaining the relative differences for $\Delta H^{\ddagger}_{intrinsic(X,Y)}$. However, at larger reaction exothermicities the $\Delta H^{\ddagger}_{activation}$ values invert. In this 'inversion region' it is possible for small differences in $\Delta H^{\ddagger}_{activation}$ to be masked by strong thermodynamic driving forces.

Applying Marcus Theory to the reagent selection can be helpful for observing an α-effect. The Marcus inversion region illustrates that large exothermicities of reaction can mask small differences in the activation barrier. Therefore, a successful investigation of the α-effect requires a multifaceted approach to experimental design.

To test this theory, previous α-effect studies from this laboratory were revisited. The α-effect was previously demonstrated in gas-phase S_N2 reactions from experiments involving the normal anions, HO^-, CH_3O^-, $C_2H_5O^-$, and the α-nucleophile HOO^- with methyl fluoride, CH_3F; anisole, $CH_3OC_6H_5$; and 4-fluoroanisole, $CH_3OC_6H_4F$. The magnitude of the α-effect ranged from 2.3 to >50. The results from this study, as well as the tabulated Marcus Barriers, are reported in Table 6.1.

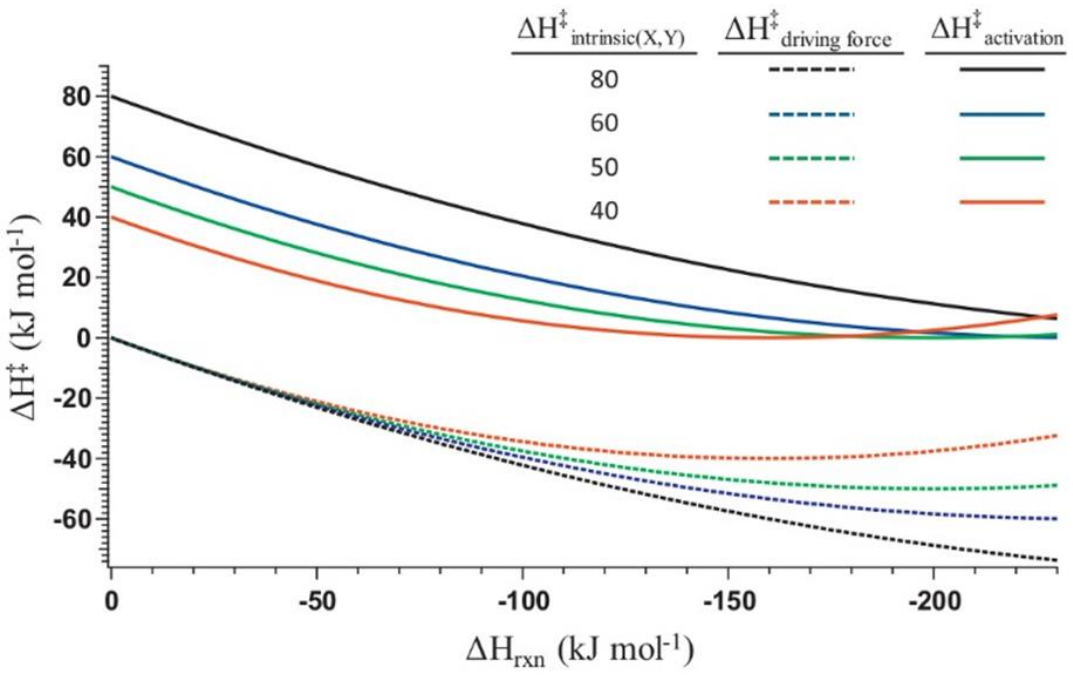

Figure 6.3 Marcus Theory relationship of $\Delta H^{\ddagger}_{activation}$ and $\Delta H^{\ddagger}_{driving\ force}$ to ΔH_{rxn}

Table 6.1 α-Effect and Marcus barriers for S_N2 reactions

						Marcus Barriers[d] (relative to reactants)				
$Nu^- + M$	PA[a]	ΔH_{rxn}[a]	S_N2 Eff[b]	α-effect[b]	$\Delta H^{\ddagger}_{overall}$[c]	$\Delta H^{\ddagger}_{(X,X)}$	$\Delta H^{\ddagger}_{(Y,Y)}$	$\Delta H^{\ddagger}_{(X,Y)}$	$\Delta H^{\ddagger}_{driving\ force}$	$\Delta H^{\ddagger}_{overall}$
$HO^- + CH_3F$	1633	–91	0.0042	0.62	–15.6	56.7	–11.0	22.9	–38.5	–15.6
$CH_3O^- + CH_3F$	1598	–70	0.0007	3.7	–14.1	43.6	–11.0	16.3	–30.4	–14.1
$C_2H_5O^- + CH_3F$	1585	–60	<0.00005	>50	–5.2	52.9	–11.0	21.0	–27.0	–6.0
$HOO^- + CH_3F$	1575	–65	0.0026		–19.4	28.1	–11.0	8.6	–28.0	–19.4
$HO^- + CH_3OC_6H_5$	1633	–162	0.13	0.69	–28.6	40.5	39.2	39.9	–68.4	–28.6
$CH_3O^- + CH_3OC_6H_5$	1598	–141	0.04	2.3	–21.6	39.4	39.2	39.3	–60.9	–21.6
$C_2H_5O^- + CH_3OC_6H_5$	1585	–131	0.01	9	–11.2	53.8	39.2	46.5	–57.7	–11.2
$HOO^- + CH_3OC_6H_5$	1575	–135	0.09		–25.6	26.7	39.2	33.0	–58.6	–25.6
$HO^- + CH_3OC_6H_4F$	1633	–174	-	-	–36.6	38.1	35.2	36.7	–73.2	–36.6
$CH_3O^- + CH_3OC_6H_4F$	1598	–153	0.10	2.3	–29.6	37.2	35.2	36.2	–65.8	–29.6
$C_2H_5O^- + CH_3OC_6H_4F$	1585	–143	0.02	12	–19.2	51.8	35.2	43.5	–62.7	–19.2
$HOO^- + CH_3OC_6H_4F$	1575	–147	0.23		–33.9	23.8	35.2	29.5	–63.4	–33.9

[a]Thermodynamic data in units of kJ mol^{-1}; Proton Affinities (PA) of the nucleophile, reaction exothermicities (ΔH_{rxn}). [b]S_N2 reaction efficiencies (S_N2 Eff), relative α-effects ($Eff_{\alpha\text{-}Nu}/Eff_{normal\text{-}Nu}$) of reactions involving CH_3F, $CH_3OC_6H_5$, and $CH_3OC_6H_4F$. [c]Transition state barriers ($\Delta H^{\ddagger}_{overall}$) calculated using G2(+) methods for methyl fluoride reactions, G3MP2 for anisoles. [d]Marcus barriers calculated using equations 6.1, 6.2, and 6.3 where ΔH_{well} (CH_3F=50, $CH_3OC_6H_5$=92, and $CH_3OC_6H_4F$=102 kJ mol^{-1})

Comparing HOO^- to HO^- does not reveal an α-effect with the neutral reagents listed, likely because the S_N2 reactions of HO^- with anisole and 4-fluoroanisole are highly exothermic (–162 and –174 kJ/mol, respectively). These reactions therefore occur in the Marcus inversion region. In addition, the proton affinity (PA) of HO^- (1633 kJ/mol) is much greater than that for HOO^- (1575 kJ/mol) suggesting different nucleophilic behavior. Conversely, the reactivity of HOO^- with the remaining alkoxides does reveal an α-effect; the exothermicities and PAs of the normal-oxyanions better match those of HOO^- than hydroxide.

6.3 Investigating the α-Effect in S_N2 and E2 Reactions

Nucleophiles may undergo both substitution (S_N2) and elimination (E2) reactions. Reagent anions were selected to be similar in both structure and basicity to produce meaningful Brønsted correlations. In this section, the reactions of the normal-oxyanions $FCH_2CH_2O^-$ and $C_6H_5CH_2O^-$ are compared to the α-oxyanion $(CH_3)_3COO^-$. The neutral reagents CH_3Cl and $(CH_3)_3CCl$ were selected to investigate S_N2 and E2 reactivity, respectively. Reactions with CH_3Cl produce Cl^- exclusively through an S_N2 reaction; Cl^- cannot be generated from CH_3Cl through an E2 reaction because CH_3Cl does not contain β-hydrogens. The reactions with $(CH_3)_3CCl$ will also produce Cl^-, but due to steric crowding at the electrophilic carbon, the reactions are assumed to produce Cl^- strictly from an E2 mechanism. The results of our kinetic studies of the six reactions are presented in Table 6.2.

Table 6.2 α-effect for S_N2 and E2 reactivity

		Thermodynamic data[a]			kinetic data[b]		α-Effect
	$Nu^- + M$	PA	ΔH_{rxn}	$\Delta H^{\ddagger}_{overall}$	k_{exp} ($\times 10^{-10}$)	Eff	$Eff_{\alpha\text{-}Nu}/Eff_{normal\text{-}Nu}$
S_N2	$FCH_2CH_2O^- + CH_3Cl$	1553(1544)	–130(–149)	–37.4	6.28±0.20	0.31	1.6
	$C_6H_5CH_2O^- + CH_3Cl$	1548(1538)	–125(–148)	–31.8	4.46±0.09	0.24	2.1
	$(CH_3)_3COO^- + CH_3Cl$	1552(1552)	–141(–164)	–44.9	9.74±0.20	0.51	
E2	$FCH_2CH_2O^- + (CH_3)_3CCl$	1553(1544)	–88.3(–80.0)	–35.1	12.3±0.2	0.56	0.9
	$C_6H_5CH_2O^- + (CH_3)_3CCl$	1548(1538)	–83.3(–73.7)	–32.2	5.17±0.10	0.27	1.9
	$(CH_3)_3COO^- + (CH_3)_3CCl$	1552(1552)	–87.3(–82.3)	–39.6	10.2±0.2	0.51	

[a]Thermodynamic data in units of kJ mol^{-1}; experimental and theoretical proton affinity (PA) and reaction enthalpy (ΔH_{rxn}), theoretical values are in parentheses and calculated using G3MP2; theoretical transition state barriers ($\Delta H^{\ddagger}_{overall}$) calculated using G3MP2. [b]Overall rate constant expressed in units of $cm^3\ s^{-1}$, Error bars represent one standard deviation (1σ) of the data, absolute uncertainty is ±30%. Reaction efficiency ($Eff = k_{exp}/k_{col}$), k_{col} calculated from PTT [Ref. 19]

The S_N2 reactions showed a small α-effect. The reaction efficiency is slightly lower for $C_6H_5CH_2O^-$ compared with $FCH_2CH_2O^-$ in agreement with the computational barriers. The theoretical reaction barrier of $C_6H_5CH_2O^-$ is higher than that of $FCH_2CH_2O^-$ by ~6 kJ mol^{-1}. The barrier for the α-oxyanion $(CH_3)_3COO^-$ is the lowest. While the magnitude of the α-effect is small, it is consistent with previous estimations concerning small differences in intrinsic reaction barriers. Although enhanced reactivity is observed with the α-nucleophile relative to proton affinity, part of this effect may arise from the larger exothermicity of the reaction (~10 kJ mol^{-1}).

The α-effect has not been previously reported in experimental elimination reactions, but has been suggested to exist in E2 reactions involving ethyl chloride from the computational work of Ren and Yamataka.[28] Ethyl chloride was not investigated due to the competing S_N2 reaction pathway. The experimental reaction efficiencies from investigating the E2 reactions with $(CH_3)_3CCl$ correlate well with the proton affinities and reaction exothermicities of the reagent anions. This is consistent with the E2 mechanism, which requires protonation of the anion. The strength of the correlation shows that the E2 mechanism is highly sensitive to the proton affinity of the anion. The α-oxyanion $(CH_3)_3COO^-$ pairs better with $FCH_2CH_2O^-$ than $C_6H_5CH_2O^-$ due to a more similar proton affinity. The proton affinity of $C_6H_5CH_2O^-$ is lower by approximately 5 kJ mol^{-1}. Although the reaction efficiency of $(CH_3)_3COO^-$ is slightly lower than that for $FCH_2CH_2O^-$, the reaction efficiencies are the same within experimental error. Due to slightly larger entropic barriers within the S_N2 mechanism, the rate constants for the reagent anions are slightly higher for the E2 mechanism than for the S_N2 mechanism even though the computational barriers for the E2 mechanism are slightly higher.

Experimental E2 reaction efficiencies involving $(CH_3)_3CCl$ from this work were combined with previously measured reaction efficiencies to form the Brønsted correlation in Figure 6.4. Brønsted correlations compare the reaction efficiency (Eff = k_{exp}/k_{col}, y-axis) to the anion proton affinity (x-axis), forming a rate-energy correlation. While anions 2 through 10 have an approximately linear-fit, the overall correlation is non-linear, and the curvature increases at lower anion proton affinities. Figure 6.4 illustrates

that the efficiencies of E2 reactions are strongly correlated to the proton affinity of the anion, but the non-linear behavior suggests significant contributions from factors other than the activation barrier. The origin of the curvature has been previously discussed, and is attributed to minor differences in the transition state structures.[29] There is a high amount of variability in an E2 transition state due to the three components: proton transfer (PT) from C_β to the nucleophile, π-bond formation between C_α and C_β, and the geometry between the leaving group and C_α. On the other hand, some of the curvature at higher anion proton affinity can be attributed to the reaction efficiencies approaching the collision rate.

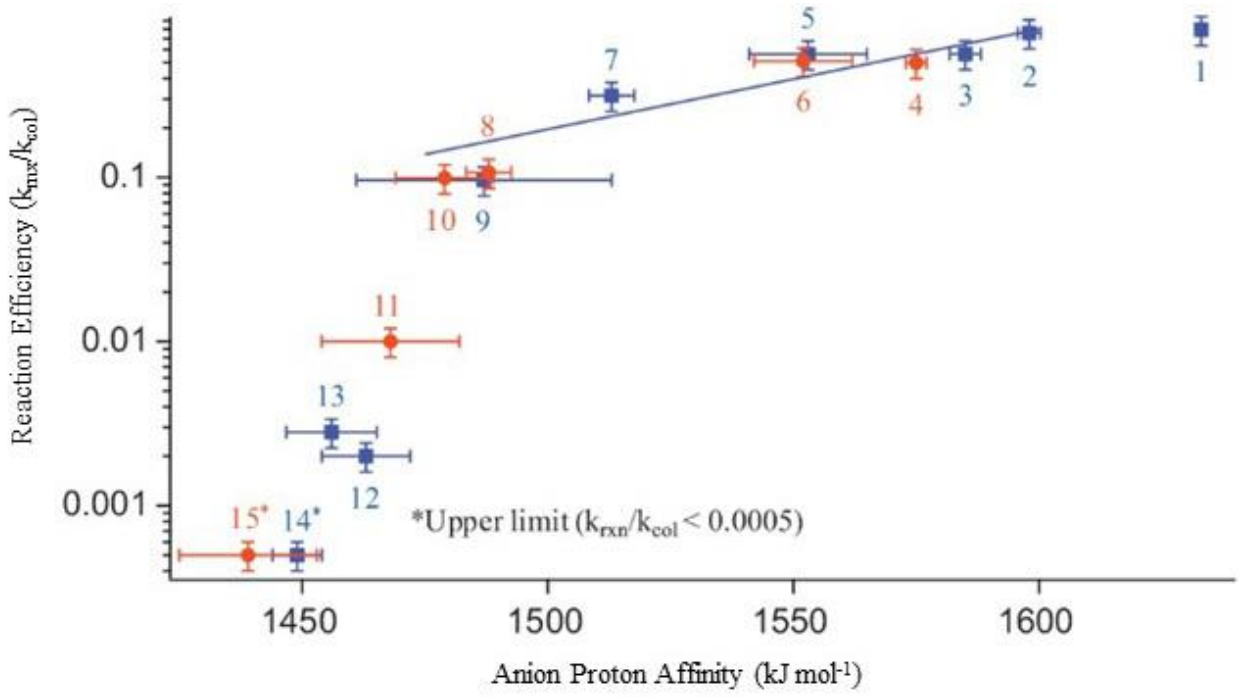

Figure 6.4 Brønsted correlation of E2 reaction efficiencies of oxyanions with $(CH_3)_3CCl$
Reaction efficiency (k_{exp}/k_{col}) vs the proton affinity (PA) for the E2 reactions of normal- and α-nucleophiles with $(CH_3)_3CCl$. Previously measured rate constants from references [Ref. 22-25]. Efficiencies calculated from PTT [Ref. 19]. (■, normal-anions; ● α-anions): 1. HO^- 2. CH_3O^- 3. $C_2H_5O^-$ 4. HOO^- 5. $CFH_2CH_2O^-$ 6. $(CH_3)_3COO^-$ 7. $CF_3CH_2O^-$ 8. ClO^- 9. $CF_3CF_2CH_2O^-$ 10. BrO^- 11. $HC(O)OO^-$ 12. $C_6H_5O^-$ 13. $HC(O)O^-$ 14. $CH_3C(O)O^-$ 15. $CH_3C(O)OO^-$.

Small deviations in the correlation between proton affinity and reaction efficiencies in Table 6.2 and Figure 6.4 suggest that a minor α-effect may occur in E2 transition states. However, a substantive intrinsic origin does not seem to prevail for an enhanced reactivity of α-nucleophiles in the E2 mechanism.

6.4 The α-Effect within Micro-Solvated Systems

The investigation of physical-organic chemistry in the gas-phase is highly desirable because intrinsic properties and reactivities may be observed in the absence of solvent. In addition, several experiments attempt to bridge the gap between condensed- and gas-phase environments by studying gas-phase reactions through micro-solvation, where a controlled number of solvent molecules are added to a reagent. The micro-solvated reactions investigated in this chapter illustrate that, while the α-effect might have a minor intrinsic contribution, solvation clearly enhanced the magnitude.[22-24]

The gas-phase nucleophilic reactions with methyl chloride proceed exclusively through an S_N2 reaction mechanism. Since there are no competing mechanisms, reaction efficiencies of normal- and α-nucleophiles with methyl chloride can be compared directly. A summary of the S_N2 reactions of un-solvated HO^-, CH_3O^-, $C_2H_5O^-$, $(CH_3)_2CHO^-$ and HOO^-;[18, 34] water micro-solvated $HO^-[H_2O]$, $CH_3O^-[H_2O]$, $C_2H_5O^-[H_2O]$, $(CH_3)_2CHO^-[H_2O]$ and $HOO^-[H_2O]$;[23] and methanol micro-solvated $CH_3O^-[CH_3OH]$, $C_2H_5O^-[CH_3OH]$, $(CH_3)_2CHO^-[CH_3OH]$ and $HOO^-[CH_3OH]$[24] with CH_3Cl are presented in Table 6.3. Methanol solvated hydroxide, $HO^-[CH_3OH]$, cannot be investigated because hydroxide will deprotonate methanol to form hydrated methoxide, $CH_3O^-[H_2O]$.

Table 6.3 Water- methanol- and un-solvated nucleophiles in reactions with methyl chloride

	thermodynamic data[a]		kinetic data[b]			product fraction[c]	
Nu^-	PA	ΔH_{rxn}	k_{exp} ($\times 10^{-11}$)	Eff	α-effect	Cl^-	$Cl^-[H_2O]$ or $Cl^-[CH_3OH]$
$HO^-[H_2O]$	1538	–101/–161	36	0.15	0.29	0.85	0.15
$CH_3O^-[H_2O]$	1520	–103/–164	10±1	0.049	0.90	0.78	0.22
$C_2H_5O^-[H_2O]$	1511	–95/–155	3.3±0.1	0.016	2.8	0.47	0.53
$(CH_3)_2CHO^-[H_2O]$	1505	–82/–143	0.54±0.05	0.0028	16	0.42	0.58
$HOO^-[H_2O]$	1493	–80/–140	9.3±0.3	0.044		0.72	0.28
$CH_3O^-[CH_3OH]$	1508	–91/–157	2.6±0.1	0.013	0.30	0.68	0.32
$C_2H_5O^-[CH_3OH]$	1500	–83/–150	0.61±0.04	0.0032	1.2	0.52	0.29[d]
$(CH_3)_2CHO^-[CH_3OH]$	1496	–71/–138	0.14±0.01	0.00075	5.2	e	e
$HOO^-[CH_3OH]$	1466	–64/–130	0.79±0.06	0.0039		0.67	0.33
HO^-	1635 (1633)	–214	190	0.67	0.78	1.0	
CH_3O^-	1601 (1598)	–202	160	0.60	0.87	1.0	
$C_2H_5O^-$	1584 (1585)	–187	130	0.60	0.87	1.0	
$(CH_3)_2CHO^-$	1574 (1576)	–171	110	0.54	0.96	1.0	
HOO^-	1574 (1575)	–186	123	0.52		1.0	

[a]Thermodynamic data in units of kJ mol^{-1} calculated using G3; proton affinities (PA) of the micro-solvated anion with experimental values in parentheses when available (Ref. 27); reaction enthalpies (ΔH_{rxn}) for the products Cl^- and clustered $Cl^-[H_2O]$ or $Cl^-[CH_3OH]$, respectively ($Cl^-/Cl^-[H_2O]$) or ($Cl^-/Cl^-[CH_3OH]$). [b]Overall rate constant expressed in units of $cm^3\ s^{-1}$ (Ref. 15, 16, 27); Error bars represent one standard deviation (1σ) of the data, absolute uncertainty is ±30%. Reaction efficiency ($Eff = k_{exp}/k_{col}$), k_{col} calculated from PTT (Ref. 19). [c]Absolute uncertainty is ±50%. [d]Additional 0.19 $Cl^-[C_2H_5OH]$ formation. [e]Because of the low reactivity, a product distribution could not be determined.

Figure 6.5 provides a Brønsted rate-energy correlation between the reaction efficiencies and proton affinities of the un- and micro-solvated nucleophilic anions. While an α-effect is not observed for the un-solvated nucleophiles, an enhanced reactivity is observed for both the water and methanol solvated HOO^-.

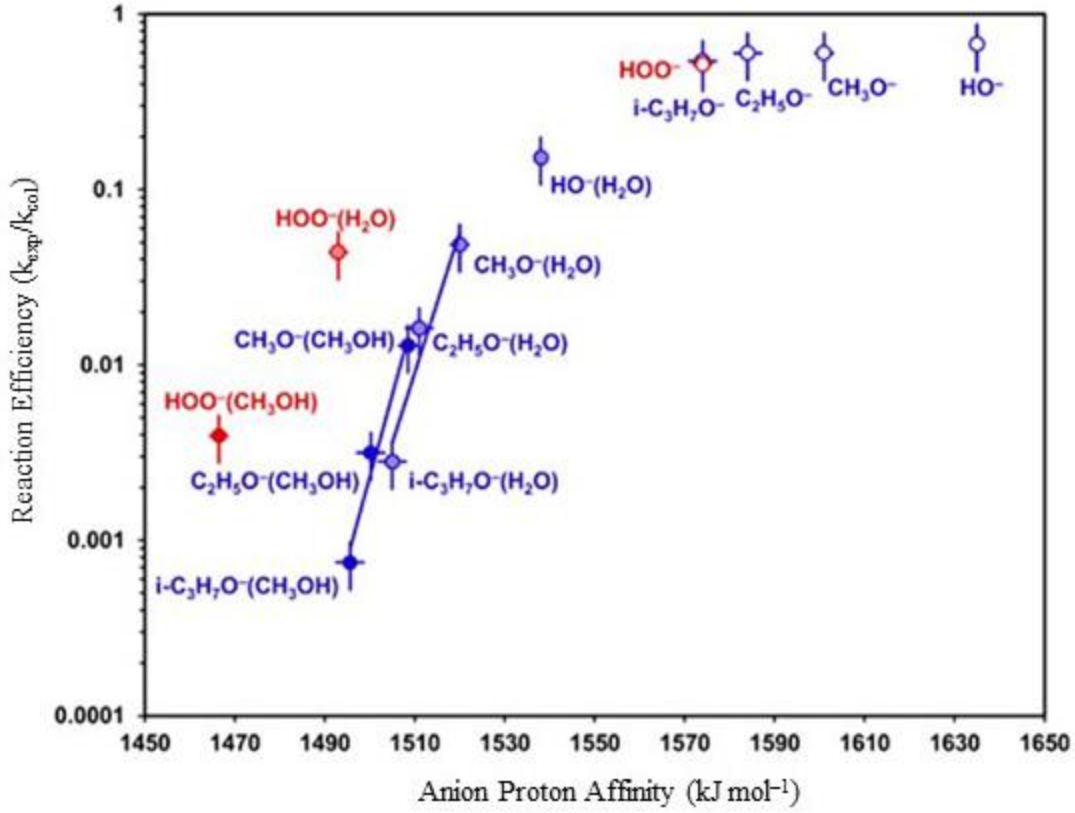

Figure 6.5 Brønsted correlation of water-, methanol-, and un-solvated nucelophiles reacting with CH_3Cl

Reaction efficiency (k_{exp}/k_{col}) vs proton affinity (PA) for the S_N2 reaction of un-solvated (○), water-solvated (shaded circles), and methanol solvated (●) anions with methyl chloride. Normal- and α-nucleophiles are represented in blue and red, respectively. The linear trend lines are fits to the normal nucleophiles data set comprising CH_3O^-, $C_2H_5O^-$, and $(CH_3)_2CHO^-$ with methanol- and water-solvation respectively.

Figure 6.5 clearly illustrates an α-effect for the reactivity of $HOO^-[H_2O]$; an α-effect is not observed for the un-solvated system. Considering the PA of $HOO^-[H_2O]$, this anion reacts more than an order of magnitude faster than is expected based on the rate-energy relationship illustrated by the other water solvated nucleophiles. Although the un-solvated nucleophiles have a large proton affinity range (~60 kJ mol^{-1}), their range of reaction efficiencies is quite small (0.52 to 0.67). In contrast, the water-solvated nucleophiles show reaction efficiencies that vary from 0.0028 to 0.15, a factor of ~50. The addition of a single water molecule to the nucleophilic reagents dramatically affects their reactivity.

The methanol-solvated reactions with methyl chloride also clearly illustrate an α-effect. Adding a methanol molecule ($\Delta PA_{average,methanol}$ = –85 kJ mol^{-1}) to the normal nucleophiles results in a greater decrease in the proton affinity than adding a water molecule ($\Delta PA_{average,water}$ = –74 kJ mol^{-1}), Table 6.3. However, solvation of HOO^- shows even larger changes in stability; the computational PA of HOO^- with the addition of methanol is ΔPA = –110 kJ mol^{-1} and with the addition of water is ΔPA = –81 kJ mol^{-1}. Considering the rate-energy correlation for the methanol-solvated–normal nucleophiles, the observed reactivity of $HOO^-[CH_3OH]$ is more than two orders of magnitude faster than expected.

Due to the larger decrease in the proton affinity of the methanol-solvated ions compared with the water-solvated ions, the relative efficiencies of the methanol solvated system are lower than the water solvated system with methyl chloride. Despite the reduction in efficiency, Figure 6.5 illustrates a similar curvature for the water and methanol solvation rate-energy relationships; the linear regressions presented are only intended to guide the eye. Furthermore, the linear regressions illustrate that both water and methanol solvation have a similar consequence on the oxy reagent α-effect studies. While the α-effect is not observed in the un-solvated reagent system, both solvent molecules allow observation of an α-effect for the S_N2 reactivity of HOO^- with methyl chloride.

Studying the α-effect between the water- or un-solvated reagents with methyl bromide is not productive because the high exothermicity of reaction will mask subtle differences in transition state barriers and reaction efficiencies, as established in the discussion of section 6.2. However, methanol solvation reduces the PA of the reagent nucleophiles, therefore reducing the exothermicity of the reaction with methyl bromide. Consequently, in addition to the reactions with methyl chloride, an α-effect is observed in the reactions of the methanol-solvated reagents with methyl bromide. The results are presented in Table 6.4.

Table 6.4 Methanol Solvated Nucleophiles Reactivity with Methyl Bromide

	thermodynamic data[a]		kinetic data[b]			product fraction[c]	
Nu^-	PA	ΔH_{rxn}	k_{exp} ($\times 10^{-11}$)	Eff	α-effect	Br^-	$Br^-[CH_3OH]$
$CH_3O^-[CH_3OH]$	1508	–123/–181	57±2	0.33	0.8	0.95	0.05
$C_2H_5O^-[CH_3OH]$	1500	–115/–174	38±2	0.23	1.1	0.89	0.08[d]
$(CH_3)_2CHO^-[CH_3OH]$	1496	–103/–162	20±1	0.13	2.0	0.91	0.09
$HOO^-[CH_3OH]$	1466	–97/–154	45±1	0.26		0.92	0.08

[a]Thermodynamic data in units of kJ mol^{-1} calculated using G3; proton affinity (PA) of the micro-solvated anion; reaction enthalpy (ΔH_{rxn}) displayed for Br^- and clustered $Br^-[CH_3OH]$ products, respectively ($Br^-/Br^-[CH_3OH]$). [b]Overall rate constant (k_{exp}) in units of cm^3 s^{-1}. Error bars represent one standard deviation (1σ), absolute uncertainty is ±30%. Reaction efficiency (Eff = k_{exp}/k_{col}), k_{col} calculated from PTT [Ref. 19]. [c]Absolute uncertainty is ±50%. [d]Additional 0.04 $Br^-[C_2H_5OH]$ formation.

Figure 6.6 shows the Brønsted rate-energy correlation between the methanol solvated system with methyl bromide (upper panel) and methyl chloride (lower panel.) The methyl bromide reactions are more efficient, likely due to the higher exothermicity of reaction and a strong thermodynamic driving force. The results illustrate an enhanced reactivity of $HOO^-[CH_3OH]$ with both methyl bromide and chloride as the efficiencies of the reactions with $HOO^-[CH_3OH]$ deviate from the rate-energy relationship displayed with the normal nucleophiles. Studying the reactivity of methanol-solvated nucleophiles with methyl bromide and chloride reveal an α-effect in two different efficiency ranges.

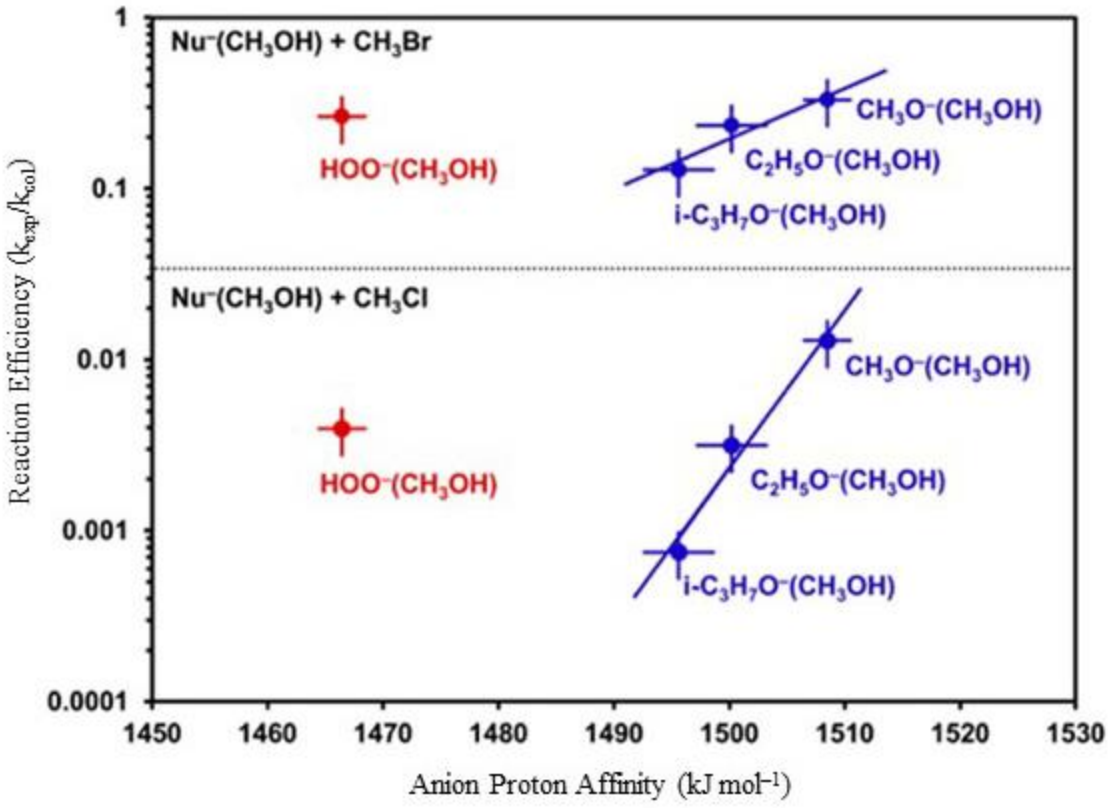

Figure 6.6 Brønsted correlation of methanol-solvated nucleophiles with CH_3Br and CH_3Cl
Reaction efficiency (k_{exp}/k_{col}) vs proton affinity (PA) for the S_N2 reaction of methanol-solvated nucleophiles with CH_3Br (upper panel) and CH_3Cl (lower panel). The linear trend lines are fits to the normal nucleophile data sets.

The product distributions and reaction exothermicities for the reactions of the water- and methanol-solvated nucleophiles with methyl bromide and chloride are summarized in Table 6.3 and Table 6.4. Although the reactions with methyl bromide and chloride may only proceed through an S_N2 reaction mechanism, two products are possible, the un-solvated (6.4) and solvated (6.5) halide ion.

$$Nu^-[CH_3OH] + CH_3X \rightarrow NuCH_3 + X^- + CH_3OH \quad \textbf{6.4}$$

$$\rightarrow NuCH_3 + X^-[CH_3OH] \quad \textbf{6.5}$$

The reactions following equation 6.5 are more exothermic, and they could reasonably be expected to dominate the product distribution. However, in all but two reactions studied, formation of the bare halide ion (equation 6.4) dominates the distribution. The remaining two reactions involving the water-solvated nucleophiles $C_2H_5O^-[H_2O]$ and $(CH_3)_2CHO^-[H_2O]$ generate roughly equal amounts of Cl^- and $Cl^-[H_2O]$. Previous studies of S_N2 reactions with micro-solvated nucleophiles list similar product distributions.[37, 38] Many factors may contribute to the preferred formation of bare product ions including steric hinderance,[39] product dynamics,[40] and redistribution of excess energy.[41] The micro-solvation study reveals similar product distributions for the normal- and α-nucleophiles suggesting that the enhanced reactivity observed with the micro-solvated HOO^- is not reflected in the product distributions.

6.5 The α-Effect and Competing Mechanisms with Methyl Formate

Methyl formate provides an interesting substrate to investigate nucleophilic-reactivity due to competing mechanisms. PT, S_N2, and $B_{AC}2$ mechanisms are in competition when a nucleophile reacts with methyl formate, Scheme 6.1. Preference for S_N2 or $B_{AC}2$ reaction channels suggests an increased nucleophilicity of the anionic reagent compared to PT channels.

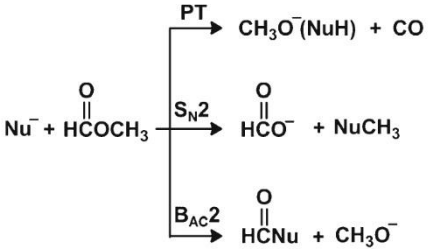

Scheme 6.1

Previously studied methyl formate reactions reported similar branching fractions (S_N2:PT:$B_{AC}2$) for HO^- (5%:61%:34%) and HOO^- (8%:64%:28%).[42] Due to the similar reactivity between the prototypical α-nucleophile HOO^- compared with HO^- the authors concluded that the α-effect is not intrinsic in

origin.[42] This conclusion was later questioned by Patterson and Fountain. Patterson and Fountain argue that, because the PA of HOO^- is ~60 kJ mol^{-1} smaller than the PA of HO^-, a similarity in reactivity supports an intrinsic α-effect.[9] The reactions of HO^- and HOO^- with methyl formate is reinvestigated and expanded by adding the normal-nucleophiles CH_3O^-, $C_2H_5O^-$, and $(CH_3)_2CHO^-$. (Actual reactivity is investigated with deuterium and ^{18}O labeled compounds to differentiate reaction pathways.) The results are tabulated in Table 6.5.

Table 6.5 The α-effect for reactions of un-solvated anions with methyl formate

			S_N2			PT		$B_{AC}2$		
Nu^-	PA[a]	k_{exp} ($\times10^{-9}$)[b]	BF(Eff)[c]	$\Delta H^{\ddagger}$[d]	α-effect	BR (Eff)[c]	$\Delta H^{\ddagger}$[d]	BR(Eff)[c]	$\Delta H^{\ddagger}$[d]	α-effect
$H^{18}O^-$	1633±2	1.73±0.03	0.08(0.05)	–39.3	1	0.59(0.47)	–83	0.33(0.20)	–53	0.9
CD_3O^-	1598±2	1.33±0.03	0.03(0.02)	–31.6	2.5	0.79(0.48)	–64	0.18(0.11)	–48	1.5
$CH_3CD_2O^-$	1585±3	1.25±0.02	<0.01	–21.8	~13	0.97(0.62)	–53	0.03(0.02)	–45	8.5
$(CH_3)_2CHO^-$	1576±4	1.20±0.02	—	–13.1	—	1.0(0.64)	–47	—	–44	—
HOO^-	1575±2	1.34±0.03	0.08(0.05)	–35.7		0.64(0.39)	–76	0.28(0.17)	–55	

[a]Experimental proton affinity (PA, Ref. 27). [b]Overall rate constants in units of $cm^3\ s^{-1}$, error bars reported as 1σ, absolute uncertainty is ±30%. [c]Branching fractions (BF), Efficiency (Eff) compares the relative rate constant for the branching fraction to the theoretical collision rate (k_{col}) calculated using PTT (Ref. 19). [d]Barrier heights and reaction exothermicity are relative to reactants and calculated with G3MP2.

All of the methyl formate reactions are very efficient. The theoretical reaction barriers support the experimental branching fractions, and the experimental results can be applied to understand intrinsic differences in each of the reaction channels. The reaction mechanisms involving methyl formate were computationally evaluated by Pliego and Riveros.[43] Their results suggest that: the PT channel occurs through a single-well potential; the S_N2 channel occurs through a double-well potential, and the $B_{AC}2$ channel occurs through a multi-well potential where the controlling barrier is for the formation of the tetrahedral intermediate.[43] These controlling barriers were theoretically computed with the G3MP2 method, and reported in Table 6.5. Both the S_N2 and $B_{AC}2$ reaction efficiencies correlate nicely with the theoretical barrier heights. However, the PT channel efficiencies seem a bit low when considering the reaction exothermicity. Pliego and Riveros modeled the PT mechanism as a direct formation of the methoxide ion bound to the neutral molecules CO and NuH.[43] This approach creates a proton abstraction process that is highly exothermic, but models a reaction that is more difficult than direct proton

abstraction. The PT process occurs on the formyl end of the molecule, while the S_N2 and $B_{AC}2$ mechanisms require the nucleophile to approach the methyl end of the ester. Nucleophilic attack at the methyl end of the ester by HO^- has been statistically modeled by RRKM theory, and the results match our observed branching fractions suggesting that the behavior of the S_N2 and $B_{AC}2$ mechanisms are statistical. The reported product fractions (S_N2:$B_{AC}2$) from RRKM theory (15%:85%) are in agreement with experimental data (20%:80%).[43]

Comparing the relative efficiencies for the nucleophilic S_N2 and $B_{AC}2$ reactions certainly favors the HOO^- anion as the proton affinity of the normal-nucleophiles decreases. It is unfortunate that the reaction of $(CH_3)_2CHO^-$ (the normal-nucleophile closest in proton affinity to HOO^-) only occurs through the PT reaction pathway, masking the nucleophilic reaction channels. This prohibits a report of an upper limit to the nucleophilic reaction channels for $(CH_3)_2CHO^-$, and therefore the magnitude of the α-effect cannot be reported. Nonetheless, a slight enhancement in the nucleophilicity for HOO^- is observed in comparison to $CH_3CD_2O^-$ and CD_3O^-. While the magnitude of the α-effect is greater for the $B_{AC}2$ reactions in solution,[5] this does not appear to be the case in gas-phase reactions with methyl formate, as the S_N2 reactions at the sp^3 carbon are the same or slightly higher than $B_{AC}2$ reactions at the sp^2 carbon.

The same reactions with methyl formate were investigated in the presence of a single water molecule. The hydrated-anionic nucleophiles were introduced into the reaction flow tube for reactions with methyl formate. The micro-solvated system exhibited a much larger α-effect than was previously observed with the solvent free reactant system. Figure 6.7 presents a Brønsted energy-rate correlation diagram comparing the reactivity of the un- and micro-solvated nucleophiles with methyl formate. The plot uses two linear regressions to exhibit the rate-energy relationship of the two respective systems (un- and micro-solvated). The plot unambiguously illustrates the enhanced reactivity of the micro-solvated α-nucleophile $HOO^-[H_2O]$ as it deviates from the rate-energy relationship followed by the normal-nucleophiles. Even the addition of a single water molecule seems to mimic the solvation environment, particularly the enhanced reactivity of HOO^- observed in solution.

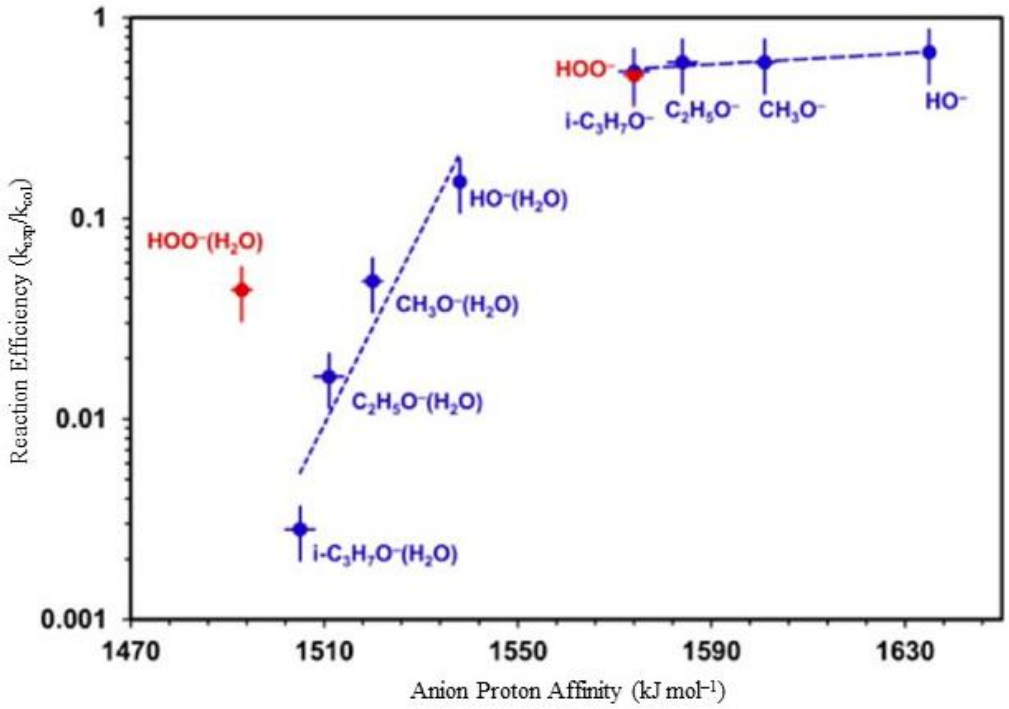

Figure 6.7 Brønsted plot: Micro-solvated and un-solvated ions with methyl formate
The reaction efficiencies (k_{exp}/k_{col}) are compared to the anion PA for the un-solvated and micro-solvated nucleophiles with methyl formate. The anion proton affinities are calculated using the G3 method. Vertical error bars represent uncertainty in the rate constants (±30%), while the horizontal error bars represent the uncertainty in the experimentally determined PA. Blue and red circles represent normal-and α-nucleophiles, respectively.

A complete report of the experimental results including kinetic measurements, branching fraction, relative reaction channel efficiency, and transition state barriers is provided in Table 6.6. The reactivity of the micro-solvated nucleophile compared with the un-solvated anion mostly differs in the $B_{AC}2$ channel, where the efficiency rapidly decreases in going from the smaller alkoxy anions to the larger anions. The larger normal-nucleophile, $(CH_3)_2CHO^-[H_2O]$, does not exhibit any $B_{AC}2$ reactivity. This is not surprising because if $(CH_3)_2CHO^-[H_2O]$ forms a tetrahedral complex as required in the $B_{AC}2$ mechanism, the intermediate will dissociate back to reactants as $(CH_3)_2CHO^-[H_2O]$ is a better leaving group than $CH_3O^-[H_2O]$.

Table 6.6 The α-effect for reactions of water-solvated anions with methyl formate

			S_N2		PT		$B_{AC}2$		
$Nu^-[H_2O]$	PA[a]	k_{exp} ($\times10^{-10}$)[b]	BF(Eff)[c]	$\Delta H^{\ddagger}$[d]	BF(Eff)[c]	$\Delta H^{\ddagger}$[d]	BF(Eff)[c]	$\Delta H^{\ddagger}$[d]	α-effect
$H^{18}O^-[H_2{}^{18}O]$	1538	13.9±0.3	—	–2	0.50(0.32)	–51	0.50(0.32)	–48	1.4
$CD_3O^-[H_2O]$	1527	6.4±0.2	0.40(0.13)	–3	0.20(0.07)	–47	0.40(0.13)	–44	3.5
$CH_3CD_2O^-[H_2O]$	1517	4.0±0.1	0.65(0.14)	3	0.25(0.06)	–41	0.10(0.02)	–43	23
$(CH_3)_2CHO^-[H_2O]$	1505	1.8±0.1	0.60(0.06)	8	0.40(0.04)	–38	—	–40	
$HOO^-[H_2O]$	1493	8.7±0.1	—	1	—	–38	1.0(0.45)	–45	

[a]Experimental proton affinity (PA) in units of kJ mol^{-1} calculated using G3. [b]Overall rate constants in units of cm^3 s^{-1}, error bars reported as 1σ, absolute uncertainty is ±30%. [c]Branching fractions (BF), Efficiency (Eff) compares the relative rate constant for the branching fraction to the theoretical collision rate (k_{col}) calculated using PTT (Ref. 19). [d]Barrier heights and reaction exothermicity are relative to reactants and calculated using G3.

It is striking that, despite the high enthalpic S_N2 transition state barriers presented in Table 6.6, the S_N2 product channel can compete with the PT and $B_{AC}2$ channels. Figure 6.8 illustrates the lowest energy transition state structures. Examination of the transition states reveals that the PT and $B_{AC}2$ reaction channels proceed through highly ordered intermediate structures. Whereas the S_N2 transition state structures for the un-solvated reaction system require the most ordered structures, the micro-solvated S_N2 transition state structures are the least ordered, and therefore the PT and $B_{AC}2$ channels must surmount high entropic barriers in the micro-solvated systems.

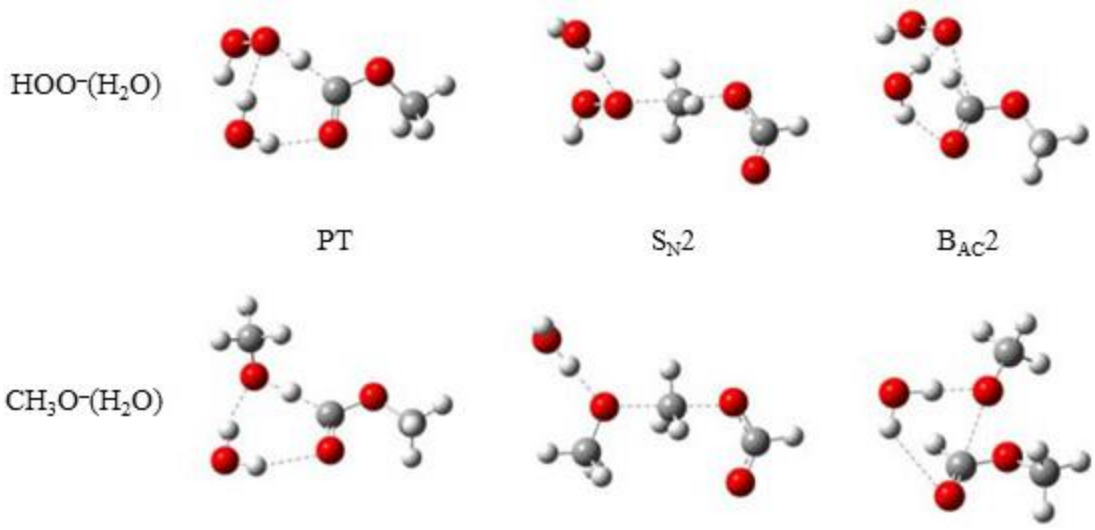

Figure 6.8 Lowest energy transition states for micro-solvated ions with methyl formate
Optimized at the MP2/6-311++G(d,p) level, the transition state geometries are illustrated for the PT, S_N2, and $B_{AC}2$ reaction pathways for $HOO^-(H_2O)$ and $CH_3O^-(H_2O)$.

Previous studies investigating substitution reactions at saturated carbon centers report that incremental micro-solvation rapidly decreases the efficiency of reaction.[23, 37, 38, 44-46] While the study regarding S_N2 reactions of micro-solvated ions with methyl chloride illustrated a decrease in the reaction efficiency by a factor of 100 (section 6.4),[23] the efficiency for reaction between the micro-solvated anions and methyl formate is only decreased by a factor of at most six. Although it is not favored entropically, the interaction of the water molecule with the carbonyl group for the PT and $B_{AC}2$ transition states (Figure 6.8) may stabilize and increase the reaction efficiency. The stabilization effect of the water molecule on the PT and $B_{AC}2$ channels is more obvious when Table 6.5 and Table 6.6 are compared. The transition states of the PT and $B_{AC}2$ channels are comparable between the un-solvated and micro-solvated systems, while the enthalpic S_N2 transition state barriers are much higher within the micro-solvated system.

Similar to the study with the un-solvated ions, the micro-solvated system illustrates an α-effect within the $B_{AC}2$ reaction pathway. The reaction of $HOO^-[H_2O]$ with methyl formate only proceeds through the $B_{AC}2$ mechanism in contrast to the un-solvated system, where the major product of HOO^- is PT. The

magnitude of the α-effect is largest when comparing the $B_{AC}2$ reactions of $HOO^-[H_2O]$ with $CH_3CD_2O^-[H_2O]$, on the order of 23. This is similar to the largest α-effect for the un-solvated system, where the α-effect for $B_{AC}2$ reaction efficiency between HOO^- and $CH_3CD_2O^-$ is on the order of 8.5.

6.6 Conclusion

Observation of the α-effect in the gas-phase was possible thanks to decades of context provided by discussion and experiments. The rate-energy relationship portrayed by Brønsted correlations provide the "gold standard" for reporting an α-effect. This relationship was not considered in early investigations of the α-effect in our lab, and resulted in a false conclusion that the α-effect is not intrinsic in origin.[42] Furthermore, the application of Marcus theory has provided a series of guidelines for designing experiments that investigate the intrinsic origin of the α-effect. Following these guidelines in experimental design has assisted the discovery of an intrinsic component of the α-effect, although pure intrinsic contributions are minor.

Furthermore, the micro-solvation studies have revealed that the large magnitudes of the α-effect reported in solution are indeed the result of differential solvation of the normal- vs. α-nucleophile. While a small intrinsic origin of the α-effect has been unveiled, the magnitude of the α-effect is clearly influenced by solvation environments, and the influence of the solvent must be considered for a complete understanding of the α-effect. Even in the presence of a single water or methanol molecule, the magnitude of the α-effect is dramatically increased, supporting both intrinsic and solvent contributions to the α-effect.

In conclusion, the α-effect is a multifaceted, complex phenomenon where several factors—both intrinsic and environmental—contribute to its magnitude. While these studies provide more context to the origin of the α-effect, a complete understanding of the α-effect will likely continue to challenge future researchers.

6.7 References

[1] J.O. Edwards, R.G. Pearson, *Factors determining nucleophilic reactivities*, J. Am. Chem. Soc., 84 (1962) 16-24.

[2] G. Klopman, K. Tsuda, J.B. Louis, R.E. Davis, *Supernucleophiles .1. alpha effect*, Tetrahedron, 26 (1970) 4549-4554.

[3] G. Klopman, R.C. Evans, *Supernucleophiles .2. Orbital interactions and nucleophilicity*, Tetrahedron, 34 (1978) 269-273.

[4] S. Oae, Y. Kadoma, *Importance of repulsion of lone electron pairs in the enhanced reactivity of 1,8-napthyridine and the large alpha-effect of hydrazine in the aminolyses of para-toluenesulfonyl chloride*, Can. J. Chem.-Rev. Can. Chim., 64 (1986) 1184-1188.

[5] E. Buncel, I.H. Um, *The alpha-effect and its modulation by solvent*, Tetrahedron, 60 (2004) 7801-7825.

[6] Y. Ren, H. Yamataka, *The alpha-effect in gas-phase S_N2 reactions: Existence and the origin of the effect*, J. Org. Chem., 72 (2007) 5660-5667.

[7] E. Buncel, S. Hoz, *Can ground-state destabilization of an alpha-nucleophile induce an alpha-effect*, Tetrahedron Lett., 24 (1983) 4777-4780.

[8] S. Hoz, *The alpha effect - on the origin of transition-state stabilization*, J. Org. Chem., 47 (1982) 3545-3547.

[9] E.V. Patterson, K.R. Fountain, *On gas phase alpha-effects. 1. The gas-phase manifestation and potential SET character*, J. Org. Chem., 71 (2006) 8121-8125.

[10] F.R. Mayo, *Free radicals, Vol. II, Jay K. Kochi, Ed., Wiley, New York, 1973. 906 pp. 42-50*, J. Polymer Sci.: Polymer Letters Edition, 12 (1974) 536-538.

[11] J.E. Dixon, T.C. Bruice, *Alpha-effect. IV. Additional observation on alpha-effect employing malachite green as substrate*, J. Am. Chem. Soc., 93 (1971) 6592-6597.

[12] J.E. Dixon, T.C. Bruice, *Alpha-effect. V. Kinetic and thermodynamic nature of alpha-effect for amine nucleophiles*, J. Am. Chem. Soc., 94 (1972) 2052-2056.

[13] M.J. Gregory, T.C. Bruice, *Alpha-effect. II. Displacements on sp^3 carbon*, J. Am. Chem. Soc., 89 (1967) 4400-4405.

[14] M.J. Gregory, T.C. Bruice, *Importance of alpha-effect in amine general base catalyzed ionization of nitroethane*, J. Am. Chem. Soc., 89 (1967) 2327-2330.

[15] R.F. Pratt, T.C. Bruice, *Lack of an alpha-effect for proton abstraction from carbon acids*, J. Org. Chem., 37 (1972) 3563-3564.

[16] J.E. McIsaac, L.R. Subbaraman, J. Subbaraman, H.A. Mulhausen, E.J. Behrman, *Nucleophilic reactivity of peroxy anions*, J. Org. Chem., 37 (1972) 1037-1041.

[17] E.A.S. Cavell, *Effect of solvent composition on the kinetics of reactions between ions and dipolar molecules*, J. Am. Chem. Soc., (1958) 4217-4222.

[18] S.M. Villano, N. Eyet, W.C. Lineberger, V.M. Bierbaum, *Reactions of alpha-nucleophiles with alkyl chlorides: Competition between S_N2 and E2 mechanisms and the gas-phase alpha-effect*, J. Am. Chem. Soc., 131 (2009) 8227-8233.

[19] J.M. Garver, S. Gronert, V.M. Bierbaum, *Experimental validation of the alpha-effect in the gas phase*, J. Am. Chem. Soc., 133 (2011) 13894-13897.

[20] J.M. Garver, Z. Yang, C.M. Nichols, B.B. Worker, S. Gronert, V.M. Bierbaum, *Resolving the alpha-effect in gas phase S_N2 reactions: A Marcus theory approach*, Int. J. Mass Spectrom., 316 (2012) 244-250.

[21] J.M. Garver, Z. Yang, N. Wehres, C.M. Nichols, B.B. Worker, V.M. Bierbaum, *The alpha-effect in elimination reactions and competing mechanisms in the gas phase*, Int. J. Mass Spectrom., 330 (2012) 182-190.

[22] D.L. Thomsen, C.M. Nichols, J.N. Reece, S. Hammerum, V.M. Bierbaum, *The alpha-effect and competing mechanisms: The gas-phase reactions of microsolvated anions with methyl formate*, J. Am. Soc. Mass Spectrom., 25 (2014) 159-168.

[23] D.L. Thomsen, J.N. Reece, C.M. Nichols, S. Hammerum, V.M. Bierbaum, *Investigating the alpha-effect in gas-phase S_N2 reactions of microsolvated anions*, J. Am. Chem. Soc., 135 (2013) 15508-15514.

[24] D.L. Thomsen, J.N. Reece, C.M. Nichols, S. Hammerum, V.M. Bierbaum, *The alpha-effect in gas-phase S_N2 reactions of microsolvated anions: Methanol as a solvent*, J. Phys. Chem. A, 118 (2014) 8060-8066.

[25] R.A. Marcus, *Theoretical relations among rate constants barriers and Brønsted slopes of chemical reactions*, J. Phys. Chem., 72 (1968) 891-899.

[26] X. Chen, J.I. Brauman, *Hydrogen bonding lowers intrinsic nucleophilicity of solvated nucleophiles*, J. Am. Chem. Soc., 130 (2008) 15038-15046.

[27] T. Su, W.J. Chesnavich, *Parametrization of the ion-polar molecule collision rate-constant by trajectory calculations*, J. Chem. Phys., 76 (1982) 5183-5185.

[28] Y. Ren, H. Yamataka, *Does alpha-effect exist in E2 reactions? A G2(+) investigation*, J. Comput. Chem., 30 (2009) 358-365.

[29] J.L. Kurz, *Relationship of barrier shape to linear free-energy slopes and curvatures*, Chem. Phys. Lett., 57 (1978) 243-246.

[30] S.M. Villano, N. Eyet, S.W. Wren, G.B. Ellison, V.M. Bierbaum, W.C. Lineberger, *Photoelectron spectroscopy and thermochemistry of the peroxyacetate anion*, Eur. J. Mass Spectrom., 16 (2010) 255-268.

[31] S.M. Villano, N. Eyet, S.W. Wren, G.B. Ellison, V.M. Bierbaum, W.C. Lineberger, *Photoelectron spectroscopy and thermochemistry of the peroxyformate anion*, J. Phys. Chem. A, 114 (2010) 191-200.

[32] J.E. Bartmess, *Negative ion energetics data in NIST chemistry WebBook*, in: P.J. Linstrom, W.G. Mallard (Eds.) NIST standard reference database number 69, National Institute of standards and Technology, Gaithersburg, MD.

[33] K.M. Ervin, V.F. DeTuro, *Anchoring the gas-phase acidity scale*, J. Phys. Chem. A, 106 (2002) 9947-9956.

[34] C.H. DePuy, S. Gronert, A. Mullin, V.M. Bierbaum, *Gas-phase S_N2 and E2 reactions of alkyl-halides*, J. Am. Chem. Soc., 112 (1990) 8650-8655.

[35] S.G. Lias, J.E. Bartmess, J.F. Liebman, J.L. Holmes, W.G. Mallard, *NIST Chemistry WebBook*, in: P.J. Lindstrom, W.G. Mallard (Eds.) Ion Energetics Data, National Institute of Standards and Technology, Gaithersburg, MD, 2014.

[36] D.K. Bohme, L.B. Young, *Kinetic studies of reactions of oxide, hydroxide, alkoxide, phenyl, and benzylic anions with methyl chloride in gas phase at 22.5 degrees*, J. Am. Chem. Soc., 92 (1970) 7354-7358.

[37] P.M. Hierl, A.F. Ahrens, M. Henchman, A.A. Viggiano, J.F. Paulson, D.C. Clary, *Nucleophilic displacement as a function of hydration number and temperature - rate constants and product distributions for $OD^-(D_2O)_{0,1,2} + CH_3Cl$ at 200-500 K*, J. Am. Chem. Soc., 108 (1986) 3142-3143.

[38] P.M. Hierl, J.F. Paulson, M.J. Henchman, *Translational energy-dependence of cross-sections for reactions of $OH^-(H_2O)_n$ with CH_3Cl and CH_3Br*, J. Phys. Chem., 99 (1995) 15655-15661.

[39] R. Otto, J. Brox, S. Trippel, M. Stei, T. Best, R. Wester, *Single solvent molecules can affect the dynamics of substitution reactions*, Nat. Chem., 4 (2012) 534-538.

[40] R. Otto, J. Brox, S. Trippel, M. Stei, T. Best, R. Wester, *Exit channel dynamics in a micro-hydrated S_N2 reaction of the hydroxyl anion*, J. Phys. Chem. A, 117 (2013) 8139-8144.

[41] T. Baer, W. Hase, *Unimolecular reaction dynamics: Theory and experiment*, Oxford University Press, New York, 1996.

[42] C.H. DePuy, E.W. Della, J. Filley, J.J. Grabowski, V.M. Bierbaum, *Absence of an alpha-effect in the gas-phase nucleophilic reactions of HOO^-*, J. Am. Chem. Soc., 105 (1983) 2481-2482.

[43] J.R. Pliego, J.M. Riveros, *The gas-phase reaction between hydroxide ion and methyl formate: A theoretical analysis of the energy surface and product distribution*, Chem.-Eur. J., 7 (2001) 169-175.

[44] D.K. Bohme, G.I. Mackay, *Bridging the gap between the gas-phase and solution - transition in the kinetics of nucleophilic displacement reactions*, J. Am. Chem. Soc., 103 (1981) 978-979.

[45] D.K. Bohme, A.B. Raksit, *Gas-phase measurements of the influence of stepwise solvation on the kinetics of nucleophilic displacement reactions with CH_3Cl and CH_3Br at room-temperature*, J. Am. Chem. Soc., 106 (1984) 3447-3452.

[46] J.V. Seeley, R.A. Morris, A.A. Viggiano, *Temperature dependences of the rate constants and branching ratios for the reactions of $F^-(H_2O)_{0-5}$ with CH_3Br*, J. Phys. Chem. A, 101 (1997) 4598-4601.

7 Appendix A

Supplimental material for construction of the ion funnel.

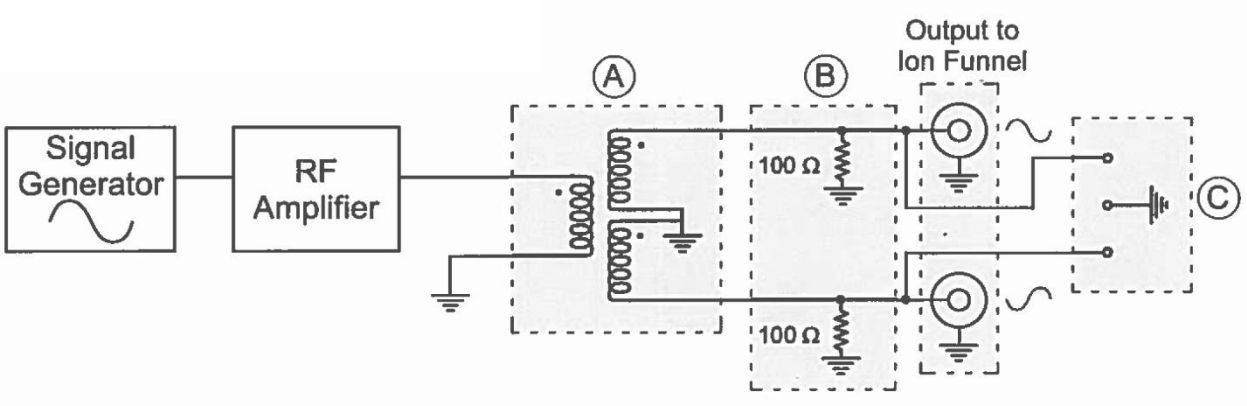

Figure A1 Schematic for Ion-Funnel Balun
Designed by R. M. Moision and R. Jones. Revised 2007.

A) Balun consists of 2 stacked FT-290-77 toroid (www.amidon-inductive.com) wrapped as a trifilar with 18 gauge magnet wire. Previous versions used 14 gauge wire. 18 gauge has proven to be sufficient. (www.amidon-inductive.com/aai_cost_toroidal.htm)
The FT-240-77, FT-290-J, or FT-240-J would also work in this circuit.

B) Two 100 Ω (carbon) resistors in parallel, resulting in a total of 50 Ω. These **must not** be wire wound. They should be non-inductive, and should be able to dissipate the amount of power that the RF amplifier produces. Surplus Sales of Nebraska has large carbon resistors (Type C). Our current setup uses four 50 Ω, 100 Watt resistors, but these are more difficult to obtain. If these large carbon resistors are used, then the appropriate resistor clips are needed for mounting. Over the frequency range typically used with the ion funnel, the massively parallel 50 Ω resistor described in the original version of this document works just fine.

C) RF Balancing posts. Placing capacitors from one post to ground can adjust the peak-to-peak voltage of the output. This can be used to equalize the peak-to-peak voltage of the two output channels. We have these on all designs, but rarely find them useful. In later designs, the 10:1 monitoring posts have also been removed.

In the circuit it is important to keep all wires equal in length within the balun as well as for each output channel. This includes the coax cable going from the balun to the chamber and any wiring within the chamber as well.

To build the trifilar, take 3 lengths of magnet wire, ~10-15 feet in length each. Place one end of each into the chuck of an electric drill. Stretch the other sides across the room and hold the strands together. Spin the 3 strands together so that they effectively form a single strand. Wrap the coiled strand around the stacked toroid. It helps to tape the two toroids together before wrapping with the magnet wire.

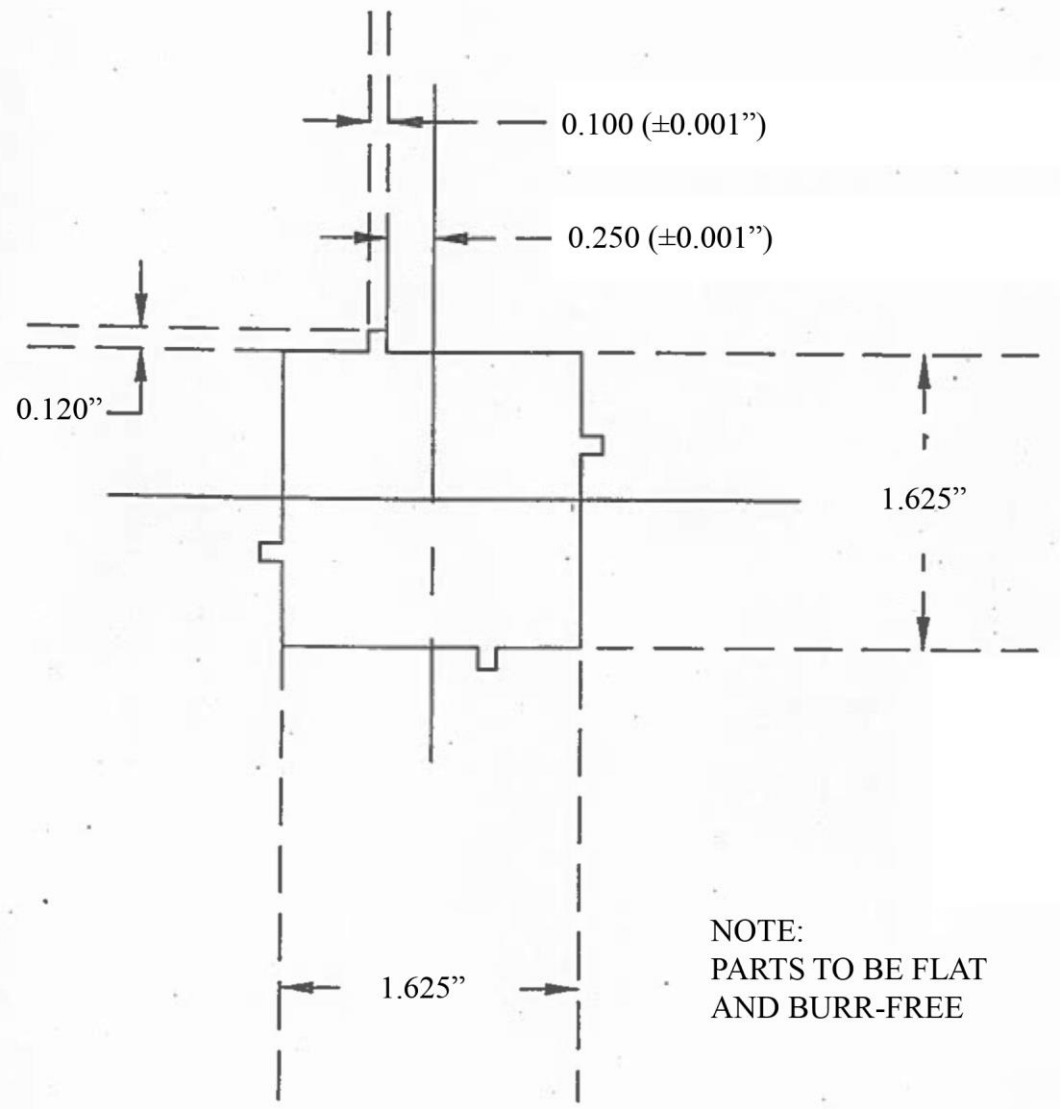

Figure A2 Lens elements for ion funnel
Material: 0.020" (±0.001") hard brass or stainless steel. All dimensions ±0.005" unless stated. Scale 1:1

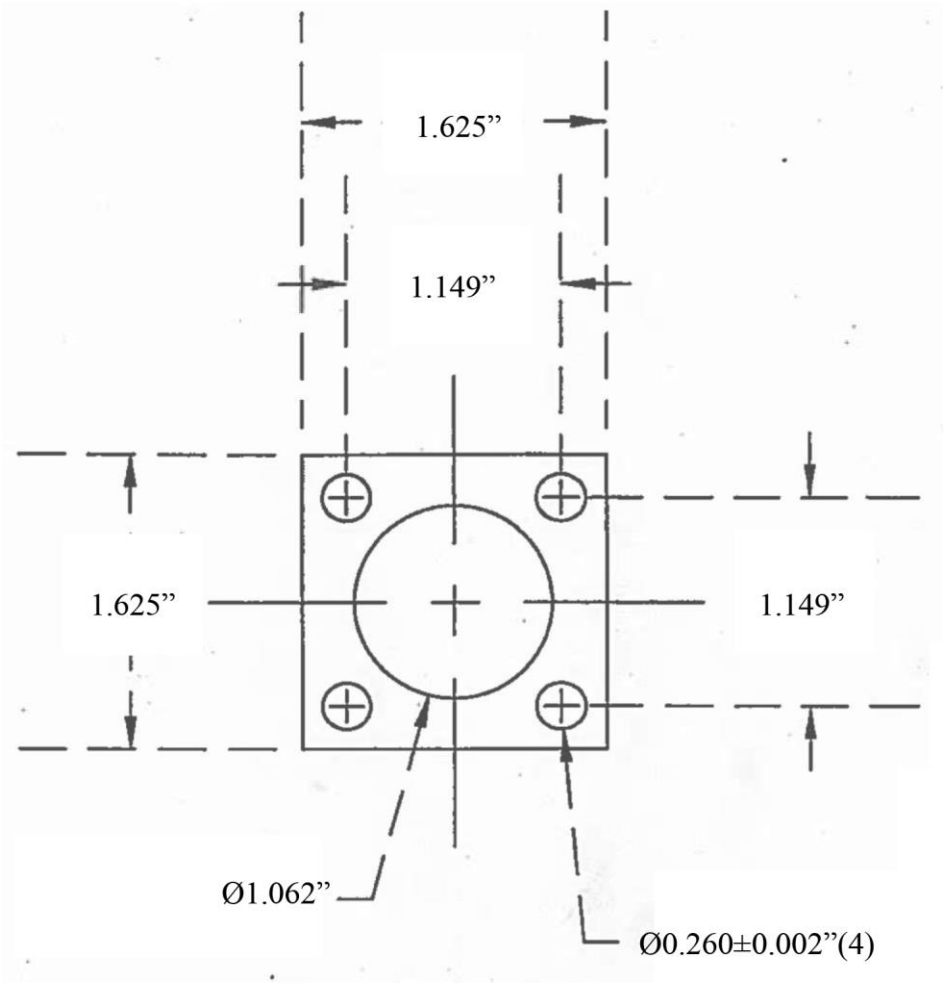

Figure A3 Insulator/Spacer elements for ion funnel
Material: 0.020” (±0.001”) Teflon. All dimensions ±0.005” unless stated. Scale 1:1

8 Appendix B

Cartesian Coordinates (Å) and Energies (Hartree) for optimized geometries for chemical species in

Chapter 4

Figure 4.1

1A, 1B, Dicyanamide, $NCNCN^-$

Atom	X	Y	Z
N	0.00000000	0.00000000	0.68821500
C	0.00000000	1.15135100	0.05646900
N	0.00000000	2.24305700	-0.39250900
C	0.00000000	-1.15135100	0.05646900
N	0.00000000	-2.24305700	-0.39250900

ZPE (Zero Point Energy) Corrected Energy: -240.516411

1A, 1B, Nitric Acid, HNO_3

Atom	X	Y	Z
N	-0.14930900	0.03441500	-0.00023500
O	-1.03699000	-0.77287500	0.00013300
O	1.14202700	-0.53580400	0.00002300
O	-0.19034500	1.24816800	0.00004200
H	1.72763000	0.24318700	0.00005800

ZPE Corrected Energy: -280.913951

2A

Atom	X	Y	Z
N	2.91132400	-0.00845300	-0.00117900
O	4.04329600	-0.47278800	-0.00329200
O	1.91729000	-0.91304000	0.00184400
O	2.61888800	1.18098600	-0.00161500
H	0.96907700	-0.42446100	0.00358100
N	-2.80699200	0.72955700	-0.00071000
C	-3.87787400	-0.03807200	-0.00208200
N	-4.90160800	-0.61700100	-0.00368000
C	-1.59651200	0.27325500	0.00338400
N	-0.45394500	-0.01094600	0.00744200

ZPE Corrected Energy: -521.470462

2A/3A

Atom	X	Y	Z
N	1.55618000	-0.38275000	0.01460000
O	2.66158700	-0.79635100	-0.37730200
O	1.28764500	-0.23147000	1.22398900
O	0.65599800	-0.10537600	-0.86877700
H	-0.41825800	2.89077500	0.75823000
N	-1.84713100	0.51939600	-0.14181100

C	-2.01031100	-0.78268800	0.00836200
N	-2.33586700	-1.90094500	0.12317400
C	-0.79528000	1.21530600	-0.08562500
N	-0.17175900	2.27559700	-0.01281100

ZPE Corrected Energy: -521.424903

3A

Atom	X	Y	Z
N	1.63350600	0.56815100	-0.16865100
C	0.45086200	1.08712500	0.15600500
N	-0.00097100	2.28852000	0.10283600
C	1.91730600	-0.70878200	-0.03657000
N	2.29435700	-1.82311100	0.03401300
H	0.73459500	2.87762000	-0.29315700
O	-0.50834900	0.16204600	0.79629300
N	-1.41748600	-0.42810100	-0.06962100
O	-1.30422400	-0.22938400	-1.26083800
O	-2.25110700	-1.10589700	0.50035800

ZPE Corrected Energy: -521.439271

3A/4A

Atom	X	Y	Z
N	-1.65616300	0.82860700	0.07158500
C	-0.36523100	0.52550700	-0.06086500
N	0.63993800	1.40719500	-0.03279800
C	-2.57937600	-0.11453000	0.01554600
N	-3.50331800	-0.84317600	-0.01025500
H	0.46400000	2.24400500	0.52290900
O	0.08657600	-0.70543500	-0.26196900
N	1.76538600	-0.26586500	0.03186500
O	2.07391900	-0.54649200	1.16396500
O	2.39984800	-0.32272100	-0.98621700

ZPE Corrected Energy: -521.415658

4A

Atom	X	Y	Z
N	1.48237400	-0.70231800	-0.10019100
C	0.50391200	0.22277200	-0.05963400
N	-0.74771200	-0.53582200	-0.24641800
C	2.73739200	-0.30856500	0.02034600
N	3.88964400	-0.09178800	0.11593200
O	0.49869200	1.43470700	0.08351400
H	-0.67769900	-1.53690900	-0.11043400
N	-2.01690300	-0.10507900	-0.00252700
O	-2.84432400	-1.00954500	0.22534800
O	-2.28211200	1.08692800	-0.06153700

ZPE Corrected Energy: -521.491439

2B

Atom	X	Y	Z
N	5.63194400	-0.21163700	0.00004900

O	6.70997800	-0.78229300	-0.00074700
O	4.55172200	-1.02672500	-0.00247000
O	5.44387000	0.99642800	0.00285300
H	3.68532500	-0.45052200	-0.00145500
N	0.00015600	1.16974600	0.00049000
C	-1.15045500	0.56395400	0.00071600
N	-2.24403100	0.13751700	0.00100000
C	1.15045800	0.56336400	-0.00011200
N	2.24380300	0.13633900	-0.00068800
H	-3.68522200	-0.44997200	0.00148300
O	-4.55143700	-1.02648700	0.00245600
N	-5.63194300	-0.21179900	-0.00036400
O	-6.70978100	-0.78283200	0.00074800
O	-5.44430700	0.99633700	-0.00372300

ZPE Corrected Energy: -802.416924

2B/3B

Atom	X	Y	Z
N	-2.79351200	1.26202100	0.04278000
O	-3.26246200	2.36037700	-0.28931300
O	-2.66628600	0.91559900	1.23721300
O	-2.41956000	0.44209300	-0.88500100
H	-3.94303400	-2.24948500	0.83816400
N	-1.15840000	-1.78113200	-0.11343000
C	-0.14010700	-0.95609800	-0.09779500
N	0.87471900	-0.38068200	-0.08725100
C	-2.39706000	-1.50766200	-0.07107200
N	-3.58030600	-1.81086800	-0.00088400
H	2.31936100	0.32579200	-0.07731100
O	3.15139900	0.92736300	-0.09589500
N	4.25349700	0.14611700	0.03480000
O	5.31289300	0.74686600	0.02385200
O	4.09335200	-1.06004100	0.14917500

ZPE Corrected Energy: -802.368530

3B

Atom	X	Y	Z
N	-1.25091600	-1.62712900	0.11572800
C	-2.46084000	-1.14340500	-0.20831000
N	-3.61515000	-1.69140100	-0.17884500
C	-0.15588800	-0.93940800	0.02604100
N	0.90400100	-0.43131900	-0.01953300
H	-3.50773300	-2.64000100	0.18622700
O	-2.47224900	0.19837200	-0.79012200
N	-2.76567300	1.22460300	0.11788300
O	-2.84604600	0.94781800	1.29407800
O	-2.89547700	2.30419100	-0.41703800
H	2.26084700	0.21994300	-0.07766000
O	3.11041700	0.84403700	-0.16269700
N	4.23348700	0.12152500	0.00996400
O	5.27777800	0.75149000	-0.07166900

O	4.12645400	-1.07803600	0.23103300

ZPE Corrected Energy: -802.390688

3B/4B

Atom	X	Y	Z
N	0.85013900	1.32885900	-0.02572000
C	2.03267600	0.68833400	-0.08840100
N	3.21327700	1.29594300	-0.09117300
C	-0.27208400	0.67006500	-0.04594100
N	-1.35405500	0.21159300	-0.05222900
H	3.25415000	2.22730200	0.31941900
O	2.14356100	-0.61858300	-0.17664500
N	3.93944900	-0.57458500	0.06856300
O	4.18994200	-0.84315800	1.21077900
O	4.49673300	-0.84079500	-0.95504000
H	-2.73168800	-0.38404100	-0.06761300
O	-3.60962100	-0.97594600	-0.10324000
N	-4.69969100	-0.19708300	0.02667200
O	-5.77027800	-0.78684100	-0.00382000
O	-4.54156700	1.00948000	0.16189800

ZPE Corrected Energy: -802.367400

4B

Atom	X	Y	Z
N	0.84668400	-0.62854900	-0.15009800
C	1.87786800	0.25303700	-0.08598900
N	3.08641800	-0.55340600	-0.20709800
C	-0.37639600	-0.18441800	-0.08953100
N	-1.51792600	0.08547300	-0.04487900
O	1.91112800	1.46323300	0.03614500
H	2.98395200	-1.55335100	-0.08507200
N	4.37251000	-0.15798600	0.04208100
O	5.16423500	-1.08829600	0.27020900
O	4.66675200	1.02485800	-0.00998500
H	-2.99495200	0.43490400	0.00674700
O	-3.95571300	0.86406700	0.04557400
N	-4.89190000	-0.10578500	0.04080400
O	-6.04831000	0.28623700	0.08304700
O	-4.52163500	-1.27153500	-0.00426900

ZPE Corrected Energy: -802.442001

5B

Atom	X	Y	Z
N	-0.76839300	2.02931900	-0.43877600
C	-1.74401900	1.04633200	-0.39111500
N	-1.23578700	-0.20471500	0.09170100
C	0.29625500	1.98773700	0.23175900
N	1.29985500	2.09450600	0.87860200
O	-2.88432900	1.20855500	-0.76059400
H	-0.25522200	-0.46586100	-0.08303000
N	-2.03606900	-1.31964900	0.29200400

O	-1.45675300	-2.40178600	0.19885100
O	-3.20818800	-1.15607600	0.59170000
H	2.13393700	1.38466300	0.74978000
O	3.58337700	-1.50396900	-0.50026200
N	2.78536000	-0.61623200	-0.19345600
O	3.18226300	0.35064000	0.56027600
O	1.59526900	-0.62309000	-0.60511300

ZPE Corrected Energy: -802.436330

5B/6B

Atom	X	Y	Z
N	-0.07544400	1.27578000	-0.75040500
C	-0.96266200	0.76628300	0.17111600
N	-2.02175200	0.14900500	-0.58952200
C	1.16129800	1.43114600	-0.51668600
N	2.25268100	1.99845200	-0.51718400
O	-0.96039700	0.83871100	1.37687100
H	-1.76907000	-0.24714700	-1.48802500
N	-3.11329900	-0.50125900	-0.05446600
O	-3.60661800	-1.37012800	-0.78399300
O	-3.53710300	-0.15333200	1.03371800
H	2.20248300	3.00670700	-0.37768800
O	1.65637800	-0.57493600	-0.44090200
N	2.73406900	-1.00076000	0.15510500
O	3.16532300	-0.39020100	1.14244600
O	3.27504100	-2.02419600	-0.29883600

ZPE Corrected Energy: -802.389883

6B

Atom	X	Y	Z
N	0.10234000	0.96567500	-0.10904900
C	0.93826400	-0.09007200	-0.08701300
N	2.28667000	0.50784500	-0.24756100
C	-1.24071500	0.87101700	-0.03636100
N	-2.10807600	1.81886500	-0.00740600
O	0.80512500	-1.29604200	0.02798100
H	2.34394900	1.50103500	-0.05796800
N	3.48311000	-0.09522800	0.01260100
O	4.40876400	0.68074800	0.31995700
O	3.59685900	-1.30595600	-0.11028600
H	-1.60447400	2.70387700	-0.04282500
O	-1.75561600	-0.45855500	0.00156000
N	-3.19534700	-0.48647000	0.04839500
O	-3.74431500	-0.56374300	-1.02316700
O	-3.67402400	-0.53962500	1.15422700

ZPE Corrected Energy: -802.405451

6B/7B

Atom	X	Y	Z
N	0.09708300	0.79699200	0.01051600
C	1.03067900	-0.18388400	0.01149800

N	2.30316600	0.51637500	-0.26224900
C	-1.20967900	0.47665200	0.09955100
N	-2.16891800	1.39458200	0.20843200
O	1.00039700	-1.38688900	0.18681900
H	2.28109600	1.51989500	-0.12725000
N	3.56297000	0.03298800	-0.04763500
O	4.43273100	0.90203300	0.15109900
O	3.77291600	-1.16908000	-0.10535000
H	-1.95341000	2.32592600	-0.14512100
O	-1.70476700	-0.73980600	0.09001500
N	-3.39958100	-0.15009700	-0.05823100
O	-3.75664800	-0.23144200	-1.20554000
O	-3.99671900	-0.34210500	0.96423900

ZPE Corrected Energy: -802.382534

7B

Atom	X	Y	Z
N	-0.00004300	-0.22366700	0.00021800
C	-1.16917200	0.46200400	-0.05395500
N	-2.20554200	-0.58414400	-0.22267300
C	1.16912600	0.46191700	0.05390500
N	2.20550200	-0.58421400	0.22249100
O	-1.47112800	1.63499000	0.01512200
H	-1.91791900	-1.51955500	0.03882800
N	-3.54921000	-0.42905000	-0.01468000
O	-4.14948300	-1.45869700	0.34496800
O	-4.07546000	0.65161500	-0.23065900
H	1.91802100	-1.51961500	-0.03918400
O	1.47116300	1.63488900	-0.01550800
N	3.54922300	-0.42900300	0.01475900
O	4.14953200	-1.45856900	-0.34515600
O	4.07545800	0.65154700	0.23121400

ZPE Corrected Energy: -802.455366

Figure 4.2

A, Dicyanamide, $NCNCN^-$

Atom	X	Y	Z
N	0.00000000	0.00000000	0.74478100
C	0.00000000	1.13336200	0.06723500
N	0.00000000	2.21606800	-0.43002100
C	0.00000000	-1.13336200	0.06723500
N	0.00000000	-2.21606800	-0.43002100

ZPE Corrected Energy: -239.913961

B, Protonated Dicyanamide, HNCNCN

Atom	X	Y	Z
N	-0.05882300	0.65888400	0.01237200
C	1.04488700	0.09161800	0.03215500
N	2.18208800	-0.30852700	-0.12907100
C	-1.25192100	0.05069700	0.00247700

N	-2.34582500	-0.39000700	-0.00244500
H	2.80012500	-0.57634700	0.62621800

ZPE Corrected Energy: -240.403638

C, Protonated Dicyanamide, $HN(CN)_2$

Atom	X	Y	Z
N	-0.04067400	0.72008800	0.00000000
C	-0.00047100	0.04615800	1.17508400
N	-0.00047100	-0.51923900	2.20601800
C	-0.00047100	0.04615800	-1.17508400
N	-0.00047100	-0.51923900	-2.20601800
H	0.29695800	1.67483600	0.00000000

ZPE Corrected Energy: -240.401951

Figure 4.3

A, $NCNCN^-[HNO_3]$

Atom	X	Y	Z
N	-2.89093300	-0.00620400	-0.02498000
O	-4.03404300	-0.43617300	-0.06566600
O	-1.92987000	-0.94897400	0.05456200
O	-2.55047400	1.16899000	-0.04876900
H	-1.00298000	-0.47765000	0.08066100
N	2.80700700	0.79202400	0.01822200
C	3.83851500	-0.03743300	-0.04062900
N	4.83623500	-0.67998700	-0.09548400
C	1.60156300	0.30097300	0.07156900
N	0.45877700	-0.01645300	0.13262600

ZPE Corrected Energy: -520.253165

B, $NCNCN^-[HNO_3]_2$

Atom	X	Y	Z
N	0.71638400	1.31037500	-0.28430800
O	1.72179900	1.90444600	-0.67210900
O	-0.28716400	1.96510800	0.16018400
O	0.63360600	0.04719500	-0.30772800
H	-1.36336300	1.13937100	0.51360800
N	-4.01124000	-1.09074700	0.32360800
C	-5.20899300	-0.80382400	-0.18095700
N	-6.30125700	-0.66398600	-0.61560000
C	-3.13864700	-0.17809100	0.50842800
N	-2.28141200	0.58313500	0.82043400
N	3.78734600	-0.84817400	0.14897400
O	3.42032800	-0.18161000	1.10348900
O	2.87034300	-1.13433100	-0.81457700
O	4.89704100	-1.30966000	-0.05115000
H	2.03283500	-0.61128400	-0.57506100

ZPE Corrected Energy: -800.578177

C, $NCNCN^-[HNO_3]_3$

Atom	X	Y	Z
N	0.49955700	-0.03549200	-0.04577400

O	-0.45034800	0.55747200	-0.61611800
O	0.33808400	-1.20657300	0.38827300
O	1.60743400	0.53506600	0.09189000
H	-1.14694700	-1.72110000	0.20587900
N	-4.37092900	-1.58158300	-0.65139500
C	-5.37286500	-1.15919600	0.12076500
N	-6.33281700	-0.79914900	0.70943400
C	-3.20628500	-1.78210700	-0.20193600
N	-2.11261400	-2.14638800	0.11324400
N	3.63362600	-2.10439400	-0.04686800
O	2.98321200	-2.01309900	-1.07446900
O	3.49401500	-1.11107100	0.88082200
O	4.41850500	-2.97999500	0.26526700
H	2.74747900	-0.52843000	0.54313500
N	0.39014900	3.71246400	0.08783800
O	0.80660200	4.84934100	-0.03039300
O	0.13077800	3.07797800	-1.09508500
O	0.17137900	3.09768900	1.11773400
H	-0.07172900	2.12467700	-0.85070300

ZPE Corrected Energy: -1080.904003

9 Bibliography

Adams, N. G. and D. Smith (1976). "The selected ion flow tube: A technique for studying ion-neutral reactions." International Journal of Mass Spectrometry and Ion Physics **21**: 349-359.

Afeefy, H. Y., J. F. Liebman, et al. (2012). Neutral Thermochemical Data, NIST Chemistry WebBook, NIST Standard Reference Database. P. J. Linstrom and W. G. Mallard. Gaithersburg, National Institute of Standards and Technology.

Agundez, M., J. Cernicharo, et al. (2010). "Astronomical identification of CN^-, the smallest observed molecular anion." Astronomy & Astrophysics **517**: 5.

Angell, C. A., Y. Ansari, et al. (2011). "Ionic Liquids: Past, present and future." Faraday Discussions **154**: 9-27.

Armand, M., F. Endres, et al. (2009). "Ionic-liquid materials for the electrochemical challenges of the future." Nature Materials **8**(8): 621-629.

Armentrout, P. B. (2000). "Entropy measurements and the kinetic method: A statistically meaningful approach." Journal of the American Society for Mass Spectrometry **11**(5): 371-379.

Armentrout, P. B., K. M. Ervin, et al. (2008). "Statistical Rate Theory and Kinetic Energy-Resolved Ion Chemistry: Theory and Applications." Journal of Physical Chemistry A **112**(41): 10071-10085.

Atterbury, C., R. A. Kennedy, et al. (2001). "A study of the reactions of trifluoromethyl sulfur pentafluoride, SF_5CF_3, with several positive ions of atmospheric interest." Physical Chemistry Chemical Physics **3**(11): 1949-1953.

Baer, T. and W. Hase (1996). Unimolecular reaction dynamics: Theory and experiment. New York, Oxford University Press.

Ball, J. A., C. A. Gottlieb, et al. (1970). "Detection of methyl alcohol in Sagittarius." Astrophysical Journal **162**(3): L203-L210.

Bartmess, J. E. "Negative ion energetics data in NIST chemistry WebBook." NIST standard reference database number 69. Retrieved November 3, 2015, from http://webbook.nist.gov.

Bartmess, J. E., J. A. Scott, et al. (1979). "Scale of Acidities in the Gas-Phase from Methanol to Phenol." Journal of the American Chemical Society **101**(20): 6046-6056.

Beynon, J. H., R. A. Saunders, et al. (1961). "High resolution mass spectra of aliphatic esters." Analytical Chemistry **33**(2): 221-225.

Bierbaum, V. M. (2015). "Go with the flow: Fifty years of innovation and ion chemistry using the flowing afterglow." International Journal of Mass Spectrometry **377**: 456-466.

Boggs, P. T., J. R. Donaldson, et al. (1992). "ODRPACK95 - software for weighted orthogonal distance regression." Acm Transactions on Mathematical Software **15**(4): 348-364.

Bohme, D. K. and G. I. Mackay (1981). "Bridging the gap between the gas-phase and solution - transition in the kinetics of nucleophilic displacement reactions." Journal of the American Chemical Society **103**(4): 978-979.

Bohme, D. K. and A. B. Raksit (1984). "Gas-phase measurements of the influence of stepwise solvation on the kinetics of nucleophilic displacement reactions with CH_3Cl and CH_3Br at room-temperature." Journal of the American Chemical Society **106**(12): 3447-3452.

Bohme, D. K. and L. B. Young (1970). "Kinetic studies of reactions of oxide, hydroxide, alkoxide, phenyl, and benzylic anions with methyl chloride in gas phase at 22.5 degrees." Journal of the American Chemical Society **92**(25): 7354-7358.

Bouchoux, G. (2006). "Evaluation of the protonation thermochemistry obtained by the extended kinetic method." Journal of Mass Spectrometry **41**(8): 1006-1013.

Bouchoux, G., F. Djazi, et al. (2003). "Application of the kinetic method to bifunctional bases MIKE and CID-MIKE test cases." International Journal of Mass Spectrometry **227**(3): 479-496.

Bouchoux, G., M. Sablier, et al. (2004). "Obtaining thermochemical data by the extended kinetic method." Journal of Mass Spectrometry **39**(9): 986-997.

Bouma, W. J., R. H. Nobes, et al. (1982). "On the nature of the methoxy cation." Organic Mass Spectrometry **17**(7): 315-317.

Bourgoin-Voillard, S., C. Afonso, et al. (2013). "Critical evaluation of kinetic method measurements: Possible origins of nonlinear effects." Journal of the American Society for Mass Spectrometry **24**(3): 365-380.

Buncel, E. and S. Hoz (1983). "Can ground-state destabilization of an alpha-nucleophile induce an alpha-effect." Tetrahedron Letters **24**(44): 4777-4780.

Buncel, E. and I. H. Um (2004). "The alpha-effect and its modulation by solvent." Tetrahedron **60**(36): 7801-7825.

Butler, J. J., D. M. P. Holland, et al. (1984). "A threshold photoelectron photooion coincidence spectrometric study of dimethyl ether (CH_3OCH_3)." International Journal of Mass Spectrometry and Ion Processes **58**(JUN): 1-14.

Cai, J. F., R. D. Topsom, et al. (1988). "Acidities of substituted acetic acids." Theochem-Journal of Molecular Structure **45**: 141-146.

Caldwell, G., R. Renneboog, et al. (1989). "Gas-phase acidities of aliphatic carboxylic-acids based on measurements of proton-transfer equilibria." Canadian Journal of Chemistry-Revue Canadienne De Chimie **67**(4): 611-618.

Carruthe, G. R. (1970). "Rocket observation of interstellar molecular hydrogen." Astrophysical Journal **161**(2): L81-L85.

Catalan, J., R. M. Claramunt, et al. (1988). "Basicity and Acidity of Azoles - the Annelation Effect in Azoles." Journal of the American Chemical Society **110**(13): 4105-4111.

Catoire, L., S. D. Chambreau, et al. (2011). "Chemical kinetics interpretation of hypergolicity of dicyanamide ionic liquid-based systems." Combustion and Flame **159**(4): 1759-1768.

Cavell, E. A. S. (1958). "Effect of solvent composition on the kinetics of reactions between ions and dipolar molecules." Journal of the Chemical Society: 4217-4222.

Cernicharo, J., M. Guelin, et al. (2008). "Detection of C_5N^- and vibrationally excited C_6H in IRC+10216." Astrophysical Journal Letters **688**(2): L83-L86.

Chambreau, S. D., S. Schneider, et al. (2008). "Fourier transform infrared studies in hypergolic ignition of ionic liquids." Journal of Physical Chemistry A **112**(34): 7816-7824.

Chen, X. and J. I. Brauman (2008). "Hydrogen bonding lowers intrinsic nucleophilicity of solvated nucleophiles." Journal of the American Chemical Society **130**(45): 15038-15046.

Cheng, X. and J. J. Grabowski (1989). "Gas-phase acidity of nitrobenzene from flowing afterglow bracketing studies." Rapid Communications in Mass Spectrometry **3**(2): 34-36.

Cheng, X. H., Z. C. Wu, et al. (1993). "Collision energy-dependence of proton-bound dimer dissociation - entropy effects, proton affinities, and intramolecular hydrogen-bonding in protonated peptides." Journal of the American Chemical Society **115**(11): 4844-4848.

Cheung, A. C., D. M. Rank, et al. (1968). "Detection of NH_3 molecules in the interstellar medium by their microwave emission." Physical Review Letters **21**(25): 1701-1705.

Cheung, A. C., D. M. Rank, et al. (1969). "Detection of water in interstellar regions by its microwave radiation." Nature **221**(5181): 626-628.

Chiappe, C. and D. Pieraccini (2005). "Ionic liquids: solvent properties and organic reactivity." Journal of Physical Organic Chemistry **18**(4): 275-297.

Chim, R. Y. L., R. A. Kennedy, et al. (2001). "Fragmentation of energy-selected $SF_5CF_3^+$ probed by threshold photoelectron photoion coincidence spectroscopy: Bond dissociation energy of SF_5-CF_3 and its atmospheric implications." Journal of Physical Chemistry A **105**(37): 8403-8412.

Chin, Y. H. and R. A. Dressler (2007). Ionic Liquids for Space Propulsion. Ionic Liquids IV: Not Just Solvents Anymore. J. F. Brennecke, R. D. Rogers and K. R. Seddon. Washington, Amer Chemical Soc. **975:** 138-160.

Cooks, R. G., J. H. Beynon, et al. (1973). Metastable Ions. Amsterdam, The Netherlands, Elsevier Scientific Publishing Company.

Cooks, R. G., J. T. Koskinen, et al. (1999). "Special feature: Commentary - The kinetic method of making thermochemical determinations." Journal of Mass Spectrometry **34**(2): 85-92.

Crowhurst, L., P. R. Mawdsley, et al. (2003). "Solvent-solute interactions in ionic liquids." Physical Chemistry Chemical Physics **5**(13): 2790-2794.

DePuy, C. H., E. W. Della, et al. (1983). "Absence of an alpha-effect in the gas-phase nucleophilic reactions of HOO^-." Journal of the American Chemical Society **105**(8): 2481-2482.

DePuy, C. H., S. Gronert, et al. (1990). "Gas-phase S_N2 and E2 reactions of alkyl-halides." Journal of the American Chemical Society **112**(24): 8650-8655.

Dixon, J. E. and T. C. Bruice (1971). "Alpha-effect. IV. Additional observation on alpha-effect employing malachite green as substrate." Journal of the American Chemical Society **93**(24): 6592-6597.

Dixon, J. E. and T. C. Bruice (1972). "Alpha-effect. V. Kinetic and thermodynamic nature of alpha-effect for amine nucleophiles." Journal of the American Chemical Society **94**(6): 2052-2056.

Drahos, L. and K. Vekey (1999). "Special feature: Commentary - How closely related are the effective and the real temperature." Journal of Mass Spectrometry **34**(2): 79-84.

Edwards, J. O. and R. G. Pearson (1962). "Factors determining nucleophilic reactivities." Journal of the American Chemical Society **84**(1): 16-24.

Eichelberger, B. R., T. P. Snow, et al. (2003). "Collision rate constants for polarizable ions." Journal of the American Society for Mass Spectrometry **14**(5): 501-505.

Ervin, K. M. (2014). "Capture Collisions of Polyynide Anions with Hydrogen Atoms: Effect of the Ion Dipole, Quadrupole, and Anisotropic Polarizability." International Journal of Mass Spectrometry **378**: 48-53.

Ervin, K. M. and P. B. Armentrout (2004). "Systematic and random errors in ion affinities and activation entropies from the extended kinetic method." Journal of Mass Spectrometry **39**(9): 1004-1015.

Ervin, K. M. and V. F. DeTuro (2002). "Anchoring the gas-phase acidity scale." Journal of Physical Chemistry A **106**(42): 9947-9956.

Eyet, N. and V. M. Bierbaum (2007). "Gas-phase acidities of thiocarboxylic acids." International Journal of Mass Spectrometry **265**(2-3): 267-270.

Federer, W., H. Villinger, et al. (1986). "Reactions of some hydrocarbon cations with nitrogen atoms." Chemical Physics Letters **123**(1-2): 12-16.

Fehsenfeld, F. C. (1971). "Ion chemistry of SF_6." Journal of Chemical Physics **54**(1): 438-439.

Fehsenfeld, F. C., E. E. Ferguson, et al. (1966). "Thermal-Energy Ion-Neutral Reaction Rates. III. The Measured Rate Constant for the Reaction $O^+(^4S)+CO_2(^1\Sigma)\rightarrow O_2^+(^2\Pi)+CO(^1\Sigma)$." Journal of Chemical Physics **44**(8): 3022-3024.

Ferguson, E. E., F. C. Fehsenfeld, et al. (1969). "Flowing afterglow measurements of ion-neutral reactions." Advances in Atomic and Molecular Physics **5**: 1-56.

Fialkov, A. B., K. Y. Kalinich, et al. (1992). Experimental determination of primary ions in flames. 24th International Symposium on Combustion/The Combustion Institute.

Fisher, E. R. and P. B. Armentrout (1991). "Kinetic-energy dependence of the reactions of O^+ and O_2^+ with CF_4 and C_2F_6." Journal of Physical Chemistry **95**(16): 6118-6124.

Foner, S. N. and R. L. Hudson (1962). "Mass spectrometric studies of metastable nitrogen atoms and molecules in active nitrogen." The Journal of Chemical Physics **37**(8): 1662-1667.

Freeman, C. G., P. W. Harland, et al. (1979). "Thermal-energy charge-transfer reactions of acetone and biacetyl." Chemical Physics Letters **64**(3): 596-600.

Frisch, M. J., G. W. Trucks, et al. (2009). Gaussian 09. Wallingford CT, Gaussian, Inc.

Garver, J. M., S. Gronert, et al. (2011). "Experimental validation of the alpha-effect in the gas phase." Journal of the American Chemical Society **133**(35): 13894-13897.

Garver, J. M., Z. Yang, et al. (2012). "Resolving the alpha-effect in gas phase S_N2 reactions: A Marcus theory approach." International Journal of Mass Spectrometry **316**: 244-250.

Garver, J. M., Z. Yang, et al. (2012). "The alpha-effect in elimination reactions and competing mechanisms in the gas phase." International Journal of Mass Spectrometry **330**: 182-190.

Gianola, A. J., T. Ichino, et al. (2004). "Thermochemistry and electronic structure of the pyrrolyl radical." Journal of Physical Chemistry A **108**(46): 10326-10335.

Gianola, A. J., T. Ichino, et al. (2005). "Photoelectron spectra and ion chemistry of imidazolide." Journal of Physical Chemistry A **109**(50): 11504-11514.

Gianola, A. J., T. Ichino, et al. (2006). "Thermochemical studies of pyrazolide." Journal of Physical Chemistry A **110**(27): 8457-8466.

Gioumousis, G. and D. P. Stevenson (1957). "Reactions of gaseous molecule ions with gaseous molecules. V. Theory." Journal of Chemical Physics **29**(2): 294-299.

Glosik, J., A. B. Rakshit, et al. (1978). "Measurement of the rates of reaction of the ground and metastable excited-states of O_2^+, NO^+ and O^+ with atmospheric gases at thermal-energy." Journal of Physics B-Atomic Molecular and Optical Physics **11**(19): 3365-3379.

Goldsmith, P. F., R. Liseau, et al. (2011). "*Herschel* measurements of molecular oxygen in Orion." Astrophysical Journal **737**(2): 17.

Gregory, M. J. and T. C. Bruice (1967). "Alpha-effect. II. Displacements on sp^3 carbon." Journal of the American Chemical Society **89**(17): 4400-4405.

Gregory, M. J. and T. C. Bruice (1967). "Importance of alpha-effect in amine general base catalyzed ionization of nitroethane." Journal of the American Chemical Society **89**(10): 2327-2330.

Gunion, R. F., M. K. Gilles, et al. (1992). "Ultraviolet photoelectron-spectroscopy of the phenide, benzyl and phenoxide anions, with ab-initio calculations." International Journal of Mass Spectrometry and Ion Processes **117**(1-3): 601-620.

Hager, J. W. (2002). "A new linear ion trap mass spectrometer." Rapid Communications in Mass Spectrometry **16**(6): 512-526.

Haney, M. A. and J. L. Franklin (1969). "Excess energies in mass spectra of some oxygen-containing organic compounds." Transactions of the Faraday Society **65**(559P): 1794-1804.

Hierl, P. M., A. F. Ahrens, et al. (1986). "Nucleophilic displacement as a function of hydration number and temperature - rate constants and product distributions for $OD^-(D_2O)_{0,1,2}$ + CH_3Cl at 200-500 K." Journal of the American Chemical Society **108**(11): 3142-3143.

Hierl, P. M., J. F. Paulson, et al. (1995). "Translational energy-dependence of cross-sections for reactions of $OH^-(H_2O)_n$ with CH_3Cl and CH_3Br." Journal of Physical Chemistry **99**(42): 15655-15661.

Hoffman, J. H. (1967). "A mass spectrometric determination of the composition of the nighttime topside ionosphere." Journal of Geophysical Research **72**(7): 1883-1888.

Hoffman, J. H., C. Y. Johnson, et al. (1969). "Daytime midlatitude ion composition measurements." Journal of Geophysical Research **74**(26): 6281-6290.

Hoz, S. (1982). "The alpha effect - on the origin of transition-state stabilization." Journal of Organic Chemistry **47**(18): 3545-3547.

Ichino, T., D. H. Andrews, et al. (2008). "Ion chemistry of 1H-1,2,3-Triazole." Journal of Physical Chemistry B **112**(2): 545-557.

Jagoda-Cwiklik, B., X. B. Wang, et al. (2007). "Microsolvation of the dicyanamide anion: $[N(CN)_2^-](H_2O)_n$ (n=0-12)." Journal of Physical Chemistry A **111**(32): 7719-7725.

Jarvis, G. K., R. A. Kennedy, et al. (2000). "Charge transfer from neutral perfluorocarbons to various cations: long-range versus short-range reaction mechanisms." International Journal of Mass Spectrometry **202**(1-3): 323-343.

Jefferts, K. B., A. A. Penzias, et al. (1971). "Detection of interstellar carbonyl sulfide." Astrophysical Journal **168**(3): L111-L113.

Jodry, J. J. and K. Mikami (2005). Ionic Liquids. Green reaction media in organic synthesis. K. Mikami. Kundli, Blackwell Publishing Ltd**:** 9-54.

Katritzky, A. R., S. Singh, et al. (2005). "1-butyl-3-methylimidazolium 3,5-dinitro-1,2,4-triazolate: a novel ionic liquid containing a rigid, planar energetic anion." Chemical Communications(7): 868-870.

Kelly, R. T., A. V. Tolmachev, et al. (2010). "The ion funnel: Theory, implementations, and applications." Mass Spectrometry Reviews **29**(2): 294-312.

King, A. B. and F. A. Long (1958). "Mass spectra of some simple esters and their interpretation by quasi-equilibrium theory." Journal of Chemical Physics **29**(2): 374-382.

Klopman, G. and R. C. Evans (1978). "Supernucleophiles .2. Orbital interactions and nucleophilicity." Tetrahedron **34**(3): 269-273.

Klopman, G., K. Tsuda, et al. (1970). "Supernucleophiles .1. alpha effect." Tetrahedron **26**(19): 4549-4554.

Knauth, D. C., B. G. Andersson, et al. (2004). "The interstellar N_2 abundance towards HD 124314 from far-ultraviolet observations." Nature **429**(6992): 636-638.

Kurz, J. L. (1978). "Relationship of barrier shape to linear free-energy slopes and curvatures." Chemical Physics Letters **57**(2): 243-246.

Lacy, J. H., J. S. Carr, et al. (1991). "Discovery of interstellar methane - observations of gaseous and solid CH_4 absorption toward young stars in molecular clouds." Astrophysical Journal **376**(2): 556-560.

Langevin, P. (1905). "A fundamental formula of kinetic theory." Annales De Chimie Et De Physique **5**: 245-288.

Li, S. Q., H. X. Gao, et al. (2014). "Borohydride Ionic Liquids and Borane/Ionic-Liquid Solutions as Hypergolic Fuels with Superior Low Ignition-Delay Times." Angewandte Chemie-International Edition **53**(11): 2969-2972.

Lias, S. G., J. E. Bartmess, et al. (1988). Gas-Phase Ion and Neutral Thermochemistry. New York, NY, American Chemical Society, American Institute of Physics, National Bureau of Standards.

Lias, S. G., J. E. Bartmess, et al. (2014). NIST Chemistry WebBook. Ion Energetics Data. P. J. Lindstrom and W. G. Mallard. Gaithersburg, MD, National Institute of Standards and Technology.

Lide, D. R., Ed. (2009). Handbook of Chemistry and Physics. New York, NY, CRC Press.

Lin, C. L. and F. Kaufman (1971). "Reactions of metastable nitrogen atoms." The Journal of Chemical Physics **55**(8): 3760-3770.

Litzinger, T. and S. Iyer (2010). "Hypergolic Reaction of Dicyanamide-Based Fuels with Nitric Acid." Energy & Fuels **25**: 72-76.

Liu, J. B., S. D. Chambreau, et al. (2011). "Thermal decomposition of 1,5-dinitrobiuret (DNB): direct dynamics trajectory simulations and statistical modeling." Journal of Physical Chemistry A **115**(28): 8064-8072.

Lotsch, B. V., J. Senker, et al. (2004). "Characterization of the thermally induced topochemical solid-state transformation of $NH_4[N(CN)_2]$ into $NCN=C(NH_2)_2$ by the means of X-ray and neutron diffraction as well as Raman and solid-state NMR spectroscopy." Inorganic Chemistry **43**(3): 895-904.

Marcus, R. A. (1968). "Theoretical relations among rate constants barriers and Brønsted slopes of chemical reactions." Journal of Physical Chemistry **72**(3): 891-899.

Mayo, F. R. (1974). "Free radicals," Vol. II, Jay K. Kochi, Ed., Wiley, New York, 1973. Journal of Polymer Science: Polymer Letters Edition **12**(9): 536-538.

McCrary, P. D., G. Chatel, et al. (2014). "Evaluating ionic liquids as hypergolic fuels: Exploring reactivity from molecular structure." Energy & Fuels **28**(5): 3460-3473.

McIsaac, J. E., L. R. Subbaraman, et al. (1972). "Nucleophilic reactivity of peroxy anions." Journal of Organic Chemistry **37**(7): 1037-1041.

McMahon, T. B. and P. Kebarle (1977). "Intrinsic acidities of substituted phenols and benzoic-acids determined by gas-phase proton-transfer equilibria." Journal of the American Chemical Society **99**(7): 2222-2230.

Meyer, J. A., D. W. Setser, et al. (1970). "Energy transfer reactions of $N_2(A^3\Sigma_u^+)$. II. Quenching and emission by oxygen and nitrogen atoms." The Journal of Physical Chemistry **74**(10): 2238-2240.

Moision, R. M. and P. B. Armentrout (2007). "An electrospray ionization source for thermochemical investigation with the guided ion beam mass spectrometer." Journal of the American Society for Mass Spectrometry **18**(6): 1124-1134.

Morris, R. A., A. A. Viggiano, et al. (1995). "Chemistry of atmospheric ions reacting with fully fluorinated compounds." International Journal of Mass Spectrometry and Ion Processes **149**: 287-298.

Nichols, C. M., Z. Yang, et al. (2013). "Gas-phase reactions of the atomic oxygen radical cation with halogenated compounds." Physical Chemistry Chemical Physics **15**: 561-567.

Nichols, C. M., Z. Yang, et al. (2013). "Gas-phase organic reactions of the atomic oxygen radical cation." International Journal of Mass Spectrometry **353**: 1-6.

Nishimura, T., Q. M. Zha, et al. (1992). "On the dissociation dynamics of energy-selected dimethyl ether ions." International Journal of Mass Spectrometry and Ion Processes **113**(3): 177-189.

Nishimura, T., Q. M. Zha, et al. (1987). "Unimolecular dissociation of energy-selected methyl formate ion." Journal of Chemical Physics **87**(8): 4589-4597.

Nold, M. J., B. A. Cerda, et al. (1999). "Proton affinities of the N- and C-terminal segments arising upon the dissociation of the amide bond in protonated peptides." Journal of the American Society for Mass Spectrometry **10**(1): 1-8.

Oae, S. and Y. Kadoma (1986). "Importance of repulsion of lone electron pairs in the enhanced reactivity of 1,8-napthyridine and the large alpha-effect of hydrazine in the aminolyses of para-toluenesulfonyl chloride." Canadian Journal of Chemistry-Revue Canadienne De Chimie **64**(6): 1184-1188.

Otto, R., J. Brox, et al. (2012). "Single solvent molecules can affect the dynamics of substitution reactions." Nature Chemistry **4**(7): 534-538.

Otto, R., J. Brox, et al. (2013). "Exit channel dynamics in a micro-hydrated S_N2 reaction of the hydroxyl anion." Journal of Physical Chemistry A **117**(34): 8139-8144.

Patterson, E. V. and K. R. Fountain (2006). "On gas phase alpha-effects. 1. The gas-phase manifestation and potential SET character." Journal of Organic Chemistry **71**(21): 8121-8125.

Pliego, J. R. and J. M. Riveros (2001). "The gas-phase reaction between hydroxide ion and methyl formate: A theoretical analysis of the energy surface and product distribution." Chemistry-a European Journal **7**(1): 169-175.

Pratt, R. F. and T. C. Bruice (1972). "Lack of an alpha-effect for proton abstraction from carbon acids." Journal of Organic Chemistry **37**(22): 3563-3564.

Reedijk, J. (1969). "Pyrazoles and imidazoles as ligands. Part I. Some simple metal(II) perchlorates and tetrafluoroborates solvated by neutral pyrazole and imidazole." Recueil Des Travaux Chimiques Des Pays-Bas **88**(12): 1451-1470.

Ren, Y. and H. Yamataka (2007). "The alpha-effect in gas-phase S_N2 reactions: Existence and the origin of the effect." Journal of Organic Chemistry **72**(15): 5660-5667.

Ren, Y. and H. Yamataka (2009). "Does alpha-effect exist in E2 reactions? A G2(+) investigation." Journal of Computational Chemistry **30**(3): 358-365.

Richter, R. and W. Lindinger (1986). Ion-molecule-reactions pertaining to etching plasmas. SASP, Symposium on Atomic and Surface Physics,contributions; February 9-15, Obertraun, Austria.

Rodgers, M. T. and P. B. Armentrout (1998). "Statistical modeling of competitive threshold collision-induced dissociation." Journal of Chemical Physics **109**(5): 1787-1800.

Rodgers, M. T., K. M. Ervin, et al. (1997). "Statistical modeling of collision-induced dissociation thresholds." Journal of Chemical Physics **106**(11): 4499-4508.

Russo, M. F., D. Bedrov, et al. (2013). "Combustion of 1,5-dinitrobiuret (DNB) in the presence of nitric acid using ReaxFF molecular dynamics simulations." Journal of Physical Chemistry A **117**(38): 9216-9223.

Schneider, S., T. Hawkins, et al. (2011). "Green Bipropellants: Hydrogen-Rich Ionic Liquids that Are Hypergolic with Hydrogen Peroxide." Angewandte Chemie-International Edition **50**(26): 5886-5888.

Schneider, S., T. Hawkins, et al. (2008). "Ionic liquids as hypergolic fuels." Energy & Fuels **22**(4): 2871-2872.

Seeley, J. V., R. A. Morris, et al. (1997). "Temperature dependences of the rate constants and branching ratios for the reactions of $F^-(H_2O)_{0-5}$ with CH_3Br." Journal of Physical Chemistry A **101**(25): 4598-4601.

Selim, E. T. M. and A. I. Helal (1981). "Heat of formation of $CH_2{=}O^+H$ fragment ion." Indian Journal of Pure & Applied Physics **19**(10): 977-980.

Shuman, N. S., W. R. Stevens, et al. (2010). "Dissociation dynamics of energy-selected acetic acid ions: The gas phase heat of formation of the acetyl ion." International Journal of Mass Spectrometry **294**(2-3): 88-92.

Smiglak, M., C. C. Hines, et al. (2010). "Ionic Liquids Based on Azolate Anions." Chemistry-a European Journal **16**(5): 1572-1584.

Smith, D. (1992). "The ion chemistry of interstellar clouds." Chemical Reviews **92**(7): 1473-1485.

Smith, D., N. G. Adams, et al. (1978). "Laboratory study of reactions of N^+, N_2^+, N_3^+, N_4^+, O^+, O_2^+, and NO^+ ions with several molecules at 300 K." Journal of Chemical Physics **69**(1): 308-318.

Smith, D., P. Spanel, et al. (1992). "A selected ion-flow tube study of the reactions of O^+, H^+ and HeH^+ with several molecular gases at 300 K." International Journal of Mass Spectrometry and Ion Processes **117**(1-3): 457-473.

Snyder, L. E., J. M. Hollis, et al. (1975). "Radio detection of interstellar sulfur-dioxide." Astrophysical Journal **198**(2): L81-L84.

Somogyi, A., M. A. Smith, et al. (2012). "Chemical ionization in the atmosphere? A model study on negatively charged "exotic" ions generated from Titan's tholins by ultrahigh resolution MS and MS/MS." International Journal of Mass Spectrometry **316**: 157-163.

Su, T. and M. T. Bowers (1973). "Ion-polar molecular collisions. Effect of ion size on ion-polar molecular rate constants. Parameterization of the Average-Dipole-Orientation Theory." International Journal of Mass Spectrometry and Ion Processes **12**: 347-356.

Su, T. and W. J. Chesnavich (1982). "Parametrization of the ion-polar molecule collision rate-constant by trajectory calculations." Journal of Chemical Physics **76**: 5183-5185.

Su, T., A. A. Viggiano, et al. (1992). "The effect of the dipole-induced dipole potential on ion polar molecule collision rate constants." Journal of Chemical Physics **96**(7): 5550-5551.

Sun, R., M. R. Siebert, et al. (2014). "Direct dynamics simulation of the activation and dissociation of 1,5-dinitrobiuret (HDNB)." Journal of Physical Chemistry A **118**(12): 2228-2236.

Taft, R. W., F. Anvia, et al. (1986). "Electrostatic proximity effects in the relative basicities and acidities of pyrazole, imidazole, pyridazine, and pyrimidine." Journal of the American Chemical Society **108**(12): 3237-3239.

Taft, R. W. and R. D. Topsom (1987). "The Nature and Analysis of Substituent Effects." Progress in Physical Organic Chemistry **16**: 1-83.

Thaddeus, P., C. A. Gottlieb, et al. (2008). "Laboratory and astronomical detection of the negative molecular ion C_3N^-." Astrophysical Journal **677**(2): 1132-1139.

Thomsen, D. L., C. M. Nichols, et al. (2014). "The alpha-effect and competing mechanisms: The gas-phase reactions of microsolvated anions with methyl formate." Journal of the American Society for Mass Spectrometry **25**(2): 159-168.

Thomsen, D. L., J. N. Reece, et al. (2013). "Investigating the alpha-effect in gas-phase S_N2 reactions of microsolvated anions." Journal of the American Chemical Society **135**(41): 15508-15514.

Thomsen, D. L., J. N. Reece, et al. (2014). "The alpha-effect in gas-phase S_N2 reactions of microsolvated anions: Methanol as a solvent." Journal of Physical Chemistry A **118**(37): 8060-8066.

Torr, M. R. and D. G. Torr (1982). "The role of metastable species in the thermosphere." Reviews of Geophysics **20**(1): 91-144.

Traeger, J. C. (1985). "Heat of formation for the formyl cation by photoionization mass-spectrometry." International Journal of Mass Spectrometry and Ion Processes **66**(3): 271-282.

Traeger, J. C., R. G. McLoughlin, et al. (1982). "Heat of formation for acetyl cation in the gas-phase." Journal of the American Chemical Society **104**(20): 5318-5322.

Tuckett, R. P. and T. Alain (2006). Chapter 3: Trifluoromethyl Sulphur Pentafluoride, SF_5CF_3: Atmospheric Chemistry and Its Environmental Importance via the Greenhouse Effect. Advances in Fluorine Science, Elsevier. **Volume 1:** 89-129.

Van Doren, J. M., S. E. Barlow, et al. (1987). "The tandem Flowing Afterglow-SIFT-DRIFT." International Journal of Mass Spectrometry and Ion Processes **81**: 85-100.

VanRaalte, D. and A. G. Harrison (1963). "Ionization and dissociation of formate esters by electron impact." Canadian Journal of Chemistry-Revue Canadienne De Chimie **41**(8): 2054-2059.

Vekey, K. (1996). "Internal energy effects in mass spectrometry." Journal of Mass Spectrometry **31**(5): 445-463.

Viggiano, A. A., R. A. Perry, et al. (1982). "Stratospheric negative-ion reaction-rates with H_2SO_4." Journal of Geophysical Research-Oceans and Atmospheres **87**(NC9): 7340-7342.

Viggiano, A. A., J. V. Seeley, et al. (1997). "Rate constants for the reactions of $XO_3^-(H_2O)_n$ (X = C, HC, and N) and $NO_3^-(HNO_3)_n$ with H_2SO_4: Implications for atmospheric detection of H_2SO_4." Journal of Physical Chemistry A **101**(44): 8275-8278.

Villano, S. M., N. Eyet, et al. (2009). "Reactions of alpha-nucleophiles with alkyl chlorides: Competition between S_N2 and E2 mechanisms and the gas-phase alpha-effect." Journal of the American Chemical Society **131**(23): 8227-8233.

Villano, S. M., N. Eyet, et al. (2010). "Photoelectron spectroscopy and thermochemistry of the peroxyacetate anion." European Journal of Mass Spectrometry **16**(3): 255-268.

Villano, S. M., N. Eyet, et al. (2010). "Photoelectron spectroscopy and thermochemistry of the peroxyformate anion." Journal of Physical Chemistry A **114**(1): 191-200.

Wang, Z. C., C. A. Cole, et al. (2015). "Reactions of azine anions with nitrogen and oxygen atoms: Implications for Titan's upper atmosphere and interstellar chemistry." Journal of the American Chemical Society **137**(33): 10700-10709.

Warneck, P. (1971). "Photoionisation von Methanol und Formaldehyd." Zeitschrift Fur Naturforschung **26**: 2047-2057.

Wayne, R. P. (1991). Chemistry of Atmospheres. New York, Oxford University Press.

Wenthold, P. G. (2000). "Determination of the proton affinities of bromo- and iodoacetonitrile using the kinetic method with full entropy analysis." Journal of the American Society for Mass Spectrometry **11**(7): 601-605.

Wenthold, P. G. and W. C. Lineberger (1999). "Negative ion photoelectron spectroscopy studies of organic reactive intermediates." Accounts of Chemical Research **32**: 597-604.

Wishart, J. F. (2009). "Energy applications of ionic liquids." Energy & Environmental Science **2**(9): 956-961.

Woon, D. E. (2015, October 13, 2015). "Interstellar and circumstellar molecules." from http://www.astrochymist.org/astrochymist_ism.html.

Yang, Z., C. A. Cole, et al. (2011). "Experimental and theoretical studies of reactions between H atoms and nitrogen-containing carbanions." Astrophysical Journal **739**(1): 10.

Young, R. A. and G. A. St. John (1968). "Experiments on $N_2(A^3\Sigma_u^+)$. I. Reaction with N." The Journal of Chemical Physics **48**(2): 895-897.

Zhang, Q. H., P. Yin, et al. (2014). "Cyanoborohydride-Based Ionic Liquids as Green Aerospace Bipropellant Fuels." Chemistry-a European Journal **20**(23): 6909-6914.

Zhang, Y. Q. and J. M. Shreeve (2010). "Dicyanoborate-Based Ionic Liquids as Hypergolic Fluids." Angewandte Chemie-International Edition **50**(4): 935-937.

Ziurys, L. M., A. J. Apponi, et al. (1994). "Detection of interstellar N_2O - A new molecule containing an N-O bond." Astrophysical Journal **436**(2): L181-L184.